



Search for Higgs boson pair production in association with top-quark pairs using 196 fb^{-1} of proton–proton collision data at $\sqrt{s} = 13$ and 13.6 TeV with the ATLAS detector

The ATLAS Collaboration

This paper presents the first search for non-resonant Higgs boson pair production in association with a top-quark pair ($t\bar{t}HH$) using proton–proton collision data collected with the ATLAS detector at the Large Hadron Collider. The data sample corresponds to an integrated luminosity of 196 fb^{-1} , comprising 140 fb^{-1} at a centre-of-mass energy of $\sqrt{s} = 13 \text{ TeV}$ and 56 fb^{-1} at 13.6 TeV . The search targets three distinct final states expected from $t\bar{t}HH$ decays: (i) one lepton (electron or muon) with at least five b -quarks, (ii) at least two b -quarks accompanied by two leptons with the same electric charges or multiple leptons, and (iii) at least three b -quarks with two photons. The $t\bar{t}HH$ production cross-section, relative to its Standard Model prediction, is measured to be $\mu_{t\bar{t}HH} = -3^{+11}_{-12}$. This result corresponds to a 95% confidence-level upper limit of 20 times the Standard Model prediction for the $t\bar{t}HH$ production cross-section, with an expected limit of 21. The Higgs effective field theory Wilson coefficient $c_{t\bar{t}HH}$ is also constrained at the same confidence level to the range of $-3.9 < c_{t\bar{t}HH} < 3.3$, compared with the expected range of $-4.0 < c_{t\bar{t}HH} < 3.5$.

Contents

1	Introduction	3
2	ATLAS detector	4
3	Data and Monte Carlo samples	5
4	Analysis strategy, object identification, and event selection	8
4.1	Object definition	8
4.2	1L selections	9
4.3	SSML selections	10
4.4	$b\bar{b}\gamma\gamma$ selections	10
5	Signal regions, control regions, and background estimation	10
5.1	The 1L channel	11
5.2	The SSML channel	11
5.3	The $b\bar{b}\gamma\gamma$ channel	13
6	Multivariate discriminants	14
7	Systematic uncertainties	15
7.1	Experimental uncertainties	15
7.2	Theoretical uncertainties	17
7.3	1L specific uncertainties	17
7.4	SSML specific uncertainties	17
7.5	$b\bar{b}\gamma\gamma$ specific uncertainties	18
8	Statistical analysis and results	18
9	Higgs effective field theory interpretation	26
10	Conclusion	27

1 Introduction

The Standard Model of particle physics (SM) has proven to be an immensely successful theory in describing fundamental particles and their interactions. A crucial aspect of this theory is the Brout–Englert–Higgs mechanism [1–3] for the electroweak symmetry breaking (EWSB), which predicts the existence of a neutral scalar particle known as the Higgs boson (H). Since its discovery in 2012 by the ATLAS and CMS collaborations [4, 5], substantial progress has been made in understanding the production processes and decay modes of the Higgs boson and its couplings to fermions and gauge bosons [6, 7]. However, the trilinear and quartic self-couplings of the Higgs boson remain only weakly constrained. These self-couplings are linked to the Higgs potential, which drives the EWSB, and can be studied through Higgs boson pair (HH) production.

Following the discovery of the Higgs boson, the search for HH production has become a central focus of the physics programme at the Large Hadron Collider (LHC). Among the primary HH production processes in proton–proton (pp) collisions at the LHC, gluon–gluon fusion (ggF) and vector-boson fusion (VBF) processes have garnered the most attention due to their higher cross-sections. Various HH decay channels, such as $b\bar{b}b\bar{b}$, $b\bar{b}\gamma\gamma$, and $b\bar{b}\tau^+\tau^-$, have been explored [8, 9]. The production of HH in association with a vector boson, known as the VHH process, has also been investigated [10, 11]. No evidence for HH production has been observed at the LHC. The combined 95% confidence level (CL) upper limit on the HH production cross-section, expressed relative to the SM prediction, is 2.9 from ATLAS [8], 3.5 from CMS [9] and 2.5 from their combination [12].

This paper presents the first search for Higgs boson pair production in association with a top-quark pair ($t\bar{t}HH$), focusing on non-resonant HH production as predicted by the SM. The $t\bar{t}HH$ process has the third largest HH production cross-section in the SM, after the ggF and VBF HH processes. Examples of the leading Feynman diagrams for the process are shown in Figure 1.

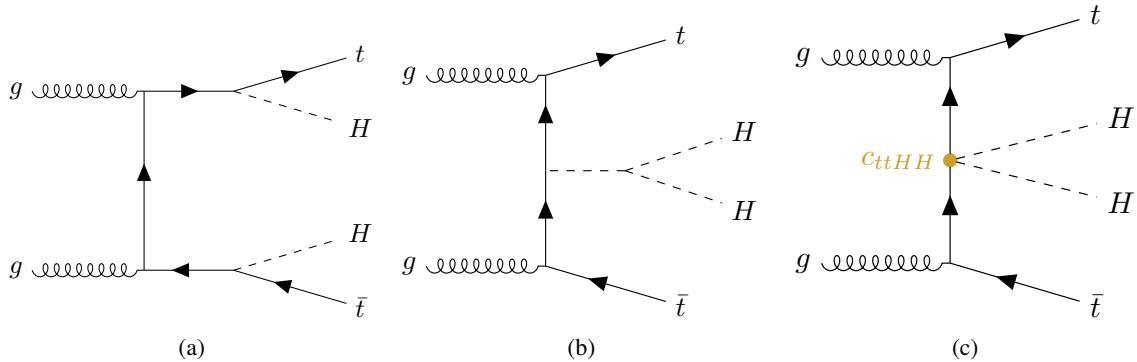


Figure 1: Examples of leading-order Feynman diagrams for the non-resonant $t\bar{t}HH$ process. Each diagram depicts a distinct subprocess arising from different Higgs boson couplings: (a) the Higgs–top Yukawa coupling, (b) the Higgs–top Yukawa coupling and Higgs boson trilinear self-coupling, and (c) the non-SM $t\bar{t}HH$ quartic coupling (highlighted with a circle), as described by the Higgs effective field theory.

In the SM, the $t\bar{t}HH$ process has a predicted cross-section of $\sigma_{t\bar{t}HH} = 0.756^{+4.3\%}_{-15.0\%}$ (scale) $\pm 3.4\%$ (PDF + α_s) fb for pp collisions at $\sqrt{s} = 13$ TeV and $0.860^{+4.2\%}_{-14.0\%}$ (scale) $\pm 3.3\%$ (PDF + α_s) fb at 13.6 TeV, calculated at next-to-leading order (NLO) in quantum chromodynamics (QCD) for a top-quark mass of $m_t = 172.5$ GeV and a Higgs boson mass of $m_H = 125$ GeV [13, 14]. The “PDF+ α_s ” uncertainty

accounts for uncertainties in the parton distribution functions and strong coupling constant, the “scale” uncertainty is due to the finite order of QCD calculations. Approximately 81% of the cross-section arises from the Higgs–top Yukawa coupling diagram shown in Figure 1 (a), while about 8% originates from the diagram involving the Higgs boson self-coupling shown in Figure 1 (b). The remaining 11% results from constructive interference between the two diagrams. Although the $t\bar{t}HH$ cross-section is sensitive to deviations of the Higgs boson self-coupling from its SM value, its dependence on the coupling modifier is considerably weaker than in the ggF and VBF HH production modes [13].

The analysis utilises the full LHC Run 2 data sample (2015–2018), corresponding to an integrated luminosity of 140 fb^{-1} collected with the ATLAS detector at a centre-of-mass energy $\sqrt{s} = 13 \text{ TeV}$ and a Run 3 data sample (2022–2023) corresponding to 56 fb^{-1} at $\sqrt{s} = 13.6 \text{ TeV}$. The analysis is performed using the framework documented in Ref. [15], developed within the ATLAS Collaboration for collision data analysis. The statistical interpretation is carried out using TRExFITTER framework [16].

Since the top quark decays almost exclusively into a W boson and a b -quark, $t\bar{t}HH$ events can result in a variety of final states with two or more b -quarks, depending on the decay modes of the W and Higgs bosons. The search leverages the large branching ratio of the $H \rightarrow b\bar{b}$ decay and the distinctive experimental signatures of leptons and photons. Three specific final states are considered. The first, labelled as 1L, is characterised by a single lepton ($\ell = \text{electron or muon}$) and at least five b -quarks, capturing signals primarily from $W \rightarrow \ell\nu$ and $HH \rightarrow b\bar{b}b\bar{b}$ decays. The second, referred to as SSML, requires two or more b -quarks together with two leptons with the same electric charges (same-sign dilepton pair) or more than two leptons. It is designed to select events in which at least one W boson decays leptonically, with additional leptons potentially arising from Higgs boson decays (e.g. $H \rightarrow \tau\tau, WW^*, ZZ^*$ decays). The third, referred to as $b\bar{b}\gamma\gamma$, consists of at least two b -quarks together with two photons, targeting $HH \rightarrow b\bar{b}\gamma\gamma$ decays.

The effect of new physics introduced by a new $t\bar{t}HH$ quartic interaction, shown in Figure 1(c), can be modelled using an effective field theory (EFT) approach. The results are interpreted in the Higgs effective field theory (HEFT) framework [17–22], as it allows the $t\bar{t}HH$ quartic interaction via the Wilson coefficient $c_{t\bar{t}HH}$ to be directly targeted without affecting other Higgs boson couplings. Unlike the ggF HH channel, which includes additional Higgs–gluon couplings, the $t\bar{t}HH$ channel is only affected by them at higher loop-order in weakly interacting theories, making the interpretation more robust.

This paper is structured as follows: Section 2 provides a brief overview of the ATLAS detector, and Section 3 describes the data and Monte Carlo (MC) samples used in the analysis. The reconstruction and identification of the physics objects, along with the event-selection criteria, are summarised in Section 4. The definitions of the signal and background regions, together with the background estimation methods, are presented in Section 5, while the multivariate techniques employed for signal–background separation are outlined in Section 6. Theoretical and experimental uncertainties are discussed in Section 7, and the final results and the HEFT interpretation are given in Sections 8 and 9, respectively. Finally, Section 10 provides the conclusions.

2 ATLAS detector

The ATLAS experiment [23, 24] at the LHC is a multipurpose particle detector with a forward–backward symmetric cylindrical geometry and a near 4π coverage in solid angle.¹ It consists of an inner tracking

¹ ATLAS uses a right-handed coordinate system with its origin at the nominal interaction point (IP) in the centre of the detector and the z -axis along the beam pipe. The x -axis points from the IP to the centre of the LHC ring, and the y -axis points upwards.

detector surrounded by a thin superconducting solenoid providing a 2 T axial magnetic field, electromagnetic (EM) and hadronic calorimeters, and a muon spectrometer. The inner detector (ID) covers the pseudorapidity range $|\eta| < 2.5$. It consists of silicon pixel, silicon microstrip, and transition radiation tracking detectors. Lead/liquid-argon (LAr) sampling calorimeters provide EM energy measurements with high granularity within the region $|\eta| < 3.2$. A steel/scintillator-tile hadronic calorimeter covers the central pseudorapidity range ($|\eta| < 1.7$). The endcap and forward regions are instrumented with LAr calorimeters for EM and hadronic energy measurements up to $|\eta| = 4.9$. The muon spectrometer surrounds the calorimeters and is based on three large superconducting air-core toroidal magnets with eight coils each. The field integral of the toroids ranges between 2.0 and 6.0 T m across most of the detector. The muon spectrometer includes a system of precision tracking chambers up to $|\eta| = 2.7$ and fast detectors for triggering up to $|\eta| = 2.4$. The luminosity is measured mainly by the LUCID-2 detector that is located close to the beampipe. A two-level trigger system was used to select events [25, 26]. The first-level trigger is implemented in hardware and used a subset of the detector information to accept events at a rate close to 100 kHz. This is followed by a software-based trigger that reduced the accepted rate of complete events to 1.25 kHz and 3 kHz on average in Run 2 and Run 3, respectively, depending on the data-taking conditions. A software suite [27] is used in data simulation, in the reconstruction and analysis of real and simulated data, in detector operations, and in the trigger and data acquisition systems of the experiment.

3 Data and Monte Carlo samples

The data used in the 1L and SSML channels were collected using single-lepton (electron or muon) triggers with varying transverse momentum (p_T) thresholds and isolation requirements [26, 28, 29]. The lowest p_T threshold ranged from 24 to 26 GeV for electrons and from 20 to 26 GeV for muons throughout the data-taking period covered by this search. Events in the $b\bar{b}\gamma\gamma$ channel were collected with diphoton triggers [26, 28], with nominal transverse momentum of 35 (25) GeV for the leading (sub-leading) photon. Events are included in the search only if all relevant detector subsystems were confirmed to be in optimal operating condition [30], resulting in a total integrated luminosity of $140.1 \pm 1.2 \text{ fb}^{-1}$ for the Run 2 data sample [31] and $56.0 \pm 1.1 \text{ fb}^{-1}$ for the Run 3 data sample [32, 33].

MC simulations play a central role in signal modelling, efficiency determination, background estimation, and event selection optimisation. The simulated samples were produced using a variety of event generators, along with different programs for parton showering, hadronisation, and underlying event modelling, collectively referred to as soft-QCD processes below. The decays of bottom and charm hadrons were simulated using the EVTGEN program [34], except for samples generated by SHERPA [35]. Top quarks were decayed at leading order (LO) using MADSPIN [36, 37] to preserve spin correlations. All simulations assumed a top-quark mass of 172.5 GeV, a Higgs boson mass of 125 GeV, and the corresponding decay branching ratios [14]. Simulated processes were normalised to the most accurate theoretical cross-section predictions available.

Table 1 summarises the nominal signal and background samples used in this search, and additional details of the signal and major background processes are provided in this section. Alternative samples employing different generators or parton-shower models are also used to evaluate modelling uncertainties. All MC

Polar coordinates (r, ϕ) are used in the transverse plane, ϕ being the azimuthal angle around the z -axis. The pseudorapidity is defined in terms of the polar angle θ as $\eta = -\ln \tan(\theta/2)$ and is equal to the rapidity $y = \frac{1}{2} \ln \left(\frac{E+p_z}{E-p_z} \right)$ in the relativistic limit. Angular distance is measured in units of $\Delta R \equiv \sqrt{(\Delta y)^2 + (\Delta \phi)^2}$.

samples were processed through an ATLAS detector simulation program [38], either using GEANT4 [39] or a fast simulation with parameterised calorimeter showers [40]. Pile-up effects, i.e. multiple interactions within the same or nearby bunch crossings, were modelled by overlaying [41] the hard-scatter events with simulated inelastic pp collisions generated using the EPOS [42] and PYTHIA [43] programs.

For samples generated with POWHEGBOX [44–49], MADGRAPH (MG5) [50], and MADGRAPH5_AMC@NLO (MG5_AMC) [51], soft-QCD processes were modelled using PYTHIA with the NNPDF2.3lo [52] parton distribution function (PDF) set and the A14 set of tuned parameters (tune) [53]. Samples generated with SHERPA used its native implementation of soft-QCD modelling. Events generated with the HERWIG7 [54–56] generator, together with the MMHT2014 NLO [57] PDF set and H7-UE tune, are used to assess systematic uncertainties associated with the modelling of soft-QCD processes.

The $t\bar{t}HH$ signal samples were generated to cover all the final states considered in this analysis, with decay filters applied to ensure orthogonality at generator level. For the 1L channel, separate samples were produced for fully hadronic, single-leptonic, and dileptonic decays of the top-quark pairs, with the Higgs boson pair decaying as $HH \rightarrow b\bar{b}b\bar{b}$. To target the SSML final state, inclusive samples were generated with all possible top-quark and Higgs boson decays except $HH \rightarrow b\bar{b}b\bar{b}$, and were filtered to contain either a same-sign dilepton pair or at least three leptons. In both channels, the ggF and VBF HH contributions are found to be negligible and therefore are not considered. Dedicated samples with $HH \rightarrow b\bar{b}\gamma\gamma$ decays were also produced. The signal samples were modelled with version 3.3.1 of the MADGRAPH (MG5) generator [50] at LO using NNPDF2.3lo, and were interfaced to PYTHIA8 for parton-shower and underlying-event modelling using the A14 tune. The renormalisation (μ_r) and factorisation (μ_f) scales were set to $H_T^{\text{scale}}/2$, where H_T^{scale} is defined as the sum of the transverse masses $\sqrt{p_T^2 + m^2}$ of all final-state partons. The $t\bar{t}HH$ samples were normalised using the SM cross-section computed at NLO in QCD [13].

Top-quark pair production ($t\bar{t}$) is a dominant background source in both the 1L and SSML channels. The process was modelled using a $t\bar{t}$ sample generated in the five-flavour scheme (5FS) with the POWHEGBOX generator at NLO, in which b -quarks are treated as massless, and the NNPDF3.0nlo [60] PDF set. The h_{damp} parameter was set to 1.5 times of the top-quark mass (m_t) in POWHEGBOX [61], and the pThard parameter was set zero in PYTHIA.² The μ_r and μ_f scales were set to the POWHEGBOX default choice of $\sqrt{m_t^2 + p_T^2}$, where p_T is the top-quark transverse momentum. The simulated sample was normalised to the SM prediction at next-to-next-to-leading order (NNLO) in QCD including next-to-next-to-leading logarithmic (NNLL) resummation, as computed with TOP++2 [62].

Top-quark pair production in association with a W boson ($t\bar{t}W$) is one of the dominant background processes in the SSML channel. It was simulated using the SHERPA generator [35], which provides matrix-element calculations at NLO accuracy in QCD for up to one additional parton, and at LO accuracy for up to two additional partons [63–65], merged with the SHERPA parton shower through the MEPS@NLO prescription [66]. The μ_r and μ_f scales were set to be $H_T^{\text{scale}}/2$ as for the $t\bar{t}HH$ signal sample. Electroweak corrections up to orders $\alpha^2\alpha_s^2$ and α^3 [67, 68] were included, along with real-emission contributions from subleading corrections at order $\alpha^3\alpha_s$ [69]. The process was normalised to the SM cross-section computed at NNLO in QCD [70].

Top-quark pair production in association with a Z boson ($t\bar{t}Z$) or a Higgs boson ($t\bar{t}H$) constitute two other important background sources in the SSML channel. The $t\bar{t}Z$ sample was simulated using MG5_AMC at NLO with the NNPDF3.0nlo PDF set, with μ_r and μ_f both set to $H_T^{\text{scale}}/2$. It was normalised to the

² The h_{damp} parameter regulates the modelling of low- and high- p_T radiation within POWHEGBOX, while pThard controls how PYTHIA vetos its own radiation to avoid double-counting emissions already generated by POWHEGBOX.

Table 1: List of MC event generators and their associated matrix-element (ME) orders, parton showers, PDFs, and underlying set of tuned parameters used for simulating signal and background processes. When different from the Run 2 configuration, Run 3 settings are indicated in parentheses.

Process	Generator	ME order	Parton Shower	PDF set	Tune
$t\bar{t}HH$	MG5	LO	PYTHIA8	NNPDF2.31o	A14
$t\bar{t}$ (5FS)	POWHEGBOX	NLO	PYTHIA8	NNPDF3.0n1o	A14
$t\bar{t}t\bar{t}$	MG5_AMC	NLO	PYTHIA8	NNPDF3.0n1o	A14
$t\bar{t}t$	MG5_AMC	LO	PYTHIA8	NNPDF2.31o	A14
$t\bar{t}W$	SHERPA	MEPS@NLO	SHERPA	NNPDF3.0nn1o	SHERPA
$t\bar{t}Z$	MG5_AMC	NLO	PYTHIA8	NNPDF3.0nn1o	A14
$t\bar{t}WW$	MG5_AMC (MG5)	LO	PYTHIA8	NNPDF3.0n1o	A14
$t\bar{t}WZ, t\bar{t}WH, t\bar{t}ZZ$	MG5	LO	PYTHIA8	NNPDF2.31o	A14
tW	POWHEGBOX	NLO	PYTHIA8	NNPDF3.0n1o	A14
tZ	MG5_AMC	LO	PYTHIA8	NNPDF3.0NLOnf4	A14
$t(q)b$ (t -channel)	POWHEGBOX	NLO	PYTHIA8	NNPDF3.0NLOnf4	A14
$t(q)b$ (s -channel)	POWHEGBOX	NLO	PYTHIA8	NNPDF3.0n1o	A14
tWZ, tHq, tHW	MG5_AMC	NLO	PYTHIA8	NNPDF3.0n1o	A14
$V/VV/VVV$ + jets	SHERPA	MEPS@NLO [†]	SHERPA	NNPDF3.0n1o	SHERPA
$\gamma\gamma$ + jets	SHERPA	NLO	SHERPA	NNPDF3.0nn1o	A14
$\gamma\gamma + t\bar{t}$	MG5	LO	PYTHIA8	NNPDF2.31o	A14
ggF H	NNLOPS [58, 59]	NLO	PYTHIA8	PDF4LHC15	AZNLO (A14)
VBF H	POWHEGBOX	NLO	PYTHIA8	PDF4LHC15 (PDF4LHC21)	AZNLO (A14)
VH	POWHEGBOX	NLO	PYTHIA8	PDF4LHC15 (PDF4LHC21)	AZNLO (A14)
$t\bar{t}H$	POWHEGBOX	NLO	PYTHIA8	NNPDF3.0n1o (PDF4LHC21)	A14
ggF HH	POWHEGBOX	NLO	PYTHIA8	PDF4LHC21	A14
VBF HH	MG5	NLO	PYTHIA8	NNPDF3.0n1o	A14

[†] For the subdominant $gg \rightarrow VV$ contribution, the ME calculation is at leading order.

SM cross-section calculated at NLO in QCD and electroweak corrections [14, 71]. The $t\bar{t}H$ sample was simulated using POWHEGBOX at NLO with the PDF set of NNPDF3.0n1o for Run 2 and PDF4LHC21 [72] for Run 3. The μ_r and μ_f scales were set to the geometric mean of the transverse mass of the three outgoing partons. The process was normalised to the SM cross-section calculated at NLO in QCD and electroweak corrections [14, 73–76].

The four-top-quark production process ($t\bar{t}t\bar{t}$) also contributes significantly in the SSML channel. It was simulated using the MADGRAPH5_AMC@NLO generator, which incorporates matrix-element calculations at NLO accuracy in QCD. The μ_r and μ_f scales were set to $H_T^{\text{scale}}/2$. The simulated sample was normalised to the SM cross-section computed at NLO in QCD, including electroweak corrections [69]. Together with the three-top-quark process ($t\bar{t}t$), modelled at LO using MADGRAPH5_AMC@NLO as described in Ref. [77], these contributions are collectively referred to as the multi-top background in the following.

In the 1L and SSML channels, additional minor background processes, such as $V/VV/VVV$ + jets and $t\bar{t} + VV$, are modelled using SHERPA at NLO and MADGRAPH at LO, respectively, as detailed in Refs. [77–79].

For the $b\bar{b}\gamma\gamma$ channel, the non-resonant diphoton background arises from processes with two prompt photons and events in which one or both photon candidates originate from misidentified jets. The normalisation of this background is determined entirely from data, while SHERPA MC samples with two

prompt photons were used to model its kinematics. The resonant background contributions from single Higgs boson production (primarily ggF H and VBF H) and non- $t\bar{t}HH$ Higgs boson pair production (mainly ggF HH and VBF HH) were modelled using MC samples, most of which were generated with the POWHEGBox generator as described in Ref. [80].

4 Analysis strategy, object identification, and event selection

Although all three channels target $t\bar{t}HH$ production, their distinct signatures and background compositions require dedicated analysis strategies. The 1L and SSML final states feature relatively high signal and background rates, enabling analyses to be performed both on the combined Run 2 and Run 3 data samples and separately for each data-taking period. In contrast, the $b\bar{b}\gamma\gamma$ final state offers a cleaner signature but suffers from limited numbers of events, motivating an analysis based solely on the combined data sample.

The 1L and SSML channels adopt similar methodologies, relying on both simulation and data for background estimation and employing transformer-based machine learning techniques [81] to enhance signal-to-background discrimination. Potential $t\bar{t}HH$ contributions are extracted through simultaneous fits to the transformer outputs in the signal regions and to selected fit variables in the background control regions. In the $b\bar{b}\gamma\gamma$ channel, potential signals are identified using a strategy analogous to Ref. [80], based on fits to the diphoton invariant-mass spectra. This method leverages the narrow Higgs boson resonance and the excellent diphoton mass resolution of the ATLAS detector, enabling a fully data-driven determination of the continuum background from the resonance sidebands.

The physics objects used in this analysis are summarised in Section 4.1, with many shared across the three channels. The event selection criteria specific to each channel are then described in Sections 4.2, 4.3, and 4.4. To be selected, an event must have a primary vertex (PV), defined as the vertex reconstructed with at least two ID tracks with $p_T > 500$ MeV. If multiple PVs are present, the one with the largest sum of p_T^2 of its associated tracks is chosen [82].

4.1 Object definition

Electrons are reconstructed by matching topological energy clusters in the EM calorimeter with tracks in the ID and are identified using likelihood-based criteria that incorporate calorimeter shower shape, track-to-cluster matching, and associated track quality requirements [83–85]. Electron candidates must have $p_T > 15$ GeV and $|\eta_{\text{cluster}}| < 2.47$, excluding the transition region between the barrel and endcap calorimeters ($1.37 < |\eta_{\text{cluster}}| < 1.52$). In the 1L channel, they are required to satisfy the *loose* identification likelihood and *loose* isolation criteria [83], whereas the SSML channel requires the *tight* identification likelihood and *tight* isolation criteria. Unless otherwise stated, the isolation criteria are based on combined tracking and calorimeter information.

Muons are reconstructed by combining tracks from the ID with those from the muon spectrometer [86, 87]. Muon candidates must have $p_T > 15$ GeV and $|\eta| < 2.5$. In the 1L channel, they must satisfy the *loose* identification quality and *loose* track-based isolation requirements, while in the SSML channel they are required to meet the *medium* identification quality and *tight* isolation criteria [88].

To select leptons originating from the primary vertex, the transverse impact parameter, normalised by its estimated uncertainty ($|d_0|/\sigma(d_0)$), must be less than five for electrons and three for muons, while the longitudinal impact parameter must satisfy $|z_0 \sin \theta| < 0.5$ mm for both lepton flavours.

Photons are reconstructed from the topological energy clusters in the EM calorimeter [83–85]. Photon candidates are required to have $|\eta_{\text{cluster}}| < 1.37$ or $1.52 < |\eta_{\text{cluster}}| < 2.37$. Photons are required to satisfy *tight* identification likelihood and *loose* track-based isolation criteria.

Jets are reconstructed using a particle-flow algorithm [89] that combines measurements from the ID and the calorimeters. The anti- k_r algorithm [90] with a radius parameter of $R = 0.4$ is employed. Jets are required to have $p_T > 20$ GeV and $|\eta| < 2.5$ and a calibration procedure is performed as described in Refs. [91, 92]. To mitigate pile-up effects, the jet-vertex tagger (JVT) [93] is applied to jets with $p_T < 60$ GeV and $|\eta| < 2.4$.

Jets originating from the hadronisation of b -quarks are identified (*b-tagged*) using the GN2 algorithm [94], a transformer-based neural network designed to predict the flavour of reconstructed jets. The network takes as input per-track quantities and their associated uncertainties, along with the jet p_T and η . Its output scores are combined into a b -tagging discriminant. Five thresholds, referred to as working points (WP), are defined with average efficiencies of 65%, 70%, 77%, 85%, and 90% for tagging b -quark jets in simulated $t\bar{t}$ events. A pseudo-continuous b -tagging (PCBT) score, w_{PCBT} , is assigned to each jet and represents the number of WPs it satisfies. The score starts at one for jets failing to satisfy any WP and increases by one for each successively tighter WP satisfied. It reaches a maximum value of $w_{\text{PCBT}} = 6$ for jets satisfying the tightest 65% WP. In the following, $N_b^{90\% (85\%, 77\%)}$ denotes the number of b -tagged jets satisfying the 90% (85%, 77%) WP. Another relevant variable is $\sum_{\text{jet}} w_{\text{PCBT}}$, defined as the sum of the w_{PCBT} scores of all jets in the event for which a valid w_{PCBT} is assigned.

The missing transverse momentum, with its magnitude denoted by E_T^{miss} , is defined as the negative vectorial sum of the p_T of all reconstructed and calibrated objects in the event. This sum also includes momenta from ID tracks matched to the primary vertex but not associated with any other reconstructed objects (soft term) [95].

A sequential overlap-removal procedure is applied independently in each channel to ensure that the same calorimeter energy deposit or track is not assigned to multiple reconstructed objects. The procedure uses the lepton selection described above for the 1L channel, whereas for the SSML channel the isolation requirements are removed from the lepton selection. For the $b\bar{b}\gamma\gamma$ channel, the leptons considered in the removal procedure are selected using the *medium* identification requirement together with *loose* isolation criteria. The impact of the overlap-removal procedure on the search is negligible.

Channel-specific event selections are then applied to maximise the sensitivity of each channel.

4.2 1L selections

In the 1L channel, candidate events are required to contain exactly one lepton (electron or muon) with transverse momentum $p_T > 27$ GeV, satisfying *tight* identification and isolation requirements. The selected lepton must be matched to a corresponding trigger-level object. E_T^{miss} is required to exceed 20 GeV, consistent with the presence of a neutrino from the leptonic top-quark decay.

Events are required to have at least six jets and at least four b -tagged jets identified with the GN2 algorithm using the 85% WP, $N_b^{85\%} \geq 4$. The nominal misidentification rates for this WP are approximately 20% for c -jets and 1% for light-flavour jets.

To mitigate the parton-shower limitations in the modelling of high jet multiplicities and low jet transverse momenta, an upper limit of eleven jets is imposed. In addition, the scalar sum of jet transverse momenta, H_T^{jets} , is required to be greater than 400 GeV.

4.3 SSML selections

The event selection for the SSML channel is based on the strategy developed for searches targeting the $t\bar{t}\bar{t}$ production process, given the similar phase space, following the procedures described in Refs. [96, 97]. Candidate events are required to contain at least two leptons with $p_T > 15$ GeV, with the leading lepton required to satisfy $p_T > 27$ GeV and to be matched to a corresponding trigger-level object. Events are categorised into two sub-channels: same-sign dilepton (SS2L) and trilepton (3L). The SS2L sub-channel includes events with exactly two leptons of the same electric charge, while the 3L sub-channel includes events with three or more leptons.

To reduce background from charge mis-identification in $Z \rightarrow e^+e^-$ processes, SS2L events with same-sign electrons must satisfy $|m_{ee} - m_Z| > 10$ GeV. In the 3L sub-channel, all opposite-sign same-flavour lepton pairs are required to meet $|m_{\ell\ell} - m_Z| > 10$ GeV to suppress contamination from Z boson decays.

4.4 $b\bar{b}\gamma\gamma$ selections

The $b\bar{b}\gamma\gamma$ channel targets the $HH \rightarrow b\bar{b}\gamma\gamma$ decays of $t\bar{t}HH$ events. Selected events must contain exactly two photons with an invariant mass in the range of $105 < m_{\gamma\gamma} < 160$ GeV. The leading (subleading) photon is required to satisfy the condition on the relative transverse momentum of $p_T/m_{\gamma\gamma} > 35\%(25\%)$, ensuring a uniform acceptance across the $m_{\gamma\gamma}$ spectrum. This selection guarantees that both photons carry sufficient transverse momentum to be compatible with a Higgs boson decay, while suppressing backgrounds containing photons originating from QCD processes. In addition, events must contain at least two b -tagged jets selected with the 90% working point, $N_b^{90\%} \geq 2$.

5 Signal regions, control regions, and background estimation

Background contributions across the three channels are estimated by using one of three approaches: fully simulation-based, hybrid simulation-data, or fully data-driven methods. Processes that are well modelled or negligible are taken directly from MC simulation, while backgrounds that are difficult to simulate reliably use MC to describe their kinematic properties and data control regions (CR) to determine their normalisation. In the $b\bar{b}\gamma\gamma$ search, where a narrow $H \rightarrow \gamma\gamma$ resonance is targeted, the continuum background is extracted from the diphoton mass sidebands in data defined as $105 < m_{\gamma\gamma} < 120$ GeV \cup $130 < m_{\gamma\gamma} < 160$ GeV. The following sections outline the specific strategies adopted for each channel.

5.1 The 1L channel

In the 1L channel, two signal-enriched regions (SR), $6b$ and $5b_{\text{Hi}}$, and two background-enriched CRs with negligible signal contamination, $5b_{\text{Lo}}$ and $4b_{\text{Hi}}$, are defined based on the number of b -tagged jets satisfying different WP criteria. These regions are summarised in Table 2. The SRs capture $\sim 1.1\%$ of all the produced inclusive $t\bar{t}HH$ signal events.

Table 2: Definition of regions in the 1L channel, along with the variables used in the fit. The quantities $N_b^{85\%}$ and $N_b^{77\%}$ represent the number of b -tagged jets identified using the 85% and 77% efficiency working points, respectively.

Region	Type	$N_b^{85\%}$	$N_b^{77\%}$	Fit variable
$4b_{\text{Hi}}$	CR	4	4	$\sum_{\text{jet}} w_{\text{PCBT}}$
$5b_{\text{Lo}}$	CR	5	≤ 4	$\sum_{\text{jet}} w_{\text{PCBT}}$
$5b_{\text{Hi}}$	SR	5	5	Transformer output
$6b$	SR	≥ 6	–	Transformer output

The dominant background in the 1L channel arises from $t\bar{t}$ events with additional heavy-flavour (HF) jets, originating from b - or c -quarks produced primarily via gluon emissions from higher-order QCD processes. Previous ATLAS and CMS analyses [98–101] have shown that MC simulations systematically underestimate the production rate of these events. To correct for this discrepancy, the normalisations of the $t\bar{t}$ +jets background components are adjusted using CRs, with corrections derived according to the flavour composition of the additional jets. Their kinematic distributions are modelled using MC simulation. The $t\bar{t}$ +jets events are categorised according to the generator-level flavour of the extra jets, identified via a hadron–jet matching algorithm described in Ref. [78]. Five categories are defined: $t\bar{t} + \geq 1c/l(\text{light})$, $t\bar{t} + 1b$, $t\bar{t} + 2b$, $t\bar{t} + 3b$, and $t\bar{t} + \geq 4b$.

The normalisation factors (NF) for each $t\bar{t}$ +jets category are determined simultaneously with the signal strength (see Section 8) using a profile likelihood fit that incorporates both the signal and CRs defined in Table 2, along with the corresponding fitting variables in each region. Pre-fit normalisations are taken directly from the generator cross-section predictions. Each category is treated as an independent process and assigned its own modelling uncertainties. The post-fit normalisations of the dominant components, $t\bar{t} + 1b$ and $t\bar{t} + 2b$, are extracted through unconstrained parameters in the fit, allowing them to adjust freely to the observed data. Due to the limited constraining power of the data, the $t\bar{t} + \geq 1c/l$, $t\bar{t} + 3b$, and $t\bar{t} + \geq 4b$ components are normalised to their MC predictions, with associated systematic uncertainties discussed in Section 7. Other minor background contributions ($V/VV/VVV$, $t\bar{t}V$, $t\bar{t}H$, multi-top and $V(V, VV)$ +jets) are also estimated by using MC simulation.

5.2 The SSML channel

In the SSML channel, the SRs are defined as follows. Events in the SS2L category are required to have at least six jets, while those in the 3L category must contain at least five jets. In both cases, at least two jets must be b -tagged using the 85% WP, i.e. $N_b^{85\%} \geq 2$. Additionally, the scalar sum of the transverse momentum of jets and leptons, $H_{\text{T}}^{\text{all}}$, must exceed 400 GeV. In this channel, the SRs capture approximately 0.75% of all produced $t\bar{t}HH$ signal events.

Background contributions in the SSML channel are classified into two main types: physics backgrounds and instrumental backgrounds. Physics backgrounds originate from processes that produce final states similar to those targeted by the SSML selection, including VV , VVV , $t\bar{t}V$, $t\bar{t}H$, $t\bar{t}VV$, and multi-top. In these processes, leptons arise from the prompt decays of heavy bosons (W , Z , and H). Among these background sources, $t\bar{t}V$, $t\bar{t}H$, and multi-top constitute the dominant contributions limiting the search sensitivity.

All physics backgrounds, except for $t\bar{t}W$, are estimated by using MC simulations. For $t\bar{t}W$, its kinematic properties are modelled using MC, while a dedicated CR is employed to constrain its normalisation using data. This is achieved through a template fit to the jet multiplicity distribution (N_j) in the $t\bar{t}W$ CR. This approach accounts for a potentially enhanced $t\bar{t}W$ production cross-section relative to the SM prediction, motivated by recent measurements [79, 102]. The selection criteria for this CR are given in Table 3. The requirements for this and other CRs described below are designed to enhance contributions from the targeted background sources while remaining orthogonal to the SR.

Instrumental backgrounds originate from leptons with misidentified charge (QmisID) and non-prompt leptons from photon conversions, heavy-flavour quark decays, and jets mis-identified as leptons (Fake/non-prompt). The main process contributing to these backgrounds is $t\bar{t}$ production. These backgrounds are challenging to simulate accurately and are therefore evaluated using a combination of MC and data-driven techniques, following the methodology described in Ref. [97].

QmisID primarily affects the SS2L ee and $e\mu$ channels, as electron identification is particularly susceptible to charge misidentification due to bremsstrahlung radiation followed by photon conversion. In Run 2 data, a boosted decision tree (BDT) based electron charge identification (ECID) tool is employed to significantly reduce the QmisID contribution [83]. The ECID tool combines tracking information with the magnitude and spatial pattern of bremsstrahlung radiation to reject electrons whose charges are likely mismeasured. However, this tool is not yet available for the Run 3 data sample, resulting in increased QmisID background.

The charge misidentification probability is derived from $Z \rightarrow e^+e^-$ events in data, selected with the requirement $|m_{ee} - m_Z| < 10$ GeV and without imposing any charge requirement. The misidentification rate is determined from the fraction of same-sign electron pairs and is parameterised as a function of the electron p_T and η . This rate is then applied to the ee and $e\mu$ events in data that satisfy the SS2L selection criteria, apart from the charge requirement, to estimate the QmisID background contribution.

Backgrounds from photon conversions, $\gamma^{(*)} \rightarrow e^+e^-$, occurring either at the primary vertex or within the detector material, can lead to only one of the electrons being reconstructed. A conversion electron is identified through its small invariant mass with a nearby reconstructed track. It is classified as an internal conversion (Int. Conv.), $\gamma^* \rightarrow e^+e^-$, if the associated track points to the primary vertex, or as a material conversion (Mat. Conv.), $\gamma \rightarrow e^+e^-$, if the track instead points to a conversion vertex in the detector material. Leptons from heavy-flavour (b - and c -quark) decays generally fail to satisfy the identification criteria designed for prompt leptons from vector boson decays. However, a small fraction satisfy the selection and contribute to the non-prompt lepton background.

Similar to the $t\bar{t}W$ background, CRs are used to improve the estimates of these fake/non-prompt lepton background contributions. MC predictions are scaled by NFs derived from a template fit to data in all the CRs, defined in Table 3. Each CR targets a specific background source: ‘Int. Conv.’ for virtual photon conversions at the primary vertex, ‘Mat. Conv.’ for real photon conversions in the detector material, ‘HF e ’ for electrons from heavy flavour decays, and ‘HF μ ’ for muons from heavy flavour decays. The selection criteria leverage the characteristic features of these background processes to enhance their contributions

Table 3: Definitions of control regions in the SSML channel. In the 3L sub-channel, leptons are labelled as ℓ_1 , ℓ_2 , and ℓ_3 in decreasing order of p_T . N_j , and $N_b^{85\%}$ denote the numbers of jets and b -tagged jets identified using the 85% working point.

Control Region	Channel	N_j	$N_b^{85\%}$	Other selection	Fit variable
$t\bar{t}W$	SS2L $e\mu, \mu\mu$	≥ 4	≥ 2	$p_T^{\ell_2} > 25 \text{ GeV}, \eta(e) < 1.5$ If $N_b^{85\%} = 2$: $H_T^{\text{all}} < 400 \text{ GeV}$ or $N_j < 6$ If $N_b^{85\%} \geq 3$: $H_T^{\text{all}} < 400 \text{ GeV}$	N_j
Int. Conv.	SS2L $ee, e\mu$	$4 \leq N_j < 6$	≥ 1	Only one e from $\gamma^* \rightarrow ee$ No e from $\gamma \rightarrow ee$	N_{events}
Mat. Conv.	SS2L $ee, e\mu$	$4 \leq N_j < 6$	≥ 1	Only one e from $\gamma \rightarrow ee$ No e from $\gamma^* \rightarrow ee$	N_{events}
HF μ	3L $e\mu\mu, \mu\mu\mu$	≥ 1	$= 1$	$E_T^{\text{miss}} > 35 \text{ GeV}$ $100 < H_T^{\text{all}} < 275 \text{ GeV}$ Total lepton charge = ± 1	$p_T^{\ell_3}$
HF e	3L $eee, ee\mu$	≥ 1	$= 1$	$E_T^{\text{miss}} > 35 \text{ GeV}$ $100 < H_T^{\text{all}} < 275 \text{ GeV}$ Total lepton charge = ± 1	$p_T^{\ell_3}$

while ensuring orthogonality among all CRs and the SR. The distributions of event variables used in the fits are listed in the table.

For the Run 3 data, photon conversion CRs (Int. Conv. and Mat. Conv.) are not used due to the larger QmisID background contribution stemming from the absence of the ECID tool. Instead, the NFs obtained from the Run 2 data are used to estimate the conversion background contributions in Run 3 data.

Fake/non-prompt lepton background contributions from light hadron decays or mis-identified jets are expected to be minimal and are estimated by using simulation without additional corrections.

5.3 The $b\bar{b}\gamma\gamma$ channel

Three SRs are defined for the $b\bar{b}\gamma\gamma$ channel using BDTs, as described in Section 6. The background model in this channel comprises a dominant non-resonant (continuum) component, along with several resonant contributions from Higgs boson production in the diphoton invariant-mass spectrum.

The continuum background primarily originates from $\gamma\gamma$ +jets events, with smaller contributions from γ +jet or dijet events where one or two jets are misidentified as photons. Due to the tight event selection, this background is dominated by processes with associated heavy-flavour production. Therefore, two dedicated samples, $\gamma\gamma b\bar{b}$ and $t\bar{t}\gamma\gamma$ are used to model the continuum background composition and kinematics. MC simulation is used solely for optimising the event selection and for training multivariate classifiers.

The continuum background is modelled with an exponential function chosen using the spurious-signal procedure [103], which evaluates a broad range of candidate parameterisations. The exponential form is retained because it satisfies statistical criteria ensuring that it does not artificially absorb or generate a signal. The exponential shape parameter is determined from data via an unbinned maximum-likelihood fit to the diphoton invariant mass distribution, $m_{\gamma\gamma}$, performed in the sidebands of all the $b\bar{b}\gamma\gamma$ SRs described in

Section 6. The fit uses independent normalisations for each region while enforcing a common exponential shape correlated across them. Allowing the shape parameter to vary independently in each SR changes the overall sensitivity by less than 1%, and the resulting parameter values are consistent across regions within statistical uncertainties.

Resonant backgrounds from single Higgs boson production and non- $t\bar{t}HH$ Higgs boson pair production processes are modelled using simulated samples and are normalised to their corresponding theoretical cross-sections. Their shapes are described by double-sided Crystal Ball (DSCB) functions [104] derived from simulation.

The complete background model is thus constructed as the sum of the analytic continuum and resonant MC templates. A combined likelihood fit simultaneously determines the normalisations and the correlated continuum shape across the signal and sideband regions, while the resonant contributions remain constrained to their theoretical predictions.

6 Multivariate discriminants

Multivariate analysis techniques are employed to exploit the kinematic differences between signal and background events that satisfy the SR selection in the 1L and SSML channels. A transformer architecture is used, incorporating the scaled dot-product attention mechanism described in Ref. [81].

MC samples are used to train the transformer models, which are designed to distinguish among various event classes, including both signals and backgrounds. The training process aims to minimise a loss function that quantifies the fraction of misclassified events within the training data samples.

Signal and background samples used to develop the transformer models are partitioned into three statistically independent subsamples: one for training (training set), one for hyper-parameter optimisation (validation set), and one for performance evaluation (test set). This strategy facilitates the study and mitigation of over-training effects. The test set is also used to predict the expected signal and background distributions of the transformer output scores for the final statistical analyses. A k -fold method, with $k = 3$ for 1L and $k = 4$ for SSML, is performed by rotating the three sets in order to evaluate independently all data samples and maximise the number of MC events used in the final statistical analyses. The training is performed separately for the Run 2 and Run 3 data samples.

The input features to the transformer consist of kinematic variables, complemented by b -tagging. These include the momentum vectors (p_T, η, ϕ) of leptons, jets and E_T^{miss} , along with the jet w_{PCBT} and the charge information for leptons.

For the 1L channel, a binary transformer classifier is trained to distinguish the $t\bar{t}HH$ signal from all background processes. In contrast, the SSML channel employs a three-class training scheme to separately identify the $t\bar{t}HH$ signal, the multi-top background, and all other backgrounds. The multi-top contribution is treated separately due to its comparatively large cross-section uncertainty. The transformer provides class-likelihood scores that are between zero and one for each event: $p_{t\bar{t}HH}$ and p_{bgd} in 1L and $p_{t\bar{t}HH}$, $p_{\text{multi-top}}$, and p_{others} in SSML. These scores are used to construct discriminants, D_{1L} for 1L and D_{SSML} for SSML, for the final signal-background separation:

$$D_{1L} = p_{t\bar{t}HH}, \quad D_{\text{SSML}} = \ln \left(\frac{p_{t\bar{t}HH}}{0.2 \cdot p_{\text{multi-top}} + 0.8 \cdot p_{\text{others}}} \right).$$

The weights assigned to the $t\bar{t}\bar{t}$ and other background components in the SSML discriminant are optimised to maximise sensitivity to the $t\bar{t}HH$ signal. These weights closely reflect the relative contributions of the corresponding background processes in the highest D_{SSML} regime.

The $b\bar{b}\gamma\gamma$ channel employs a set of BDTs to define SRs of varying purities, rather than serving as the final discriminant. Signal-to-background discrimination is achieved through a multi-BDT strategy, implemented using the XGBOOST algorithm [105] and the OPTUNA framework [106] for hyperparameter optimisation.

Four independent BDTs, shown in Figure 2, are trained on the combined Run 2 and Run 3 data samples to distinguish the $t\bar{t}HH$ signal from the four major backgrounds: $\gamma\gamma b\bar{b}$, $t\bar{t}\gamma\gamma$, $t\bar{t}H$, and other Higgs processes. Key input features include the reconstructed di-Higgs boson invariant mass and the kinematics of photons and b -tagged jets. Training is validated with independent test samples, and overtraining is assessed by comparing training and test BDT-score distributions. Three mutually exclusive SRs (SR1, SR2, and SR3), ordered from the lowest to highest sensitivity, are defined for events with $N_b^{90\%} \geq 3$ using three thresholds ($c_i^1 < c_i^2 < c_i^3$) on each of the four BDTs ($i = 1, 2, 3, 4$). SR3 contains events satisfying all highest thresholds (c_i^3), SR2 consists of events satisfying the intermediate thresholds (c_i^2) but fail to satisfy the SR3 requirement. Finally SR1 includes events satisfying the baseline thresholds (c_i^1), excluding those already assigned to SR2 or SR3. The threshold values, c_i^k , are optimised to maximise the expected signal significance within the diphoton mass window $120 < m_{\gamma\gamma} < 130$ GeV, while ensuring at least three sideband events in each SR. In the $b\bar{b}\gamma\gamma$ channel, the SRs retain approximately 0.05% of all $t\bar{t}HH$ signal.

7 Systematic uncertainties

Systematic uncertainties in the $t\bar{t}HH$ search are categorised into three main groups: experimental uncertainties, which affect reconstructed objects such as leptons, photons, and jets; theoretical uncertainties, related to the modelling of signal and background processes; and data-driven uncertainties, associated with background estimates derived from data. These uncertainties impact both the shape of kinematic distributions and the normalisation of signal and background contributions. While the specific objects and processes may vary across channels, the methodologies for evaluating experimental and theoretical uncertainties are similar. In contrast, the estimation of uncertainties for data-driven background contributions is channel-specific. In the 1L and SSML channels, systematic variations are propagated through the transformer-output templates used in the binned fit. For the $b\bar{b}\gamma\gamma$ channel, the uncertainties are incorporated via the $m_{\gamma\gamma}$ model (signal DSCB parameters and background-shape parameters) entering the unbinned fit in each category. The following sections first describe systematic uncertainties common to all three channels, followed by channel-specific uncertainties and their respective impacts.

7.1 Experimental uncertainties

Jet-related uncertainties arise from several sources, including the jet energy scale (JES), jet energy resolution (JER), flavour tagging, and JVT used for pile-up rejection. JES and JER uncertainties are evaluated using control samples where jets recoil against well-calibrated reference objects – such as photons, Z bosons, or other calibrated jets [91]. Flavour tagging uncertainties originate from uncertainties in tagging efficiencies and misidentification rates. These are assessed using $t\bar{t}$ events for b - and c -jets, and Z +jets events for light-quark and gluon jets [107–109]. Additional uncertainties are considered for the JVT efficiency [93].

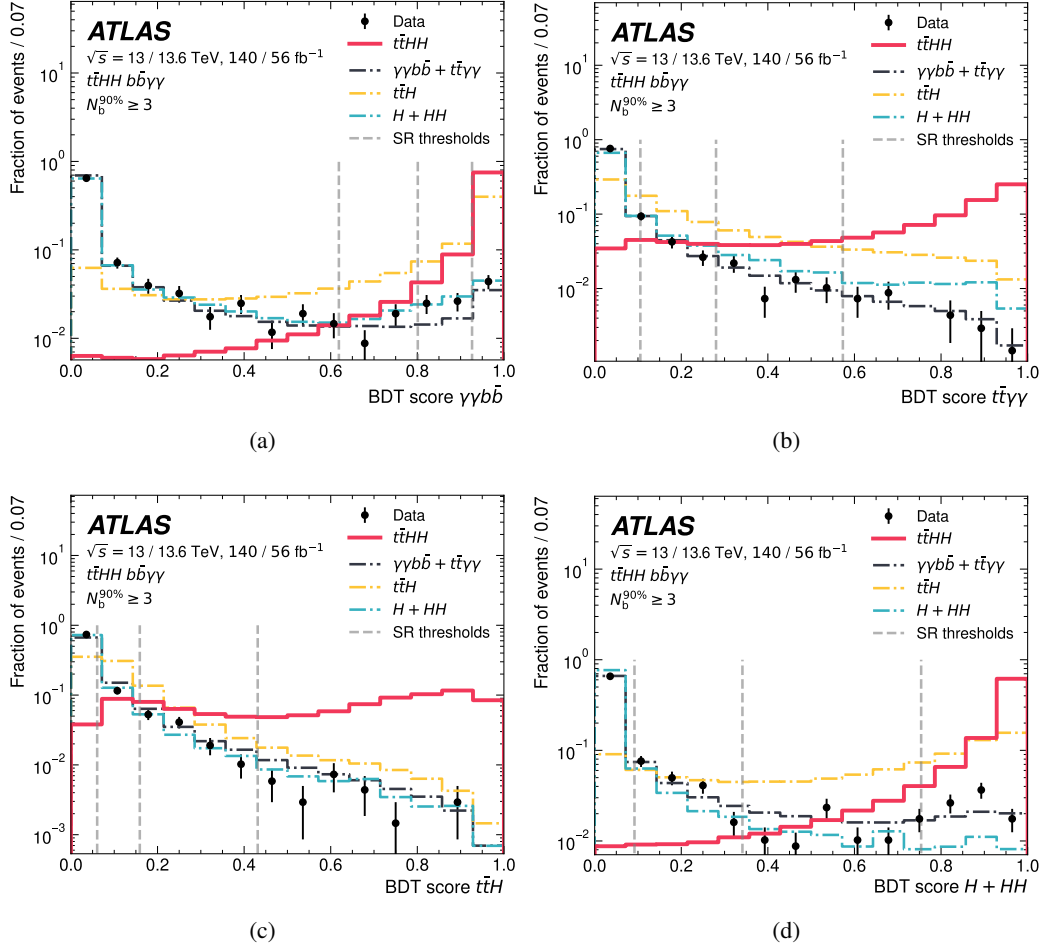


Figure 2: BDT score distributions obtained from the combined Run 2 and Run 3 data samples, used to discriminate the $t\bar{t}HH$ signal from the main background processes: (a) $\gamma\gamma b\bar{b}$, (b) $t\bar{t}\gamma\gamma$, (c) $t\bar{t}H$, and (d) single Higgs boson and di-Higgs boson production. All histograms are normalised to unity. Vertical dashed lines indicate the BDT score thresholds used to define the signal regions, whose boundaries are determined simultaneously across the four BDT scores.

Furthermore, a separate uncertainty is applied in simulation to account for differences in detector response between b -jets, light-quark jets and gluon jets.

Uncertainties in the reconstruction, identification, isolation and trigger efficiencies of electrons, photons, and muons are also considered, along with uncertainties in their energy scale and resolution [83, 88]. The latter uncertainties for jets and leptons are propagated to the calculation of E_T^{miss} , which also incorporates contributions from the modelling of the underlying event and the reconstruction efficiency of tracks used to compute the soft term [110].

The uncertainty in the integrated luminosity is 0.83% [31] for the Run 2 data sample, and 2.0% [32, 33] for the Run 3 data sample. These values are derived using the LUCID-2 detector [111], supplemented by measurements from the inner detector and calorimeters. An additional uncertainty is considered for corrections applied to the pile-up profile in simulated samples.

7.2 Theoretical uncertainties

Uncertainties in the modelling of signal and background processes arise from several sources: the PDFs, α_s , missing higher-order QCD corrections in the partonic MEs, and initial- and final-state radiation (ISR and FSR). PDF uncertainties are evaluated following the PDF4LHC recommendations [72], while α_s uncertainties are estimated by varying its value within the current measurement range. Uncertainties due to missing high-order corrections are assessed by varying the renormalisation and factorisation scales relative to their central values. Generator-related uncertainties are determined by comparing nominal predictions with those obtained using alternative generators or parton shower models, as specified in Table 1. ISR and FSR uncertainties are evaluated by varying the renormalisation scales in the parton shower, as well as the renormalisation and factorisation scales in the MEs.

7.3 1L specific uncertainties

Modelling uncertainties for $t\bar{t}$ +jets are evaluated by comparing the nominal POWHEG+PYTHIA 8 (5FS) sample with four alternative samples: POWHEG+PYTHIA 8 configurations with $pT_{\text{hard}}=1$ and with $h_{\text{damp}} = 3m_t$, a POWHEG+HERWIG 7 sample, and a POWHEGBOXRES +HERWIG7 (4FS) sample. Each alternative generator and each $t\bar{t}$ +jets component ($t\bar{t} + c/l$, $t\bar{t} + 1b$, $t\bar{t} + 2b$, $t\bar{t} + 3b$, and $t\bar{t} + \geq 4b$) is treated independently. The normalisations of the $t\bar{t} + 1b$ and $t\bar{t} + 2b$ components are constrained in data through two independent free NFs. For these two, the alternative samples are normalised to the nominal phase space, so that the uncertainties account for shape and acceptance effects, separated from overall normalisation variations. For the $t\bar{t} + 3b$, $t\bar{t} + \geq 4b$, and the subdominant $t\bar{t} + c/l$ components, additional normalisation uncertainties of 40%, 50%, and 6%, respectively, are assigned. These values are derived, for each component, from the sum in quadrature of the relative differences between the nominal prediction and all alternative samples. In this case, the alternative samples are not normalised to the nominal phase space. The resulting uncertainty includes their intrinsic normalisation differences and therefore includes normalisation, shape, and acceptance effects.

7.4 SSML specific uncertainties

For the SSML channel, a conservative uncertainty is assigned to the $t\bar{t}t\bar{t}$ production. The ATLAS Collaboration has previously measured the $t\bar{t}t\bar{t}$ cross-section to be about two standard deviations above the SM prediction [97]. To account for both the 15% theoretical uncertainty [69] and the discrepancy with the ATLAS measurement, normalisation uncertainties of $^{+70\%}_{-15\%}$ are applied, similar to the approach taken in Ref. [112]. These uncertainties are also applied to the minor $t\bar{t}t\bar{t}$ background in the 1L channel.

Uncertainties in the fake/non-prompt lepton and QmisID background contributions are evaluated following the methodology outlined in Ref. [97]. For the fake/non-prompt lepton background, only shape uncertainties in the distributions used in the template fit are considered, as their normalisations are free parameters in the fit. These uncertainties are estimated by comparing data with the background predictions in regions kinematically similar to the control regions. For the heavy-flavour non-prompt background, a loose lepton selection is employed, while for the conversion background, comparisons are made using $\mu\mu\gamma^{(*)}$ events in the 3L sub-channel.

Additional systematic uncertainties associated with the ECID are also included. As discussed in Section 5.2, the photon-conversion backgrounds for Run 3 are estimated by using the NFs derived from Run 2 data.

Extra systematic uncertainties are applied to account for differences in event yields between the Run 3 and the Run 2 extrapolations without the ECID tool.

7.5 $b\bar{b}\gamma\gamma$ specific uncertainties

The dominant uncertainty in the continuum $\gamma\gamma$ +jets background arises from the choice of analytic function for its modelling. This background modelling uncertainty is evaluated using the *spurious signal* method that quantifies the fitted signal yield obtained when a signal-plus-background fit is applied to background-only templates [103]. In all categories, the resulting bias is treated as a systematic uncertainty in the signal yield.

For resonant processes, a conservative 100% uncertainty is assigned to single and di-Higgs boson processes to account for modelling limitations in heavy-flavour–jet-associated production. An exception is made for $t\bar{t}H$ production with additional heavy-flavour jets, for which a 50% normalisation uncertainty is assigned, derived from the measurement in Ref. [98, 99].

8 Statistical analysis and results

To assess the compatibility of the observed data with background expectations and to search for the presence of a $t\bar{t}HH$ signal, simultaneous maximum-likelihood fits are performed across the SRs and CRs. In the 1L and SSML channels, binned likelihood fits to data are performed using the transformer discriminant in the SRs and the fit variables listed in Tables 2 and 3 for the CRs. For the $b\bar{b}\gamma\gamma$ channel, an unbinned maximum-likelihood fit is performed to the diphoton invariant mass $m_{\gamma\gamma}$ in each of the three BDT-defined SRs.

The parameter-of-interest (POI) in the fit is the signal strength, $\mu_{t\bar{t}HH}$, defined as the ratio of the observed $t\bar{t}HH$ signal cross-section to the SM expectation. The fit also includes normalisation parameters, which constrain background contributions using data from CRs in the 1L and SSML channels, and background parameters for the $b\bar{b}\gamma\gamma$ channel. Systematic uncertainties are incorporated via nuisance parameters (NPs).

Likelihood functions are constructed separately for each SR and CR. In the 1L and SSML channels, the likelihood is built from binned Poisson probabilities of the corresponding fitting variable. In the $b\bar{b}\gamma\gamma$ channel, the likelihood is unbinned and defined as the product of per-event probability densities evaluated at the observed $m_{\gamma\gamma}$. Gaussian or log-normal constraints are applied to the NPs in both cases. These individual likelihoods are then aggregated across all regions to form the final likelihood function, which is subsequently maximised in the fit.

For the 1L and SSML channels, the final likelihood function is:

$$\mathcal{L}(\mu_{t\bar{t}HH}, \vec{\kappa}, \vec{\theta}) = \prod_{\text{Regions}} \left[\prod_i^{N_{\text{bins}}} \text{Pois}(n_i | \nu_i(\mu_{t\bar{t}HH}, \vec{\kappa}, \vec{\theta})) \right] \cdot G(\vec{\theta}).$$

where $\text{Pois}(n_i | \nu_i(\mu_{t\bar{t}HH}, \vec{\kappa}, \vec{\theta}))$ represents the Poisson probability for bin i , with n_i and $\nu_i(\mu_{t\bar{t}HH}, \vec{\kappa}, \vec{\theta})$ representing the observed and expected event counts, respectively. The variables $\vec{\kappa}$ and $\vec{\theta}$ correspond to

NFs and NPs. The expected count in each bin is given by

$$\nu_i(\mu_{t\bar{t}HH}, \vec{\kappa}, \vec{\theta}) = \mu_{t\bar{t}HH} S_i(\vec{\theta}) + B_i(\vec{\kappa}, \vec{\theta}). \quad (1)$$

where S_i is the expected signal yield from the SM, and B_i is the estimated background contribution. The function $G(\vec{\theta})$ encodes the prior constraints on the NPs.

For $b\bar{b}\gamma\gamma$, the final likelihood function has the form:

$$\mathcal{L}(\mu_{t\bar{t}HH}, \vec{\kappa}, \vec{\theta}) = \prod_r \left[\text{Pois}(n_r | \nu_r(\mu_{t\bar{t}HH}, \vec{\kappa}, \vec{\theta})) \times \prod_i^{n_r} f_r(m_{\gamma\gamma}^i, \vec{\kappa}, \vec{\theta}) \right] \cdot G(\vec{\theta}).$$

Here n_r and ν_r are the observed and expected event counts in region r , respectively. The function $f_r(m_{\gamma\gamma}^i, \vec{\kappa}, \vec{\theta})$ represents the probability density for the diphoton mass of event i in the region r , summing over both signal and background contributions, analogous to Eq. 1. The vector $\vec{\kappa}$ parameterises the background model and $G(\vec{\theta})$ represents the NP constraints as described above.

For the 1L and SSML channels, the Run 2 and Run 3 data samples are first fitted independently and then combined. In contrast, the $b\bar{b}\gamma\gamma$ channel employs a single fit to the two data samples, motivated by the limited numbers of events and the similarity of their kinematic distributions. Experimental systematic uncertainties are assumed to be correlated across channels within the same run period, but uncorrelated between run periods except for most of the jet-related uncertainties, which are treated as correlated. Theoretical uncertainties in the process cross-sections are considered correlated across both run periods and all channels, while other modelling uncertainties are uncorrelated across run periods to account for differences in the MC generator configurations used in the two runs. The NFs for the $t\bar{t} + 1b$, $t\bar{t} + 2b$, and $t\bar{t}W$ processes, introduced to account for differences between data and theoretical predictions, are treated as correlated between the run periods, while all other NFs, related to instrumental backgrounds in the SSML channel, are kept uncorrelated.

The fits are performed under the signal-plus-background hypothesis. Good agreement is observed between the data and background expectations across all fit variables, for all channels and data-taking periods. Figures 3 and 4 show the post-fit background composition in the 1L and SSML CRs, respectively, for the combined Run 2 and Run 3 data samples. In the 1L channel, the post-fit NFs for the $t\bar{t} + 1b$ and $t\bar{t} + 2b$ processes are 1.2 ± 0.4 and 0.91 ± 0.11 , respectively, while in the SSML channel the $t\bar{t}W$ NF is 1.04 ± 0.20 . These NFs are consistent within uncertainties between Run 2 and Run 3.

The corresponding post-fit discriminant distributions are shown in Figure 5 for the 1L channel and in Figure 6 for the SSML channel, presented separately for the Run 2 and Run 3 data samples. Figure 7 shows the post-fit diphoton invariant mass distribution for the $b\bar{b}\gamma\gamma$ channel, combining the Run 2 and Run 3 data samples. The measured signal-strength values are all compatible with the SM prediction of unity, $\mu_{t\bar{t}HH}^{1L} = -5_{-15}^{+15}$ from 1L, $\mu_{t\bar{t}HH}^{SSML} = 5_{-21}^{+17}$ from SSML, and $\mu_{t\bar{t}HH}^{b\bar{b}\gamma\gamma} = -13_{-6}^{+35}$ from $b\bar{b}\gamma\gamma$. The asymmetry in the measured signal-strength uncertainty in the $b\bar{b}\gamma\gamma$ channel arises from the physical constraint that the total expected event yield must remain non-negative. Combining three channels yields a best-fit signal-strength value of $\mu_{t\bar{t}HH} = -3_{-12}^{+11}$. Distributions of some representative kinematic variables in the signal regions are shown in Figure 8 for 1L and in Figure 9 for SSML, again demonstrating good agreement between the observed data and the post-fit background predictions.

Upper limits on the signal strength at the 95% CL are derived using the modified frequentist method [113], commonly referred to as the CL_s method, and employing the \tilde{q}_μ test statistic in the asymptotic approximation [114]. The observed (expected) 95% CL upper limits on the signal strength are 26 (29), 40 (38), and

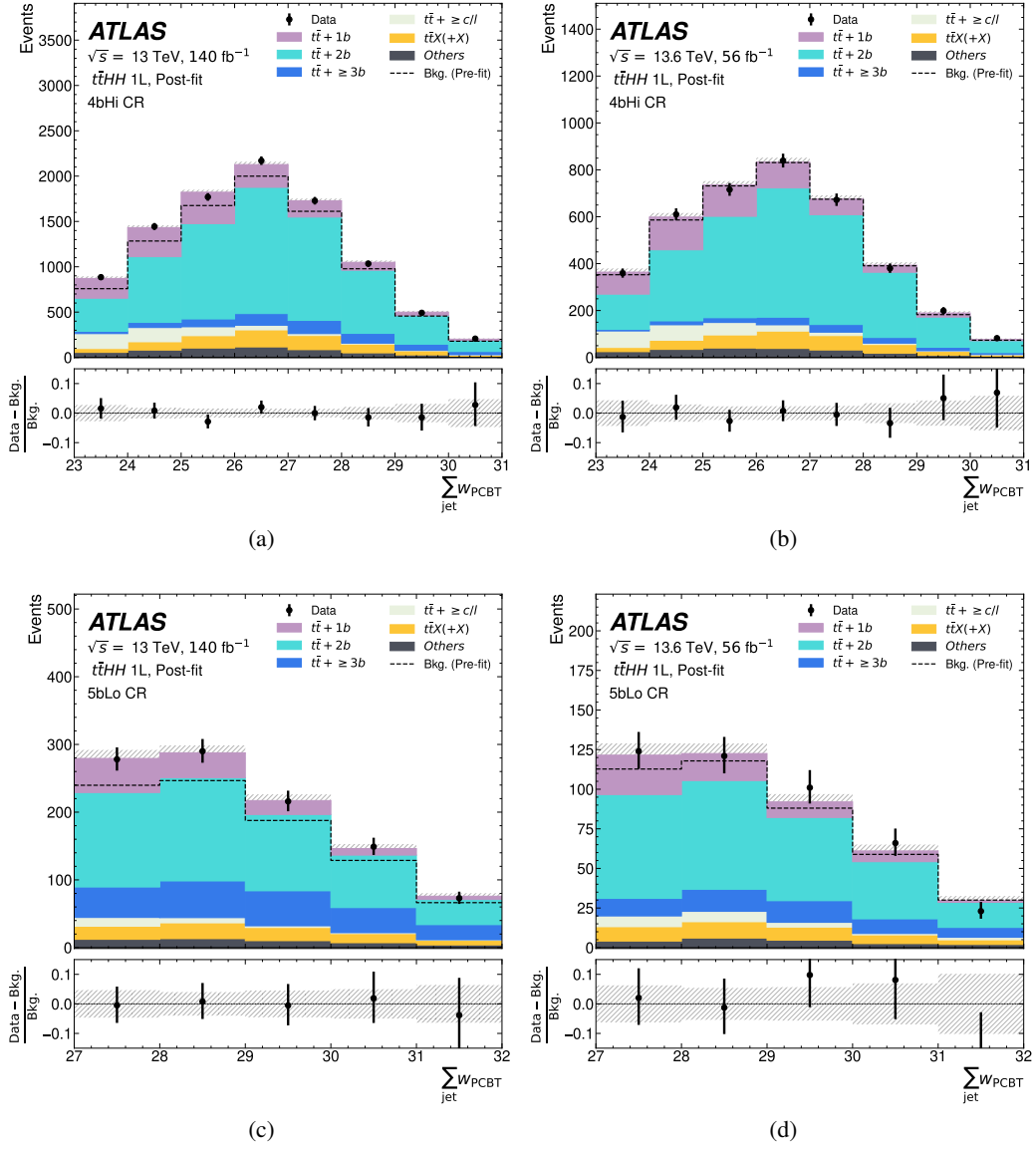


Figure 3: Distributions of the sum of jet pseudo-continuous b -tagging scores in the $4b_{\text{Hi}}$ and $5b_{\text{Lo}}$ control regions of the 1L channel for the (a, c) Run 2 and (b, d) Run 3 data samples, comparing the data with the post-fit background predictions. The lower panels display the relative differences between the data and the background predictions. The hatched bands indicate the combined statistical and systematic uncertainties in the background predictions. For reference, the pre-fit background predictions are overlaid as dashed histograms.

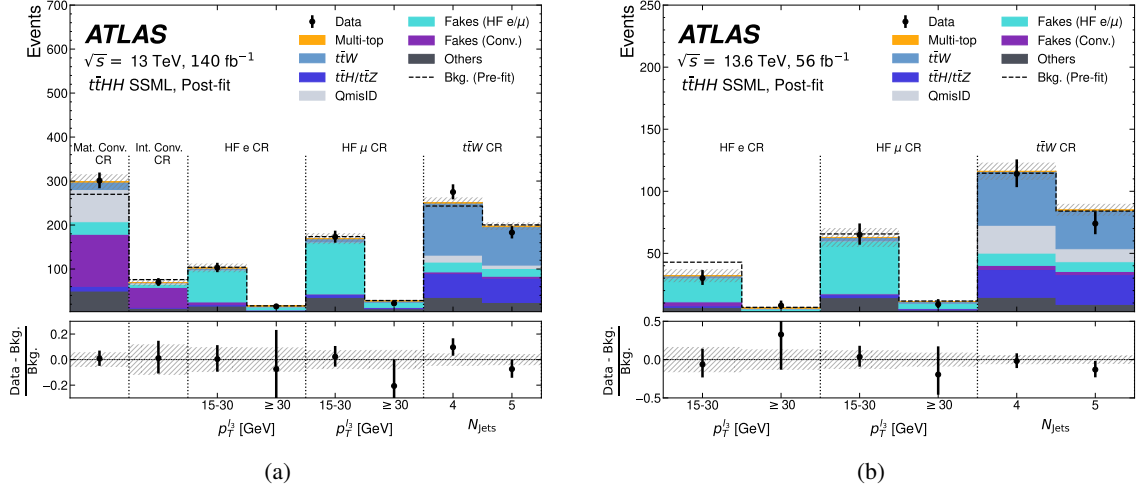


Figure 4: Distributions of the fit variables of the SSML control regions, using the same binning as in the fit, for the (a) Run 2 and (b) Run 3 data samples, comparing the data with the post-fit background predictions. The lower panels display the relative differences between the data and the background predictions. The hatched bands indicate the combined statistical and systematic uncertainties in the background predictions. For reference, the pre-fit background predictions are overlaid as dashed histograms.

75 (79) for the 1L, SSML, and $b\bar{b}\gamma\gamma$ channels, respectively. In all cases, the expected limits are computed under the background-only hypothesis ($\mu_{t\bar{t}HH} = 0$). Combining the three channels results in an observed upper limit of 20 at 95% CL, compared with an expected limit of 21. Figure 10 shows the observed and expected limits for the individual 1L, SSML, and $b\bar{b}\gamma\gamma$ channels, as well as their combination. For the 1L and SSML channels, the results from the Run 2 and Run 3 data samples are compatible within uncertainties, with the Run 2 data sample providing more stringent limits due to its larger integrated luminosity.

Table 4 summarises the breakdown of contributions to the observed and expected uncertainties, $\Delta\mu_{t\bar{t}HH}$, in the signal strength of the combined 1L, SSML, and $b\bar{b}\gamma\gamma$ analysis from different groups of uncertainty sources. These breakdowns are derived by performing conditional profile-likelihood fits in which all NPs associated with a given uncertainty group are fixed to their best-fit values, while all remaining parameters are profiled. The uncertainty attributed to each group is then defined as the difference in quadrature between the total post-fit uncertainty and the uncertainty from the corresponding conditional fit. The expected breakdowns are evaluated assuming $\mu_{t\bar{t}HH} = 1$, and correlations among different groups are neglected. The systematic uncertainties are categorised into signal modelling, background modelling, number of MC events and detector systematic uncertainties, with the background-modelling contribution further decomposed by background source. The uncertainties from the floating NFs, which are limited by the available number of data events, are included in the data statistical uncertainty category. Data statistical and systematic uncertainties contribute comparably to the total uncertainty, while background modelling dominates the systematic uncertainty.

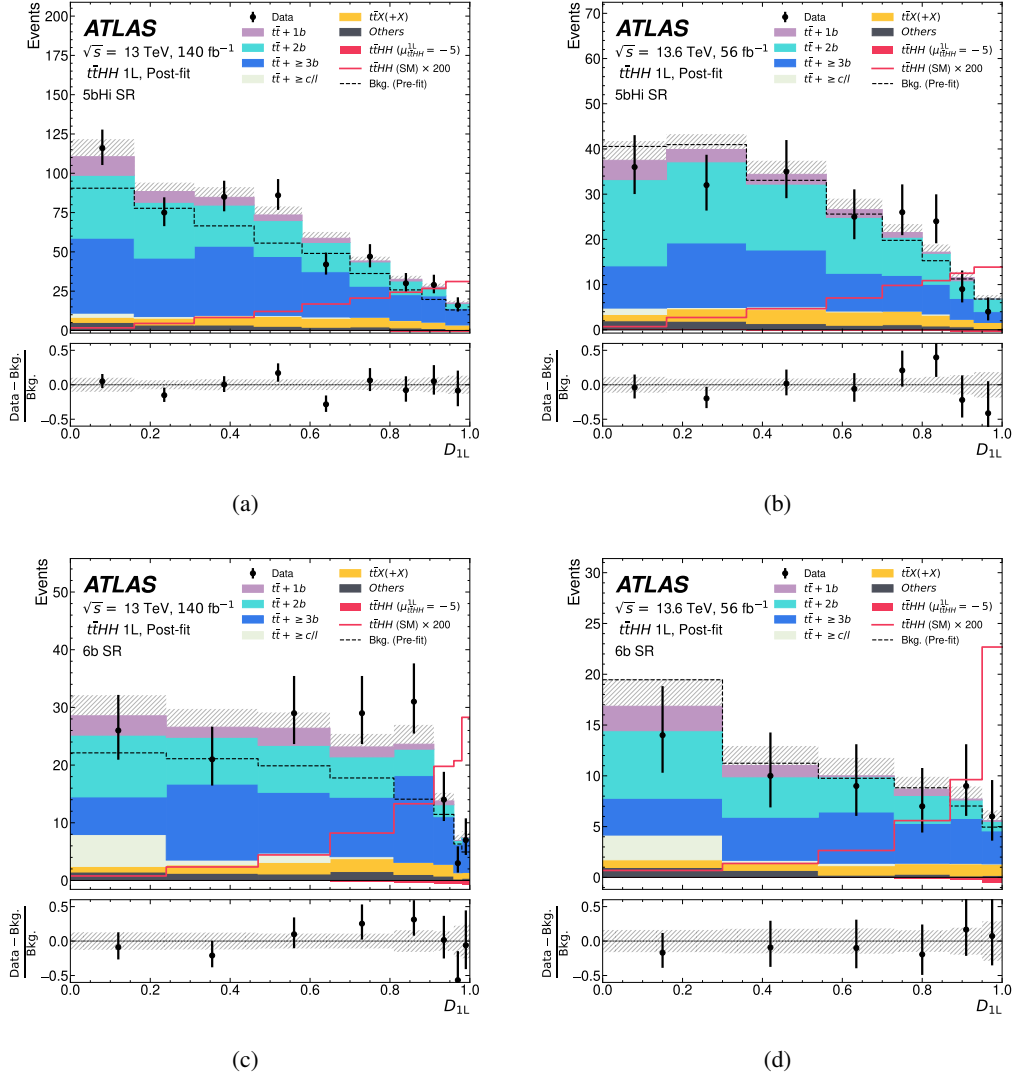


Figure 5: Distributions of the D_{1L} discriminant in the $5b_{Hi}$ and $6b$ signal regions of the 1L channel for the (a, c) Run 2 and (b, d) Run 3 data samples, comparing the data with the post-fit signal-plus-background predictions. The observed $t\bar{t}HH$ signal in this channel, corresponding to a measured signal strength of $\mu_{t\bar{t}HH}^{1L} = -5_{-15}^{+15}$, is displayed as a negatively stacked contribution. The lower panels display the relative differences between the data and the background predictions. The hatched bands indicate the combined statistical and systematic uncertainties in the background predictions. For reference, the pre-fit background predictions are overlaid as dashed lines, and the SM $t\bar{t}HH$ signal distribution – scaled up by a factor of 200 – are shown as solid lines.

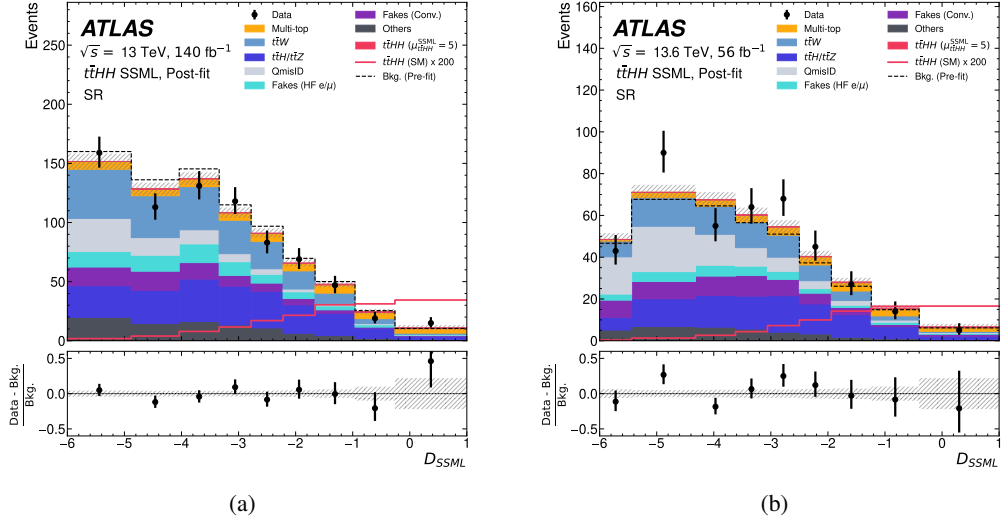


Figure 6: Distributions of the D_{SSML} discriminant in the SSML signal regions for the (a) Run 2 and (b) Run 3 data samples, comparing the data with the post-fit signal-plus-background predictions. The observed $t\bar{t}HH$ signal in this channel, corresponding to a measured signal strength of $\mu_{t\bar{t}HH}^{SSML} = 5^{+17}_{-21}$, is displayed stacked on top of the backgrounds. The first and last bins include contributions from underflow and overflow, respectively. The lower panels display the relative differences between the data and the background predictions. The hatched bands indicate the combined statistical and systematic uncertainties in the background predictions. For reference, the pre-fit background predictions are overlaid as dashed lines, and the SM $t\bar{t}HH$ signal distribution – scaled up by a factor of 200 – are shown as solid lines.

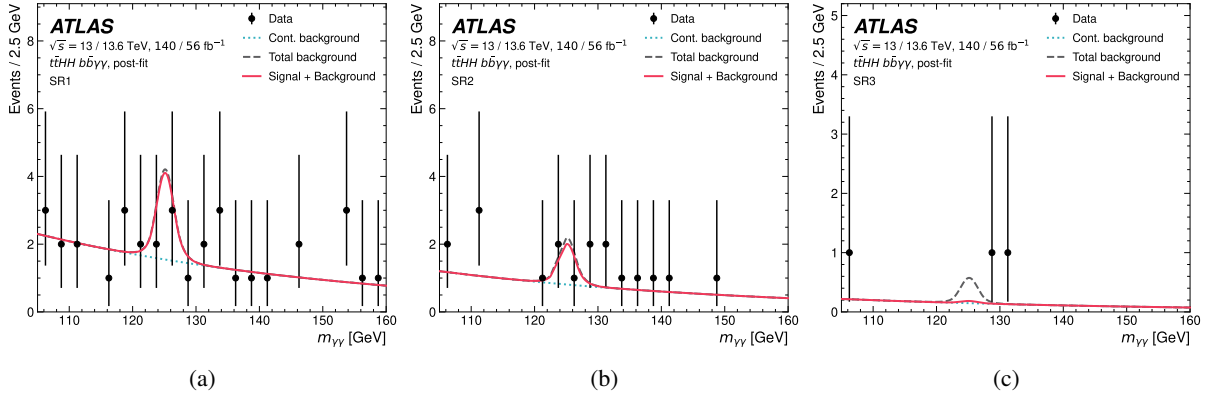


Figure 7: Comparison of the $m_{\gamma\gamma}$ distributions between the observed data and the signal-plus-background fitted estimate (solid) for the $b\bar{b}\gamma\gamma$ channel in the three signal regions: (a) SR1, (b) SR2 and (c) SR3, where SR1 is the least sensitive and SR3 the most sensitive. The continuous background (dotted) and the total background (dashed) are also shown. The observed $t\bar{t}HH$ signal strength in this channel is $\mu_{t\bar{t}HH}^{b\bar{b}\gamma\gamma} = -13^{+35}_{-6}$.

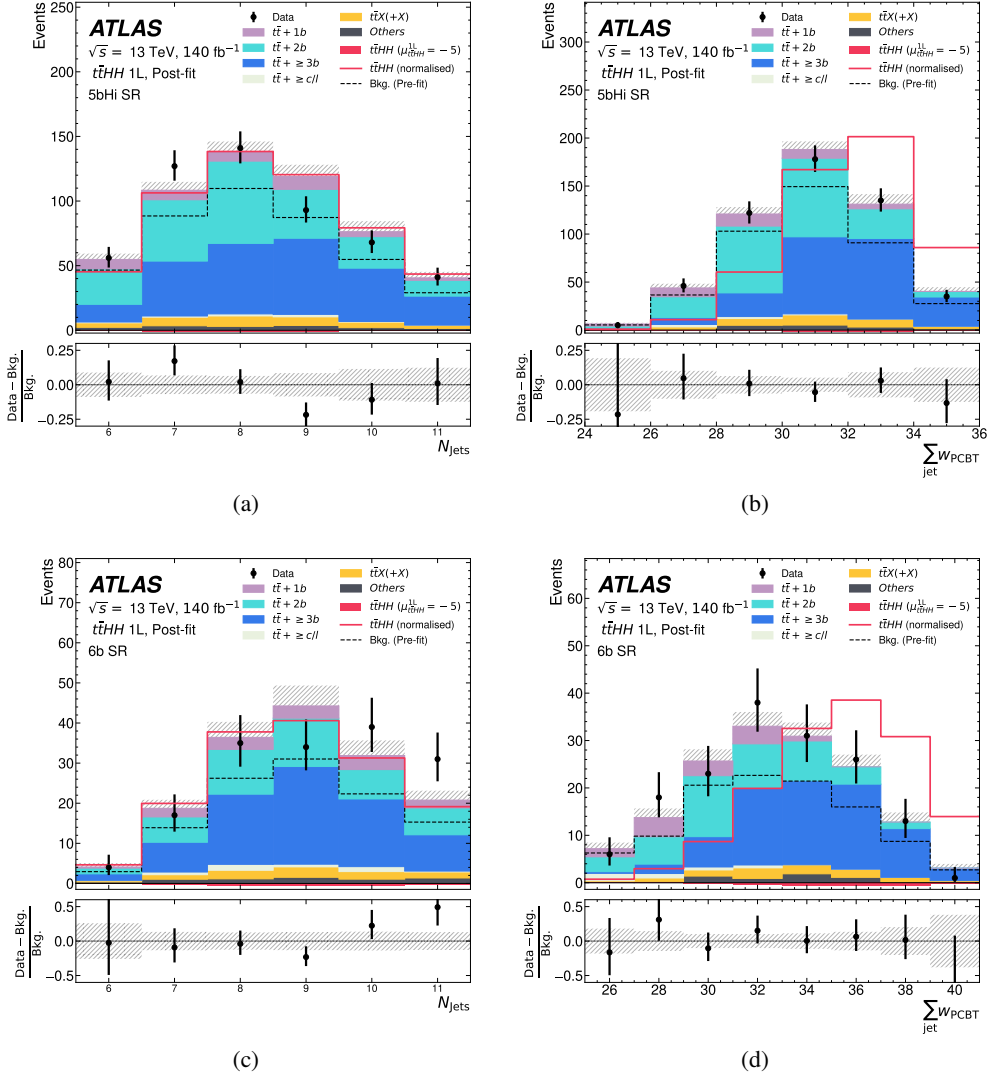


Figure 8: Distributions of the (a, c) jet multiplicity and (b, d) sum of pseudo-continuous b -tagging scores in the (a, b) $5b_{\text{Hi}}$ and (c, d) $6b$ signal regions of the 1L channel for the Run 2 data sample, comparing the data with the post-fit signal-plus-background predictions. The fitted $t\bar{t}HH$ signal in this channel, $\mu_{t\bar{t}HH}^{1L} = -5_{-15}^{+15}$, is shown as a negatively stacked contribution. The lower panels display the relative differences between the data and the background predictions. The hatched bands indicate the combined statistical and systematic uncertainties in the background predictions. For reference, the pre-fit backgrounds are overlaid as dashed lines, and the SM $t\bar{t}HH$ signal distributions – normalised to the total background yield – are shown as solid lines.

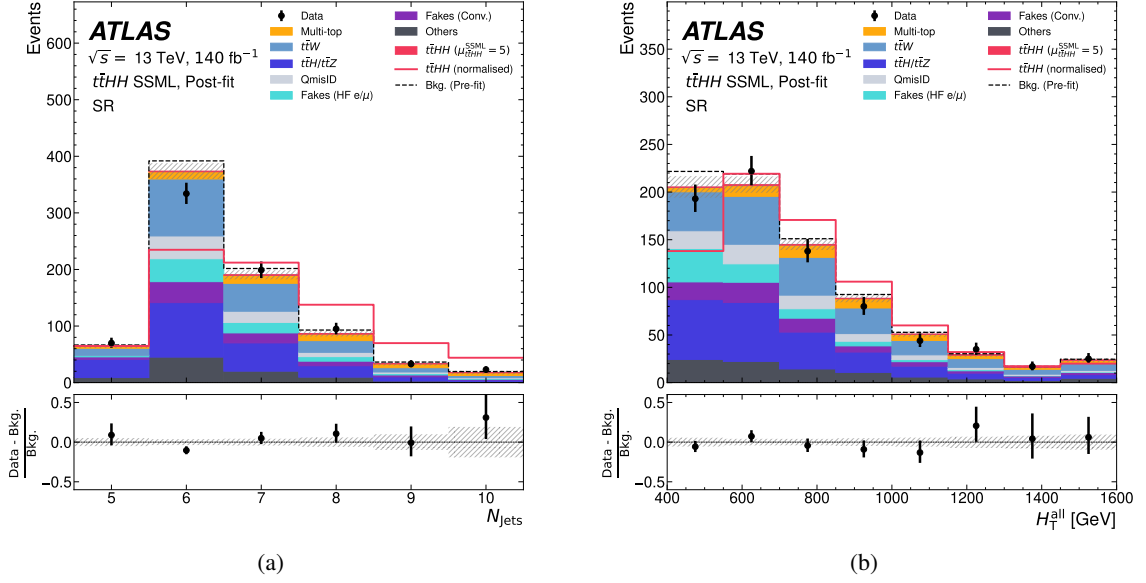


Figure 9: Distributions of the (a) jet multiplicity and (b) H_T^{all} in the SSML signal region for the Run 2 data sample, comparing the data with the post-fit signal-plus-background predictions. The fitted $t\bar{t}HH$ signal in this channel, $\mu_{t\bar{t}HH}^{\text{SSML}} = 5_{-21}^{+17}$, is shown stacked on top of the backgrounds. The first and last bins include contributions from underflow and overflow, respectively. The lower panels display the relative differences between the data and the background predictions. The hatched bands indicate the combined statistical and systematic uncertainties in the background predictions. For reference, the pre-fit backgrounds are overlaid as dashed lines, and the SM $t\bar{t}HH$ signal distributions – normalised to the total background yield – are shown as solid lines.

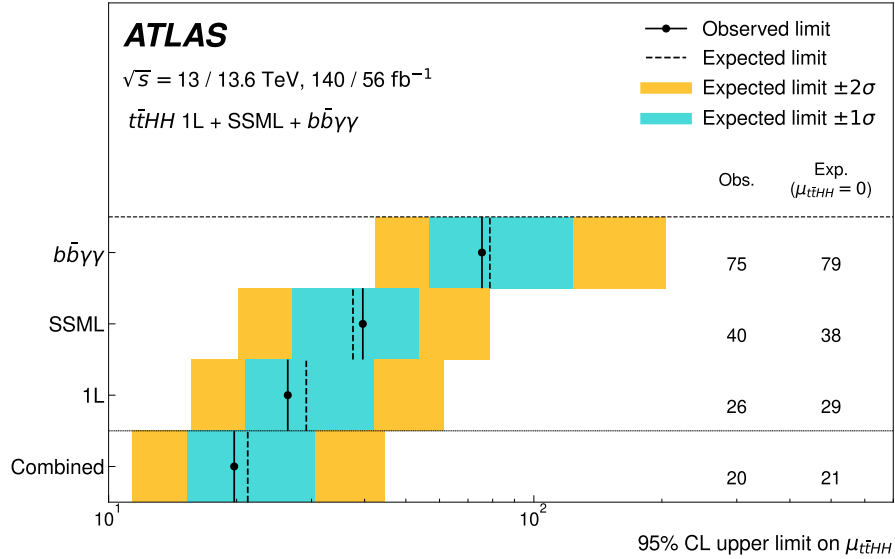


Figure 10: Observed and expected 95% CL upper limits on the signal strength from the individual 1L, SSML, and $b\bar{b}\gamma\gamma$ channels, and from their combination. The expected limits are derived under the background-only hypothesis, i.e. assuming $\mu_{t\bar{t}HH} = 0$.

Table 4: Breakdowns of the contributions to the observed and expected uncertainties, $\Delta\mu_{t\bar{t}HH}$, in the signal strength of the combined 1L, SSML, and $b\bar{b}\gamma\gamma$ analysis for different groups of uncertainty sources, neglecting correlations among groups.

Uncertainty Source	Observed	Expected
Signal modelling	(+0.9, -1.8)	(+1.3, -1.0)
Background modelling	(+6.8, -8.2)	(+5.7, -6.2)
$t\bar{t}$ + jets	(+5.3, -6.5)	(+4.7, -5.0)
$t\bar{t}t\bar{t}$	(+4.6, -6.4)	(+2.9, -4.0)
$t\bar{t}H$	(+2.1, -1.6)	(+2.0, -1.9)
others	(+0.9, -0.7)	(+0.9, -0.8)
MC statistical	(+2.8, -3.7)	(+2.5, -2.7)
Detector systematic	(+2.2, -3.4)	(+1.9, -1.5)
Total systematic	(+8.3, -9.4)	(+7.3, -7.4)
Data statistical	(+7.2, -6.8)	(+7.2, -6.7)
Total	(+11.0, -11.6)	(+10.3, -10.0)

9 Higgs effective field theory interpretation

Beyond-the-SM (BSM) self-interactions of the Higgs boson, or its non-standard interactions with other gauge fields and fermions, could lead to modifications to the $t\bar{t}HH$ event rate as well as affect the kinematic properties of the signal events. The results obtained with the two most sensitive channels of this analysis, i.e. the 1L and SSML channels, are thus interpreted in the context of the HEFT formalism, with a focus on anomalous interactions between Higgs boson pairs and top quark pairs.

Similarly to the SM effective field theory (SMEFT) [115, 116], HEFT assumes the SM field content. However, unlike in SMEFT, where the Higgs boson is part of an SU(2) doublet alongside unphysical Goldstone bosons, in HEFT the Higgs boson is a gauge singlet. This allows the Higgs boson dynamics to be decoupled from the symmetry-breaking pattern [117]. Consequently, HEFT enables more general deviations in Higgs boson couplings, which must be independently constrained through precision measurements, and features a more intricate power counting compared to SMEFT [118–120]. The HEFT approach employed in this study is implemented in a model specifically developed for this purpose and is interfaced through MADGRAPH [51] using the FeynRules UFO model format [121, 122].

State-of-the-art constraints on $c_{t\bar{t}HH}$ have been derived from the ggF HH channel by both the ATLAS [8] and CMS [9] collaborations, ($-0.19 < c_{t\bar{t}HH} < 0.7$ and $-0.28 < c_{t\bar{t}HH} < 0.59$, respectively), which remains the most sensitive channel to date for $c_{t\bar{t}HH}$. However, assuming a weakly interacting ultraviolet completion [123], ggF is parameterised by two additional Higgs–gluon couplings, c_{ggH} and c_{ggHH} , in comparison with $t\bar{t}HH$ where these enter at higher loop order. As a result, obtaining robust bounds from ggF is more challenging unless further assumptions are imposed. The quoted limits are obtained by setting all other couplings of the Higgs boson to their SM values. Relaxing this assumption requires a multidimensional fit, weakening the obtained constraints. The work presented here aims to provide a complementary constraint on $c_{t\bar{t}HH}$ independent of the ggF HH channel. The underlying assumption of the analysis, that only $c_{t\bar{t}HH}$ differs from its SM value, is consistent with those used to derive the values for the ggF HH channel. In this context, only cross-section effects are considered, while acceptance and

kinematic shape variations are not explicitly parameterised. Acceptance effects are evaluated for values of $c_{i\bar{i}HH}$ close to the exclusion limits and are covered by an additional 30% uncertainty in the signal yield included in the measurement. An estimate of the kinematic-shape effects is found to impact the 95% CL interval on $c_{i\bar{i}HH}$ by at most 10%, which is not included in the quoted limits.

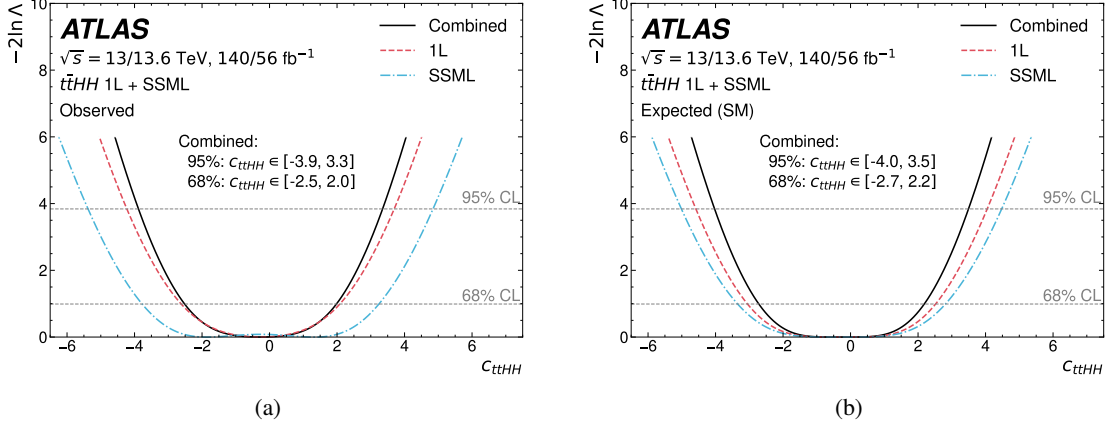


Figure 11: (a) Observed and (b) expected values of the profile likelihood as a function of $c_{i\bar{i}HH}$ for the 1L channel (dashed curve), the SSML channel (dot-dashed curve), and their combination (solid curve).

The constraints on $c_{i\bar{i}HH}$ are extracted from the same phase space as the rest of the analysis using the same multivariate discriminant described in Section 6 and in the same analysis regions. The results are presented in Figure 11. The $c_{i\bar{i}HH}$ is constrained, at the 95% CL, in the range of $-3.9 < c_{i\bar{i}HH} < 3.3$ for the observed results, while the expected range is $-4.0 < c_{i\bar{i}HH} < 3.5$. The expected profile exhibits a double-minimum structure due to the quadratic dependence of the signal cross-section on $c_{i\bar{i}HH}$. Given the observed results, the two minima are nearly degenerate, resulting in an almost flat region in the likelihood scan.

Benefiting from the quadratic dependence of the cross-section on $c_{i\bar{i}HH}$, the bounds derived in this analysis are only about one order of magnitude weaker than those obtained in the ggF HH channel in Ref. [8], even though the predicted cross-section for $i\bar{i}HH$ production is smaller by a factor of about 40.

10 Conclusion

The non-resonant production of Higgs boson pairs in association with top-quark pairs, $i\bar{i}HH$, is predicted to be a rare process in the SM. This paper describes the first search for this process using the full Run 2 data sample, corresponding to 140 fb^{-1} of pp collisions at $\sqrt{s} = 13 \text{ TeV}$ collected between 2015 and 2018, and a Run 3 data sample of 56 fb^{-1} at $\sqrt{s} = 13.6 \text{ TeV}$ collected between 2022 and 2023, recorded with the ATLAS detector at the LHC.

The presented $i\bar{i}HH$ search targets the 1L, SSML, and $b\bar{b}\gamma\gamma$ final states. The background contributions are estimated through a combination of simulation and data-driven techniques. Machine-learning-based discriminants are employed to improve separation between signal and background.

No significant excess above the background expectation is observed in any channel. A simultaneous fit across all the channels and analysis regions yields a measured signal-strength value of $\mu_{i\bar{i}HH} = -3_{-12}^{+11}$,

consistent with the SM prediction, and results in an observed upper limit of $\mu_{t\bar{t}HH} < 20$ at 95% CL. The results are further interpreted within the Higgs effective field theory framework, leading to a 95% CL interval on the $t\bar{t}HH$ quartic interaction parameter of $-3.9 < c_{t\bar{t}HH} < 3.3$.

Acknowledgements

We thank CERN for the very successful operation of the LHC and its injectors, as well as the support staff at CERN and at our institutions worldwide without whom ATLAS could not be operated efficiently.

The crucial computing support from all WLCG partners is acknowledged gratefully, in particular from CERN, the ATLAS Tier-1 facilities at TRIUMF/SFU (Canada), NDGF (Denmark, Norway, Sweden), CC-IN2P3 (France), KIT/GridKA (Germany), INFN-CNAF (Italy), NL-T1 (Netherlands), PIC (Spain), RAL (UK) and BNL (USA), the Tier-2 facilities worldwide and large non-WLCG resource providers. Major contributors of computing resources are listed in Ref. [124].

We gratefully acknowledge the support of ANPCyT, Argentina; YerPhI, Armenia; ARC, Australia; BMWFW and FWF, Austria; ANAS, Azerbaijan; CNPq and FAPESP, Brazil; NSERC, NRC and CFI, Canada; CERN; ANID, Chile; CAS, MOST and NSFC, China; Minciencias, Colombia; MEYS CR, Czech Republic; DNRF and DNSRC, Denmark; IN2P3-CNRS and CEA-DRF/IRFU, France; SRNSFG, Georgia; BMFTR, HGF and MPG, Germany; GSRI, Greece; RGC and Hong Kong SAR, China; ICHEP and Academy of Sciences and Humanities, Israel; INFN, Italy; MEXT and JSPS, Japan; CNRST, Morocco; NWO, Netherlands; RCN, Norway; MNiSW, Poland; FCT, Portugal; MNE/IFA, Romania; MSTDI, Serbia; MSSR, Slovakia; ARIS and MVZI, Slovenia; DSI/NRF, South Africa; MICIU/AEI, Spain; SRC and Wallenberg Foundation, Sweden; SERI, SNSF and Cantons of Bern and Geneva, Switzerland; NSTC, Taipei; TENMAK, Türkiye; STFC/UKRI, United Kingdom; DOE and NSF, United States of America.

Individual groups and members have received support from BCKDF, CANARIE, CRC and DRAC, Canada; CERN-CZ, FORTE and PRIMUS, Czech Republic; COST, ERC, ERDF, Horizon 2020 and Marie Skłodowska-Curie Actions, European Union; Investissements d’Avenir Labex, Investissements d’Avenir Idex and ANR, France; DFG and AvH Foundation, Germany; Herakleitos, Thales and Aristeia programmes co-financed by EU-ESF and the Greek NSRF, Greece; BSF-NSF and MINERVA, Israel; NCN and NAWA, Poland; La Caixa Banking Foundation, CERCA and AGAUR programs from Generalitat de Catalunya and PROMETEO and GenT Programmes Generalitat Valenciana, Spain; Göran Gustafssons Stiftelse, Sweden; The Royal Society and Leverhulme Trust, United Kingdom; Eric and Wendy Schmidt Fund for Strategic Innovation, United States of America.

In addition, individual members wish to acknowledge support from Chile: Agencia Nacional de Investigación y Desarrollo (ANID FONDECYT reg. 1230987, FONDECYT 1230812, FONDECYT 1240864, Fondecyt 3240661, Fondecyt Regular 1240721); China: Chinese Ministry of Science and Technology (MOST-2023YFA1605700, MOST-2023YFA1609300), National Natural Science Foundation of China (NSFC 12275265, NSFC-W2543005); Czech Republic: Czech Science Foundation (GACR - 24-11373S), Ministry of Education Youth and Sports (ERC-CZ-LL2327, FORTE CZ.02.01.01/00/22_008/0004632), PRIMUS Research Programme (PRIMUS/21/SCI/017); EU: H2020 European Research Council (ERC - 101002463); European Union: European Research Council (BARD No. 101116429, ERC - 948254, ERC 101089007), European Regional Development Fund (HE COFUND GA No.101081355, ERDF), Marie Skłodowska-Curie Actions (GAP-101168829); France: Agence Nationale de la Recherche (ANR-21-CE31-0013, ANR-22-EDIR-0002, ANR-24-CE31-0504-01); Germany: Deutsche Forschungsgemeinschaft (DFG

- 469666862); China: Research Grants Council (GRF); Italy: Ministero dell'Università e della Ricerca (NextGenEU 153D23001490006 M4C2.1.1, NextGenEU 153D23000820006 M4C2.1.1, NextGenEU 153D23001490006 M4C2.1.1, SOE2024_0000023); Japan: Japan Society for the Promotion of Science (JSPS KAKENHI JP25H0063, JSPS KAKENHI JP22H01227, JSPS KAKENHI JP22H04944, JSPS KAKENHI JP22KK0227, JSPS KAKENHI JP24K23939, JSPS KAKENHI JP24KK0251, JSPS KAKENHI JP25H00650, JSPS KAKENHI JP25H01291, JSPS KAKENHI JP25K01023); Norway: Research Council of Norway (RCN-314472); Poland: Polish National Science Centre (NCN 2021/42/E/ST2/00350, NCN OPUS 2023/51/B/ST2/02507, NCN OPUS nr 2022/47/B/ST2/03059, NCN UMO-2019/34/E/ST2/00393, UMO-2022/47/O/ST2/00148, UMO-2023/49/B/ST2/04085, UMO-2023/51/B/ST2/00920, UMO-2024/53/N/ST2/00869); Spain: Agència de Gestió d'Ajuts Universitaris i de Recerca. (AGAUR - 2023 BP 00141), Ministry of Science and Innovation (RYC2019-028510-I, RYC2020-030254-I, RYC2021-031273-I, RYC2022-038164-I), Ministerio de Ciencia, Innovación y Universidades/Agencia Estatal de Investigación (PID2022-142604OB-C22); Sweden: Carl Trygger Foundation (Carl Trygger Foundation CTS 22:2312), Swedish Research Council (Swedish Research Council 2023-04654, VR 2021-03651, VR 2022-03845, VR 2022-04683, VR 2023-03403, VR 2024-05451, VR 2025-05940), Knut and Alice Wallenberg Foundation (KAW 2023.0366); Switzerland: Swiss National Science Foundation (SNSF - PCEFP2_194658); United Kingdom: The Binks Trust, Royal Society (NIF-R1-231091); United States of America: U.S. Department of Energy (ECA DE-AC02-76SF00515), John Templeton Foundation (John Templeton Foundation 63206), Neubauer Family Foundation.

References

- [1] F. Englert and R. Brout, *Broken Symmetry and the Mass of Gauge Vector Mesons*, [*Phys. Rev. Lett.* **13** \(1964\) 321](#), ed. by J. C. Taylor.
- [2] P. W. Higgs, *Broken Symmetries and the Masses of Gauge Bosons*, [*Phys. Rev. Lett.* **13** \(1964\) 508](#), ed. by J. C. Taylor.
- [3] G. S. Guralnik, C. R. Hagen and T. W. B. Kibble, *Global Conservation Laws and Massless Particles*, [*Phys. Rev. Lett.* **13** \(1964\) 585](#), ed. by J. C. Taylor.
- [4] ATLAS Collaboration, *Observation of a new particle in the search for the Standard Model Higgs boson with the ATLAS detector at the LHC*, [*Phys. Lett. B* **716** \(2012\) 1](#), arXiv: [1207.7214 \[hep-ex\]](#).
- [5] CMS Collaboration, *Observation of a new boson at a mass of 125 GeV with the CMS experiment at the LHC*, [*Phys. Lett. B* **716** \(2012\) 30](#), arXiv: [1207.7235 \[hep-ex\]](#).
- [6] ATLAS Collaboration, *A detailed map of Higgs boson interactions by the ATLAS experiment ten years after the discovery*, [*Nature* **607** \(2022\) 52](#), arXiv: [2207.00092 \[hep-ex\]](#), Erratum: [*Nature* **612** \(2022\) E24](#).
- [7] CMS Collaboration, *A portrait of the Higgs boson by the CMS experiment ten years after the discovery*, [*Nature* **607** \(2022\) 60](#), arXiv: [2207.00043 \[hep-ex\]](#), Erratum: [*Nature* **623** \(2023\) E4](#).
- [8] ATLAS Collaboration, *Combination of Searches for Higgs Boson Pair Production in pp Collisions at $\sqrt{s} = 13$ TeV with the ATLAS detector*, [*Phys. Rev. Lett.* **133** \(2024\) 101801](#), arXiv: [2406.09971 \[hep-ex\]](#).
- [9] CMS Collaboration, *Combination of searches for nonresonant Higgs boson pair production in proton–proton collisions at $\sqrt{s} = 13$ TeV*, (2025), arXiv: [2510.07527 \[hep-ex\]](#).
- [10] ATLAS Collaboration, *Search for Higgs boson pair production in association with a vector boson in pp collisions at $\sqrt{s} = 13$ TeV with the ATLAS detector*, [*Eur. Phys. J. C* **83** \(2023\) 519](#), arXiv: [2210.05415 \[hep-ex\]](#).
- [11] CMS Collaboration, *Search for Higgs boson pair production with one associated vector boson in proton–proton collisions at $\sqrt{s} = 13$ TeV*, [*JHEP* **10** \(2024\) 061](#), arXiv: [2404.08462 \[hep-ex\]](#).
- [12] ATLAS and CMS collaborations, *Combination of ATLAS and CMS searches for Higgs boson pair production at $\sqrt{s} = 13$ TeV*, (2026), arXiv: [2602.23991 \[hep-ex\]](#).
- [13] R. Frederix et al., *Higgs pair production at the LHC with NLO and parton-shower effects*, [*Phys. Lett. B* **732** \(2014\) 142](#), arXiv: [1401.7340 \[hep-ph\]](#).
- [14] D. de Florian et al., *Handbook of LHC Higgs Cross Sections: 4. Deciphering the Nature of the Higgs Sector*, (2017), arXiv: [1610.07922 \[hep-ph\]](#).
- [15] ATLAS Collaboration, *Easyjet analysis framework*, version 1.0.0, 2025, URL: <https://doi.org/10.5281/zenodo.15927813>.
- [16] M. Aly et al., *TRExFitter*, version 1.4.0, 2025, URL: <https://doi.org/10.5281/zenodo.16684099>.

- [17] F. Feruglio, *The Chiral approach to the electroweak interactions*, *Int. J. Mod. Phys. A* **8** (1993) 4937, arXiv: [hep-ph/9301281](#).
- [18] G. Buchalla and O. Catà, *Effective Theory of a Dynamically Broken Electroweak Standard Model at NLO*, *JHEP* **07** (2012) 101, arXiv: [1203.6510 \[hep-ph\]](#).
- [19] R. Alonso, M. Gavela, L. Merlo, S. Rigolin and J. Yepes, *Corrigendum to “The effective chiral Lagrangian for a light dynamical “Higgs Particle”* [*Phys. Lett. B* 722 (2013) 330–335], *Physics Letters B* **726** (2013) 926, ISSN: 0370-2693.
- [20] I. Brivio et al., *Disentangling a dynamical Higgs*, *JHEP* **03** (2014) 024, arXiv: [1311.1823 \[hep-ph\]](#).
- [21] G. Buchalla, O. Catà and C. Krause, *Complete electroweak chiral Lagrangian with a light Higgs at NLO*, *Nucl.Phys.B* **880** (2014) 552.
- [22] I. Brivio and M. Trott, *The standard model as an effective field theory*, *Phys.Rept.* **793** (2019) 1.
- [23] ATLAS Collaboration, *The ATLAS Experiment at the CERN Large Hadron Collider*, *JINST* **3** (2008) S08003.
- [24] ATLAS Collaboration, *The ATLAS experiment at the CERN Large Hadron Collider: a description of the detector configuration for Run 3*, *JINST* **19** (2024) P05063, arXiv: [2305.16623 \[physics.ins-det\]](#).
- [25] ATLAS Collaboration, *Performance of the ATLAS trigger system in 2015*, *Eur. Phys. J. C* **77** (2017) 317, arXiv: [1611.09661 \[hep-ex\]](#).
- [26] ATLAS Collaboration, *The ATLAS trigger system for LHC Run 3 and trigger performance in 2022*, *JINST* **19** (2024) P06029, arXiv: [2401.06630 \[hep-ex\]](#).
- [27] ATLAS Collaboration, *Software and computing for Run 3 of the ATLAS experiment at the LHC*, *Eur. Phys. J. C* **85** (2025) 234, arXiv: [2404.06335 \[hep-ex\]](#),
Erratum: *Eur. Phys. J. C* **85** (2025) 907.
- [28] ATLAS Collaboration, *Performance of electron and photon triggers in ATLAS during LHC Run 2*, *Eur. Phys. J. C* **80** (2020) 47, arXiv: [1909.00761 \[hep-ex\]](#).
- [29] ATLAS Collaboration, *Performance of the ATLAS muon triggers in Run 2*, *JINST* **15** (2020) P09015, arXiv: [2004.13447 \[physics.ins-det\]](#).
- [30] ATLAS Collaboration, *ATLAS data quality operations and performance for 2015–2018 data-taking*, *JINST* **15** (2020) P04003, arXiv: [1911.04632 \[physics.ins-det\]](#).
- [31] ATLAS Collaboration, *Luminosity determination in pp collisions at $\sqrt{s} = 13$ TeV using the ATLAS detector at the LHC*, *Eur. Phys. J. C* **83** (2023) 982, arXiv: [2212.09379 \[hep-ex\]](#).
- [32] ATLAS Collaboration, *Preliminary analysis of the luminosity calibration of the ATLAS 13.6 TeV data recorded in 2022*, ATL-DAPR-PUB-2023-001, 2023, URL: <https://cds.cern.ch/record/2853525>.
- [33] ATLAS Collaboration, *Preliminary analysis of the luminosity calibration for the ATLAS 13.6 TeV data recorded in 2023*, ATL-DAPR-PUB-2024-001, 2024, URL: <https://cds.cern.ch/record/2900949>.

- [34] D. J. Lange, *The EvtGen particle decay simulation package*, *Nucl. Instrum. Meth. A* **462** (2001) 152.
- [35] E. Bothmann et al., *Event generation with Sherpa 2.2*, *SciPost Phys.* **7** (2019) 034, arXiv: [1905.09127 \[hep-ph\]](#).
- [36] S. Frixione, E. Laenen, P. Motylinski and B. R. Webber, *Angular correlations of lepton pairs from vector boson and top quark decays in Monte Carlo simulations*, *JHEP* **04** (2007) 081, arXiv: [hep-ph/0702198](#).
- [37] P. Artoisenet, R. Frederix, O. Mattelaer and R. Rietkerk, *Automatic spin-entangled decays of heavy resonances in Monte Carlo simulations*, *JHEP* **03** (2013) 015, arXiv: [1212.3460 \[hep-ph\]](#).
- [38] ATLAS Collaboration, *The ATLAS Simulation Infrastructure*, *Eur. Phys. J. C* **70** (2010) 823, arXiv: [1005.4568 \[physics.ins-det\]](#).
- [39] S. Agostinelli et al., *GEANT4 – a simulation toolkit*, *Nucl. Instrum. Meth. A* **506** (2003) 250.
- [40] ATLAS Collaboration, *The simulation principle and performance of the ATLAS fast calorimeter simulation FastCaloSim*, ATL-PHYS-PUB-2010-013, 2010, URL: <https://cds.cern.ch/record/1300517>.
- [41] ATLAS Collaboration, *Emulating the impact of additional proton–proton interactions in the ATLAS simulation by presampling sets of inelastic Monte Carlo events*, *Comput. Softw. Big Sci.* **6** (2022) 3, arXiv: [2102.09495 \[hep-ex\]](#).
- [42] S. Porteboeuf, T. Pierog and K. Werner, ‘Producing Hard Processes Regarding the Complete Event: The EPOS Event Generator’, *e μ 45th Rencontres de Moriond on QCD and High Energy Interactions*, Gioi Publishers, 2010 135, arXiv: [1006.2967 \[hep-ph\]](#).
- [43] T. Sjöstrand et al., *An introduction to PYTHIA 8.2*, *Comput. Phys. Commun.* **191** (2015) 159, arXiv: [1410.3012 \[hep-ph\]](#).
- [44] S. Frixione, G. Ridolfi and P. Nason, *A positive-weight next-to-leading-order Monte Carlo for heavy flavour hadroproduction*, *JHEP* **09** (2007) 126, arXiv: [0707.3088 \[hep-ph\]](#).
- [45] P. Nason, *A new method for combining NLO QCD with shower Monte Carlo algorithms*, *JHEP* **11** (2004) 040, arXiv: [hep-ph/0409146](#).
- [46] S. Frixione, P. Nason and C. Oleari, *Matching NLO QCD computations with parton shower simulations: the POWHEG method*, *JHEP* **11** (2007) 070, arXiv: [0709.2092 \[hep-ph\]](#).
- [47] S. Alioli, P. Nason, C. Oleari and E. Re, *A general framework for implementing NLO calculations in shower Monte Carlo programs: the POWHEG BOX*, *JHEP* **06** (2010) 043, arXiv: [1002.2581 \[hep-ph\]](#).
- [48] E. Re, *Single-top Wt-channel production matched with parton showers using the POWHEG method*, *Eur. Phys. J. C* **71** (2011) 1547, arXiv: [1009.2450 \[hep-ph\]](#).
- [49] S. Alioli, P. Nason, C. Oleari and E. Re, *NLO single-top production matched with shower in POWHEG: s- and t-channel contributions*, *JHEP* **09** (2009) 111, arXiv: [0907.4076 \[hep-ph\]](#), Erratum: *JHEP* **02** (2010) 011.

- [50] J. Alwall, M. Herquet, F. Maltoni, O. Mattelaer and T. Stelzer, *MadGraph 5: going beyond*, *JHEP* **06** (2011) 128, arXiv: [1106.0522 \[hep-ph\]](#).
- [51] J. Alwall et al., *The automated computation of tree-level and next-to-leading order differential cross sections, and their matching to parton shower simulations*, *JHEP* **07** (2014) 079, arXiv: [1405.0301 \[hep-ph\]](#).
- [52] NNPDF Collaboration, R. D. Ball et al., *Parton distributions with LHC data*, *Nucl. Phys. B* **867** (2013) 244, arXiv: [1207.1303 \[hep-ph\]](#).
- [53] ATLAS Collaboration, *ATLAS Pythia 8 tunes to 7 TeV data*, ATL-PHYS-PUB-2014-021, 2014, URL: <https://cds.cern.ch/record/1966419>.
- [54] M. Bähr et al., *Herwig++ physics and manual*, *Eur. Phys. J. C* **58** (2008) 639, arXiv: [0803.0883 \[hep-ph\]](#).
- [55] J. Bellm et al., *Herwig 7.1 Release Note*, (2017), arXiv: [1705.06919 \[hep-ph\]](#).
- [56] J. Bellm et al., *Herwig 7.2 release note*, *Eur. Phys. J. C* **80** (2020) 452, arXiv: [1912.06509 \[hep-ph\]](#).
- [57] L. A. Harland-Lang, A. D. Martin, P. Motylinski and R. S. Thorne, *Parton distributions in the LHC era: MMHT 2014 PDFs*, *Eur. Phys. J. C* **75** (2015) 204, arXiv: [1412.3989 \[hep-ph\]](#).
- [58] K. Hamilton, P. Nason, E. Re and G. Zanderighi, *NNLOPS simulation of Higgs boson production*, *JHEP* **10** (2013) 222, arXiv: [1309.0017 \[hep-ph\]](#).
- [59] K. Hamilton, P. Nason and G. Zanderighi, *Finite quark-mass effects in the NNLOPS POWHEG+MiNLO Higgs generator*, *JHEP* **05** (2015) 140, arXiv: [1501.04637 \[hep-ph\]](#).
- [60] NNPDF Collaboration, R. D. Ball et al., *Parton distributions for the LHC run II*, *JHEP* **04** (2015) 040, arXiv: [1410.8849 \[hep-ph\]](#).
- [61] ATLAS Collaboration, *Studies on top-quark Monte Carlo modelling for Top2016*, ATL-PHYS-PUB-2016-020, 2016, URL: <https://cds.cern.ch/record/2216168>.
- [62] M. Czakon and A. Mitov, *Top++: A program for the calculation of the top-pair cross-section at hadron colliders*, *Comput. Phys. Commun.* **185** (2014) 2930, arXiv: [1112.5675 \[hep-ph\]](#).
- [63] F. Cascioli, P. Maierhöfer and S. Pozzorini, *Scattering Amplitudes with Open Loops*, *Phys. Rev. Lett.* **108** (2012) 111601, arXiv: [1111.5206 \[hep-ph\]](#).
- [64] A. Denner, S. Dittmaier and L. Hofer, *COLLIER: A fortran-based complex one-loop library in extended regularizations*, *Comput. Phys. Commun.* **212** (2017) 220, arXiv: [1604.06792 \[hep-ph\]](#).
- [65] F. Buccioni et al., *OpenLoops 2*, *Eur. Phys. J. C* **79** (2019) 866, arXiv: [1907.13071 \[hep-ph\]](#).
- [66] S. Höche, F. Krauss, M. Schönherr and F. Siegert, *QCD matrix elements + parton showers. The NLO case*, *JHEP* **04** (2013) 027, arXiv: [1207.5030 \[hep-ph\]](#).
- [67] S. Kallweit, J. M. Lindert, P. Maierhöfer, S. Pozzorini and M. Schönherr, *NLO QCD+EW predictions for V + jets including off-shell vector-boson decays and multijet merging*, *JHEP* **04** (2016) 021, arXiv: [1511.08692 \[hep-ph\]](#).

- [68] C. Gütschow, J. M. Lindert and M. Schönherr, *Multi-jet merged top-pair production including electroweak corrections*, [Eur. Phys. J. C **78** \(2018\) 317](#), arXiv: [1803.00950 \[hep-ph\]](#).
- [69] R. Frederix, D. Pagani and M. Zaro, *Large NLO corrections in $t\bar{t}W^\pm$ and $t\bar{t}\bar{t}$ hadroproduction from supposedly subleading EW contributions*, [JHEP **02** \(2018\) 031](#), arXiv: [1711.02116 \[hep-ph\]](#).
- [70] L. Buonocore et al., *Precise Predictions for the Associated Production of a W Boson with a Top-Antitop Quark Pair at the LHC*, [Phys. Rev. Lett. **131** \(2023\) 231901](#), arXiv: [2306.16311 \[hep-ph\]](#).
- [71] S. Frixione, V. Hirschi, D. Pagani, H. -. Shao and M. Zaro, *Electroweak and QCD corrections to top-pair hadroproduction in association with heavy bosons*, [JHEP **06** \(2015\) 184](#), arXiv: [1504.03446 \[hep-ph\]](#).
- [72] J. Butterworth et al., *PDF4LHC recommendations for LHC Run II*, [J. Phys. G **43** \(2016\) 023001](#), arXiv: [1510.03865 \[hep-ph\]](#).
- [73] W. Beenakker et al., *NLO QCD corrections to $t\bar{t}H$ production in hadron collisions*, [Nucl. Phys. B **653** \(2003\) 151](#), arXiv: [hep-ph/0211352](#).
- [74] S. Dawson, C. Jackson, L. H. Orr, L. Reina and D. Wackerroth, *Associated Higgs boson production with top quarks at the CERN Large Hadron Collider: NLO QCD corrections*, [Phys. Rev. D **68** \(2003\) 034022](#), arXiv: [hep-ph/0305087](#).
- [75] Y. Zhang, W.-G. Ma, R.-Y. Zhang, C. Chen and L. Guo, *QCD NLO and EW NLO corrections to $t\bar{t}H$ production with top quark decays at hadron collider*, [Phys. Lett. B **738** \(2014\) 1](#), arXiv: [1407.1110 \[hep-ph\]](#).
- [76] S. Frixione, V. Hirschi, D. Pagani, H.-S. Shao and M. Zaro, *Weak corrections to Higgs hadroproduction in association with a top-quark pair*, [JHEP **09** \(2014\) 065](#), arXiv: [1407.0823 \[hep-ph\]](#).
- [77] ATLAS Collaboration, *Measurement of the Higgs boson production in association with top quarks in multilepton final states in pp collisions at $\sqrt{s} = 13$ TeV with the ATLAS detector*, (2025), arXiv: [2510.23755 \[hep-ex\]](#).
- [78] ATLAS Collaboration, *Measurement of the associated production of a top-antitop-quark pair and a Higgs boson decaying into a $b\bar{b}$ pair in pp collisions at $\sqrt{s} = 13$ TeV using the ATLAS detector at the LHC*, [Eur. Phys. J. C **85** \(2025\) 210](#), arXiv: [2407.10904 \[hep-ex\]](#).
- [79] ATLAS Collaboration, *Measurement of the total and differential cross-sections of $t\bar{t}W$ production in pp collisions at $\sqrt{s} = 13$ TeV with the ATLAS detector*, [JHEP **05** \(2024\) 131](#), arXiv: [2401.05299 \[hep-ex\]](#).
- [80] ATLAS Collaboration, *Study of Higgs boson pair production in the $HH \rightarrow b\bar{b}\gamma\gamma$ final state with 308fb^{-1} of data collected at $\sqrt{s} = 13$ TeV and 13.6 TeV by the ATLAS experiment*, (2025), arXiv: [2507.03495 \[hep-ex\]](#).
- [81] A. Vaswani et al., *Attention Is All You Need*, (2023), arXiv: [1706.03762 \[cs.CL\]](#).
- [82] ATLAS Collaboration, *Vertex Reconstruction Performance of the ATLAS Detector at $\sqrt{s} = 13$ TeV*, ATL-PHYS-PUB-2015-026, 2015, URL: <https://cds.cern.ch/record/2037717>.

- [83] ATLAS Collaboration, *Electron and photon performance measurements with the ATLAS detector using the 2015–2017 LHC proton–proton collision data*, [JINST **14** \(2019\) P12006](#), arXiv: [1908.00005 \[hep-ex\]](#).
- [84] ATLAS Collaboration, *Electron and photon efficiencies in LHC Run 2 with the ATLAS experiment*, [JHEP **05** \(2024\) 162](#), arXiv: [2308.13362 \[hep-ex\]](#).
- [85] ATLAS Collaboration, *Electron and photon energy calibration with the ATLAS detector using LHC Run 2 data*, [JINST **19** \(2024\) P02009](#), arXiv: [2309.05471 \[hep-ex\]](#).
- [86] ATLAS Collaboration, *Muon reconstruction and identification efficiency in ATLAS using the full Run 2 pp collision data set at $\sqrt{s} = 13$ TeV*, [Eur. Phys. J. C **81** \(2021\) 578](#), arXiv: [2012.00578 \[hep-ex\]](#).
- [87] ATLAS Collaboration, *Studies of the muon momentum calibration and performance of the ATLAS detector with pp collisions at $\sqrt{s} = 13$ TeV*, [Eur. Phys. J. C **83** \(2023\) 686](#), arXiv: [2212.07338 \[hep-ex\]](#).
- [88] ATLAS Collaboration, *Muon reconstruction performance of the ATLAS detector in proton–proton collision data at $\sqrt{s} = 13$ TeV*, [Eur. Phys. J. C **76** \(2016\) 292](#), arXiv: [1603.05598 \[hep-ex\]](#).
- [89] ATLAS Collaboration, *Jet reconstruction and performance using particle flow with the ATLAS Detector*, [Eur. Phys. J. C **77** \(2017\) 466](#), arXiv: [1703.10485 \[hep-ex\]](#).
- [90] M. Cacciari, G. P. Salam and G. Soyez, *The anti- k_t jet clustering algorithm*, [JHEP **04** \(2008\) 063](#), arXiv: [0802.1189 \[hep-ph\]](#).
- [91] ATLAS Collaboration, *Jet energy scale and resolution measured in proton–proton collisions at $\sqrt{s} = 13$ TeV with the ATLAS detector*, [Eur. Phys. J. C **81** \(2021\) 689](#), arXiv: [2007.02645 \[hep-ex\]](#).
- [92] ATLAS Collaboration, *New techniques for jet calibration with the ATLAS detector*, [Eur. Phys. J. C **83** \(2023\) 761](#), arXiv: [2303.17312 \[hep-ex\]](#).
- [93] ATLAS Collaboration, *Performance of pile-up mitigation techniques for jets in pp collisions at $\sqrt{s} = 8$ TeV using the ATLAS detector*, [Eur. Phys. J. C **76** \(2016\) 581](#), arXiv: [1510.03823 \[hep-ex\]](#).
- [94] ATLAS Collaboration, *Transforming jet flavour tagging at ATLAS*, (2025), arXiv: [2505.19689 \[hep-ex\]](#).
- [95] ATLAS Collaboration, *The performance of missing transverse momentum reconstruction and its significance with the ATLAS detector using 140fb^{-1} of $\sqrt{s} = 13$ TeV pp collisions*, [Eur. Phys. J. C **85** \(2025\) 606](#), arXiv: [2402.05858 \[hep-ex\]](#).
- [96] ATLAS Collaboration, *Search for $t\bar{t}H/A \rightarrow t\bar{t}\bar{t}$ production in the multilepton final state in proton–proton collisions at $\sqrt{s} = 13$ TeV with the ATLAS detector*, [JHEP **07** \(2023\) 203](#), arXiv: [2211.01136 \[hep-ex\]](#).
- [97] ATLAS Collaboration, *Observation of four-top-quark production in the multilepton final state with the ATLAS detector*, [Eur. Phys. J. C **83** \(2023\) 496](#), arXiv: [2303.15061 \[hep-ex\]](#), Erratum: [Eur. Phys. J. C **84** \(2024\) 156](#).

- [98] ATLAS Collaboration, *Measurements of inclusive and differential fiducial cross-sections of $t\bar{t}$ production with additional heavy-flavour jets in proton–proton collisions at $\sqrt{s} = 13$ TeV with the ATLAS detector*, [JHEP **04** \(2019\) 046](#), arXiv: [1811.12113 \[hep-ex\]](#).
- [99] ATLAS Collaboration, *Measurement of $t\bar{t}$ production in association with additional b -jets in the $e\mu$ final state in proton–proton collisions at $\sqrt{s} = 13$ TeV with the ATLAS detector*, [JHEP **01** \(2025\) 068](#), arXiv: [2407.13473 \[hep-ex\]](#).
- [100] ATLAS Collaboration, *Measurement of top-quark pair production in association with charm quarks in proton–proton collisions at $\sqrt{s} = 13$ TeV with the ATLAS detector*, [Phys. Lett. B **860** \(2025\) 139177](#), arXiv: [2409.11305 \[hep-ex\]](#).
- [101] CMS Collaboration, *Inclusive and differential cross section measurements of $t\bar{t}b\bar{b}$ production in the lepton+jets channel at $\sqrt{s} = 13$ TeV*, [JHEP **05** \(2024\) 042](#), arXiv: [2309.14442 \[hep-ex\]](#).
- [102] CMS Collaboration, *Measurement of the cross section of top quark–antiquark pair production in association with a W boson in proton–proton collisions at $\sqrt{s} = 13$ TeV*, [JHEP **07** \(2023\) 219](#), arXiv: [2208.06485 \[hep-ex\]](#).
- [103] ATLAS Collaboration, *Recommendations for the Modeling of Smooth Backgrounds*, ATL-PHYS-PUB-2020-028, 2020, URL: <https://cds.cern.ch/record/2743717>.
- [104] ATLAS Collaboration, *Search for Scalar Diphoton Resonances in the Mass Range 65–600 GeV with the ATLAS Detector in pp Collision Data at $\sqrt{s} = 8$ TeV*, [Phys. Rev. Lett. **113** \(2014\) 171801](#), arXiv: [1407.6583 \[hep-ex\]](#).
- [105] T. Chen and C. Guestrin, *XGBoost: A Scalable Tree Boosting System*, (2016), arXiv: [1603.02754 \[cs.LG\]](#).
- [106] T. Akiba, S. Sano, T. Yanase, T. Ohta and M. Koyama, *Optuna: A Next-generation Hyperparameter Optimization Framework*, (2019), arXiv: [1907.10902 \[cs.LG\]](#).
- [107] ATLAS Collaboration, *Calibration of the light-flavour jet mistagging efficiency of the b -tagging algorithms with Z +jets events using 139fb^{-1} of ATLAS proton–proton collision data at $\sqrt{s} = 13$ TeV*, [Eur. Phys. J. C **83** \(2023\) 728](#), arXiv: [2301.06319 \[hep-ex\]](#).
- [108] ATLAS Collaboration, *ATLAS flavour-tagging algorithms for the LHC Run 2 pp collision dataset*, [Eur. Phys. J. C **83** \(2023\) 681](#), arXiv: [2211.16345 \[physics.data-an\]](#).
- [109] ATLAS Collaboration, *Measurement of the c -jet mistagging efficiency in $t\bar{t}$ events using pp collision data at $\sqrt{s} = 13$ TeV collected with the ATLAS detector*, [Eur. Phys. J. C **82** \(2022\) 95](#), arXiv: [2109.10627 \[hep-ex\]](#).
- [110] ATLAS Collaboration, *Performance of missing transverse momentum reconstruction with the ATLAS detector using proton–proton collisions at $\sqrt{s} = 13$ TeV*, [Eur. Phys. J. C **78** \(2018\) 903](#), arXiv: [1802.08168 \[hep-ex\]](#).
- [111] G. Avoni et al., *The new LUCID-2 detector for luminosity measurement and monitoring in ATLAS*, [JINST **13** \(2018\) P07017](#).
- [112] ATLAS Collaboration, *Measurement of the Higgs boson production in association with top quarks in multilepton final states in pp collisions at $\sqrt{s} = 13$ TeV with the ATLAS detector*, (2025), arXiv: [2510.23755 \[hep-ex\]](#).

- [113] A. L. Read, *Presentation of search results: the CL_s technique*, *J. Phys. G* **28** (2002) 2693.
- [114] G. Cowan, K. Cranmer, E. Gross and O. Vitells, *Asymptotic formulae for likelihood-based tests of new physics*, *Eur. Phys. J. C* **71** (2011) 1554, arXiv: [1007.1727 \[physics.data-an\]](https://arxiv.org/abs/1007.1727), Erratum: *Eur. Phys. J. C* **73** (2013) 2501.
- [115] W. Buchmüller and D. Wyler, *Effective lagrangian analysis of new interactions and flavour conservation*, *Nucl. Phys. B* **268** (1986) 621.
- [116] B. Grzadkowski, M. Iskrzyński, M. Misiak and J. Rosiek, *Dimension-Six Terms in the Standard Model Lagrangian*, *JHEP* **10** (2010) 085, arXiv: [1008.4884 \[hep-ph\]](https://arxiv.org/abs/1008.4884).
- [117] S. Weinberg, *Nonlinear Realizations of Chiral Symmetry*, *Phys. Rev.* **166** (5 1968) 1568.
- [118] B. Gavela, E. E. Jenkins, A. V. Manohar and L. Merlo, *Analysis of General Power Counting Rules in Effective Field Theory*, *Eur. Phys. J. C* **76** (2016) 485, arXiv: [1601.07551 \[hep-ph\]](https://arxiv.org/abs/1601.07551).
- [119] G. Buchalla, O. Cata and C. Krause, *On the Power Counting in Effective Field Theories*, *Phys. Lett. B* **731** (2013) 80, arXiv: [1312.5624 \[hep-ph\]](https://arxiv.org/abs/1312.5624).
- [120] I. Brivio, R. Gröber and K. Schmid, *The Art of Counting: a reappraisal of the HEFT expansion*, In preparation.
- [121] A. Alloul, N. D. Christensen, C. Degrande, C. Duhr and B. Fuks, *FeynRules 2.0 - A complete toolbox for tree-level phenomenology*, *Comput. Phys. Commun.* **185** (2014) 2250, arXiv: [1310.1921 \[hep-ph\]](https://arxiv.org/abs/1310.1921).
- [122] C. Degrande et al., *UFO - The Universal FeynRules Output*, *Comput. Phys. Commun.* **183** (2012) 1201, arXiv: [1108.2040 \[hep-ph\]](https://arxiv.org/abs/1108.2040).
- [123] C. Arzt, M. B. Einhorn and J. Wudka, *Patterns of deviation from the standard model*, *Nucl. Phys. B* **433** (1995) 41, arXiv: [hep-ph/9405214](https://arxiv.org/abs/hep-ph/9405214).
- [124] ATLAS Collaboration, *ATLAS Computing Acknowledgements*, ATL-SOFT-PUB-2026-001, 2026, URL: <https://cds.cern.ch/record/2952666>.

The ATLAS Collaboration

G. Aad ¹⁰², E. Aakvaag ¹⁷, B. Abbott ¹²², S. Abdelhameed ^{118a}, K. Abeling ⁵⁴, N.J. Abicht ⁴⁸, S.H. Abidi ³⁰, M. Aboeela ⁴⁴, A. Aboulhorma ^{36e}, H. Abramowicz ¹⁵⁵, B.S. Acharya ^{68a,68b,m}, A. Ackermann ^{62a}, C. Adam Bourdarios ⁴, L. Adamczyk ^{85a}, S.V. Addepalli ¹⁴⁷, M.J. Addison ¹⁰¹, J. Adelman ¹¹⁷, A. Adiguzel ^{22c}, T. Adye ¹³⁶, A.A. Affolder ¹³⁸, Y. Afik ³⁹, M.N. Agaras ¹³, A. Aggarwal ¹⁰⁰, C. Agheorghiesei ^{28c}, A. Ahmad ^{83a}, F. Ahmadov ^{38,ad}, S. Ahuja ⁹⁵, S. Ahuja ¹⁶⁶, X. Ai ^{113c}, G. Aielli ^{75a,75b}, A. Aikot ¹⁶⁶, M. Ait Tamliah ^{36e}, T.P.A. Åkesson ⁹⁸, D. Akiyama ¹⁷¹, N.N. Akolkar ²⁵, S. Aktas ¹⁶⁹, G.L. Alberghi ^{24b}, J. Albert ¹⁶⁸, U. Alberti ²⁰, P. Albicocco ⁵², S. Alderweireldt ⁵¹, Z.L. Alegria ¹²³, M. Aleksa ³⁷, I.N. Aleksandrov ³⁸, C. Alexa ^{28b}, T. Alexopoulos ¹⁰, F. Alfonsi ^{24b}, M. Algren ⁵⁵, M. Alhroob ¹⁷⁰, B. Ali ¹³⁴, H.M.J. Ali ^{91,v}, S. Ali ³², S.W. Alibocus ⁹², M. Aliev ^{34c}, G. Alimonti ^{70a}, C. Allaire ⁶⁵, B.M.M. Allbrooke ¹⁵⁰, D.R. Allen ¹²³, J.S. Allen ¹⁰¹, J.F. Allen ⁵¹, C.S. Alley ¹, E.R. Almazan ¹³⁸, A. Aloisio ^{71a,71b}, F. Alonso ⁹⁰, C. Alpigiani ¹⁴¹, A. Alvarez Fernandez ¹⁰⁰, M. Alves Cardoso ⁵⁵, M.G. Alviggi ^{71a,71b}, M. Aly ¹⁰¹, Y. Amaral Coutinho ^{81b}, A. Ambler ¹⁰⁴, C. Amelung ³⁷, M. Amerl ¹⁰¹, T. Amezza ¹²⁹, B. Amini ⁵³, K. Amirie ¹⁵⁹, A. Amirkhanov ³⁸, D. Amperiadou ¹⁵⁶, S. An ⁸², C. Anastopoulos ¹⁴³, T. Andeen ¹¹, J.K. Anders ⁹², A.C. Anderson ⁵⁸, A. Andreazza ^{70a,70b}, S. Angelidakis ⁹, A. Angerami ⁴¹, A.V. Anisenkov ³⁸, A. Annovi ^{73a}, C. Antel ³⁷, E. Antipov ¹⁴⁹, M. Antonelli ⁵², F. Anulli ^{74a}, M. Aoki ⁸², T. Aoki ¹⁵⁷, M.A. Aparo ¹³, L. Aperio Bella ⁴⁷, M. Apicella ³¹, C. Appelt ¹⁵⁵, A. Apyan ²⁷, M. Arampatzi ¹⁰, S.J. Arbiol Val ⁸⁶, C. Arcangeletti ⁵², A.T.H. Arce ⁵⁰, J-F. Arguin ¹⁰⁸, S. Argyropoulos ¹⁵⁶, J.-H. Arling ⁴⁷, O. Arnaez ⁴, H. Arnold ¹⁴⁹, G. Artoni ^{74a,74b}, H. Asada ¹¹¹, S. Asatryan ¹⁷⁶, N.A. Asbah ³⁷, R.A. Ashby Pickering ¹⁷⁰, A.M. Aslam ⁹⁵, J. Assahsah ^{36d}, K. Assamagan ³⁰, R. Astalos ^{29a}, K.S.V. Astrand ⁹⁸, S. Atashi ¹⁶³, R.J. Atkin ^{34a}, H. Atmani ^{36f}, P.A. Atmasiddha ¹³⁰, K. Augsten ¹³⁴, A.D. Auriol ⁴⁰, V.A. Austrup ¹⁰¹, A.S. Avad ⁹⁴, G. Avolio ³⁷, K. Axiotis ⁵⁵, A. Azzam ¹³, D. Babal ^{29b}, H. Bachacou ¹³⁷, K. Bachas ^{156,p}, A. Bachiou ³⁵, E. Bachmann ⁴⁹, M.J. Backes ^{62a}, A. Badea ³⁹, T.M. Baer ¹⁰⁶, M. Bahmani ¹⁹, D. Bahner ⁵³, K. Bai ¹²⁵, L. Baines ⁹⁴, O.K. Baker ¹⁷⁵, D. Bakshi Gupta ⁸, L.E. Balabram Filho ^{81b}, V. Balakrishnan ¹²², R. Balasubramanian ⁴, P. Balek ^{85a}, E. Ballabene ^{24b,24a}, F. Balli ¹³⁷, L.M. Baltes ^{62a}, W.K. Balunas ¹²⁸, I. Bamwidhi ^{118b}, E. Banas ⁸⁶, M. Bandieramonte ¹³¹, A. Bandyopadhyay ²⁵, S. Bansal ²⁵, L. Barak ¹⁵⁵, M. Barakat ⁴⁷, E.L. Barberio ¹⁰⁵, D. Barberis ^{18b}, M. Barbero ¹⁰², M.Z. Barel ¹¹⁶, T. Barillari ¹¹⁰, M-S. Barisits ³⁷, T. Barklow ¹⁴⁷, P. Baron ¹³⁵, D.A. Baron Moreno ¹⁰¹, A. Baroncelli ⁶¹, A.J. Barr ¹²⁸, J.D. Barr ⁹⁶, F. Barreiro ⁹⁹, J. Barreiro Guimarães da Costa ¹⁴, M.G. Barros Teixeira ^{132a}, F. Bartels ^{62a}, R. Bartoldus ¹⁴⁷, A.E. Barton ⁹¹, P. Bartos ^{29a}, M. Baselga ⁴⁸, S. Bashiri ⁸⁶, A. Bassalat ^{65,b}, M.J. Basso ^{160a}, S. Bataju ⁴⁴, R. Bate ¹⁶⁷, R.L. Bates ⁵⁸, S. Batlamous ⁹⁹, M. Battaglia ¹³⁸, D. Battulga ¹⁹, M. Baucé ^{74a,74b}, L. Bauckhage ⁴⁷, P. Bauer ²⁵, L.T. Bayer ⁴⁷, L.T. Bazzano Hurrell ³¹, T. Beau ¹²⁹, J.Y. Beaucamp ⁹⁰, S. Beauceron ¹²⁹, P.H. Beauchemin ¹⁶², P. Bechtel ²⁵, H.P. Beck ^{20,o}, K. Becker ¹⁷⁰, A.J. Beddall ⁸⁰, V.A. Bednyakov ³⁸, C.P. Bee ¹⁴⁹, L.J. Beemster ¹⁶, M. Begalli ^{81d}, M. Begel ³⁰, J.K. Behr ⁴⁷, J.F. Beirer ³⁷, F. Beisiegel ²⁵, M. Belfkir ^{118b}, G. Bella ¹⁵⁵, L. Bellagamba ^{24b}, A. Bellerive ³⁵, C.D. Bellgraph ⁶⁷, P. Bellos ²¹, I. Benaoumeur ²¹, D. Benčekroun ^{36a}, F. Bendebba ^{36a}, Y. Benhammou ¹⁵⁵, K.C. Benkendorfer ¹⁶⁸, L. Beresford ⁴⁷, M. Beretta ⁵², E. Bergeas Kuutmann ¹⁶⁴, N. Berger ⁴, B. Bergmann ¹³⁴, J. Beringer ^{18a}, M. Berkat ¹³⁷, G. Bernardi ⁵, C. Bernius ¹⁴⁷, F.U. Bernlochner ²⁵, A. Berrocal Guardia ¹³, T. Berry ⁹⁵, P. Berta ¹³⁵, A. Berti ^{132a},

R. Bertrand ¹⁰², A. Besir¹⁶, S. Bethke ¹¹⁰, A. Betti ^{74a,74b}, T.F. Beumker ¹⁷⁴, A.J. Bevan ⁹⁴,
 L. Bezio ⁵⁵, N.K. Bhalla ⁵³, S. Bharthuar ¹¹⁰, S. Bhatta ¹⁴⁹, P. Bhattarai ¹⁴⁷, Z.M. Bhatti ¹¹⁹,
 K.D. Bhide ⁵³, V.S. Bhopatkar ¹²³, R.M. Bianchi ¹³¹, G. Bianco ^{24b,24a}, O. Biebel ¹⁰⁹,
 M. Biglietti ^{76a}, P. Bijl⁵³, C.S. Billingsley⁴⁴, Y. Bimghi ^{36f}, M. Bindi ⁵⁴, A. Bingham ¹⁷⁴,
 A. Bingul ^{22b}, C. Bini ^{74a,74b}, G.A. Bird ³³, M. Biros ¹³⁵, S. Biryukov ¹⁵⁰, T. Bisanz ⁴⁸,
 E. Bisceglie ^{24b,24a}, J.P. Biswal ¹³⁶, D. Biswas ¹⁴⁵, M. Biyabi ¹⁴, I. Bloch ⁴⁷, A. Blue ⁵⁸,
 U. Blumenschein ⁹⁴, V.S. Bobrovnikov ³⁸, L. Boccardo ^{56b,56a}, M. Boehler ⁵³, B. Boehm ¹⁶⁹,
 D. Bogavac ¹³, L.S. Boggia ¹²⁹, V. Boisvert ⁹⁵, P. Bokan ¹⁶⁴, T. Bold ^{85a}, M. Bomben ⁵,
 M. Bona ⁹⁴, M. Boonekamp ¹³⁷, A.G. Borbély ⁵⁸, G. Borissov ⁹¹, A. Borkar ¹⁶⁹,
 D. Bortoletto ¹²⁸, D. Boscherini ^{24b}, M. Bosman ¹³, K. Bouaouda ^{36a}, L. Boudet ¹³⁷,
 J. Boudreau ¹³¹, E.V. Bouhova-Thacker ⁹¹, D. Boumediene ⁴⁰, R. Bouquet ^{56b,56a}, A. Boveia ¹²¹,
 D. Boye ³⁰, I.R. Boyko ³⁸, L. Bozianu ⁵⁵, J. Bracnik ²¹, N. Brahimi ⁴, G. Brandt ¹⁷⁴,
 O. Brandt ³³, B. Brau ¹⁰³, R. Brener ¹⁷², L. Brenner ¹¹⁶, R. Brenner ¹⁶⁴, S. Bressler ¹⁷²,
 M. Brettell ⁹⁶, G. Brianti ¹¹⁶, D. Britton ⁵⁸, D. Britzger ¹¹⁰, I. Brock ²⁵, R. Brock ¹⁰⁷,
 H. Bronson¹³⁰, G. Brooijmans ⁴¹, A.J. Brooks⁶⁷, E.M. Brooks ^{160b}, E. Brost ³⁰,
 L.M. Brown ^{168,160a}, L.E. Bruce ⁶⁰, T.L. Bruckler ¹²⁸, P.A. Bruckman de Renstrom ⁸⁶,
 B. Brüers ⁴⁷, A. Bruni ^{24b}, G. Bruni ^{24b}, D. Brunner ^{46a,46b}, M. Bruschi ^{24b}, N. Bruscinò ^{74a,74b},
 T. Buanes ¹⁷, Q. Buat ¹⁴¹, D. Buchin ¹¹⁰, A.G. Buckley ⁵⁸, J. Bucko ¹³⁵, M. Bühring ⁴⁹,
 O. Bulekov ⁸⁰, B.A. Bullard ¹⁴⁷, T.O. Buratovich ⁹⁰, S. Burdin ⁹², C.D. Burgard ⁴⁸,
 A.M. Burger ⁸⁹, B. Burghgrave ⁸, O. Burlayenko ⁵³, J. Burleson ¹⁶⁵, J.C. Burzynski ¹²²,
 V. Büscher ¹⁰⁰, P.J. Bussey ⁵⁸, O. But ²⁵, J.M. Butler ²⁶, C.M. Buttar ⁵⁸, J.M. Butterworth ⁹⁶,
 P. Butti³⁷, W. Buttinger ¹³⁶, C.J. Buxo Vazquez ¹⁰⁷, A.R. Buzykaev ³⁸, S. Cabrera Urbán ¹⁶⁶,
 L. Cadamuro ⁶⁵, H. Cai ³⁷, Y. Cai ^{24b,112c,24a}, Y. Cai ^{112a}, M.A. Cairo¹³⁰, V.M.M. Cairo ³⁷,
 O. Cakir ^{3a}, N. Calace ³⁷, P. Calafiura ^{18a}, G. Calderini ¹²⁹, P. Calfayan ³⁵, L. Calic ⁹⁸,
 G. Callea ⁵⁸, L.P. Caloba^{81b}, D. Calvet ⁴⁰, S. Calvet ⁴⁰, R. Camacho Toro ¹²⁹, S. Camarda ³⁷,
 D. Camarero Munoz ²⁷, P. Camarri ^{75a,75b}, C. Camincher ³⁷, M. Campanelli ⁹⁶, A. Camplani ⁴²,
 V. Canale ^{71a,71b}, A.C. Canbay ^{3a}, E. Canonero ⁹⁵, J. Cantero ¹⁶⁶, F. Capocasa ²⁷, P. Cappelli ²⁷,
 M. Capua ^{43b,43a}, A. Carbone ^{70a,70b}, R. Cardarelli ^{75a}, J.C.J. Cardenas ⁸, M.P. Cardiff ²⁷,
 G. Carducci ^{43b,43a}, T. Carli ³⁷, G. Carlino ^{71a}, J.I. Carlotto ¹³, B.T. Carlson ^{131,q},
 E.M. Carlson ¹⁶⁸, L. Carminati ^{70a,70b}, A. Carnelli ⁴, M. Carnesale ³⁷, S. Caron ¹¹⁵,
 E. Carquin ^{139g}, I.B. Carr ¹⁰⁵, S. Carrá ^{72a,72b}, G. Carratta ^{24b,24a}, C. Carrion Martinez ¹⁶⁶,
 A.M. Carroll ¹²⁵, N. Cartalade ⁴⁰, M.P. Casado ^{13,h}, P. Casolaro ^{71a,71b}, M. Caspar ⁴⁷,
 F. Cassinese ⁹⁰, W.R. Castiglioni ³⁹, F.L. Castillo ⁴, L. Castillo Garcia ¹³,
 V. Castillo Gimenez ¹⁶⁶, N.F. Castro ^{132a,132e}, A. Catinaccio ³⁷, J.R. Catmore ¹²⁷, T. Cavaliere ⁴,
 V. Cavaliere ³⁰, E. Celebi ⁸⁰, S. Cella ³⁰, V. Cepaitis ⁵⁵, K. Cerny ¹²⁴, A.S. Cerqueira ^{81a},
 A. Cerri ^{73a,aq}, L. Cerrito ^{75a,75b}, F. Cerutti ^{18a}, B. Cervato ^{70a,70b}, A. Cervelli ^{24b},
 G. Cesarini ⁵², S.A. Cetin ⁸⁰, P.M. Chabrilat ¹²⁹, R. Chakkappai ⁶⁵, S. Chakraborty ¹⁷⁰,
 A. Chambers ⁶⁰, J. Chan ^{18a}, J.D. Chapman ³³, E. Chapon ¹³⁷, B. Chargeishvili ^{153b},
 D.G. Charlton ²¹, C. Chauhan ¹³³, Y. Che ^{112a}, S. Chekanov ⁶, G.A. Chelkov ^{38,a}, H. Chen ³⁰,
 J. Chen ^{142a}, J. Chen ¹⁴⁶, M. Chen ⁵⁹, S. Chen ⁸⁷, S.J. Chen ^{112a}, X. Chen ^{142a}, X. Chen ^{15,ai},
 Z. Chen ⁶¹, C.L. Cheng ¹⁷³, H.C. Cheng ^{63a}, S. Cheong ¹⁴⁷, A. Cheplakov ³⁸,
 E. Cherepanova ¹¹⁶, E. Cheu ⁷, K. Cheung ⁶⁴, L. Chevalier ¹³⁷, G. Chiarelli ^{73a}, G. Chiodini ^{69a},
 A.S. Chisholm ²¹, A. Chitan ^{28b}, M. Chitishvili ¹⁶⁶, M.V. Chizhov ^{38,r}, K. Choi ¹¹, Y. Chou ¹⁴¹,
 E.Y.S. Chow ¹¹⁵, K.L. Chu ¹⁷², M.C. Chu ^{63a}, Z. Chubinidze ⁵², J. Chudoba ¹³³,
 J.J. Chwastowski ⁸⁶, D. Cieri ¹¹⁰, K.M. Ciesla ^{85a}, V. Cindro ⁹³, A. Ciocio ^{18a}, F. Ciroto ^{71a,71b},
 Z.H. Citron ¹⁷², M. Citterio ^{70a}, D.A. Ciubotaru^{28b}, A. Clark ⁵⁵, P.J. Clark ⁵¹, N. Clarke Hall ⁹⁶,
 C. Clarry ¹⁵⁹, S.E. Clawson ⁴⁷, C. Clement ^{46a,46b}, L. Clissa ^{24b,24a}, Y. Coadou ¹⁰²,

M. Cobal [ID 68a,68c](#), A. Coccaro [ID 56b](#), M.G. Cochran Branson [ID 141](#), R.F. Coelho Barrue [ID 132a](#),
R. Coelho Lopes De Sa [ID 103](#), S. Coelli [ID 70a](#), M.M. Cohen [ID 130](#), L.S. Colangeli [ID 159](#), B. Cole [ID 41](#),
P. Collado Soto [ID 99](#), J. Collot [ID 59](#), M.R. Coluccia [ID 69a](#), I. Combes⁶⁵, P. Conde Muiño [ID 132a,132g](#),
M.P. Connell [ID 34c](#), S.H. Connell [ID 34c](#), E.I. Conroy [ID 128](#), M. Contreras Cossio [ID 11](#), F. Conventi [ID 71a,ak](#),
A.M. Cooper-Sarkar [ID 128](#), L. Corazzina [ID 74a,74b](#), F.A. Corchia [ID 24b,24a](#), A. Cordeiro Oudot Choi [ID 141](#),
L.D. Corpe [ID 40](#), M. Corradi [ID 74a,74b](#), F. Corriveau [ID 104,ab](#), A. Cortes-Gonzalez [ID 157](#), M.J. Costa [ID 166](#),
F. Costanza [ID 4](#), D. Costanzo [ID 143](#), J. Couthures [ID 4](#), G. Cowan [ID 95](#), K. Cranmer [ID 173](#), L. Cremer [ID 48](#),
D. Cremonini [ID 24b,24a](#), S. Crépé-Renaudin [ID 59](#), F. Crescioli [ID 129](#), T. Cresta [ID 72a,72b](#), M. Cristinziani [ID 145](#),
M. Cristoforetti [ID 77a,77b](#), E. Critelli [ID 96](#), A. Cueto [ID 99](#), H. Cui [ID 96](#), Z. Cui [ID 7](#), B.M. Cunnett [ID 150](#),
W.R. Cunningham [ID 58](#), E. Cuppini¹¹⁰, F. Curcio [ID 166](#), J.R. Curran [ID 51](#),
M.J. Da Cunha Sargedas De Sousa [ID 56b,56a](#), J.V. Da Fonseca Pinto [ID 81b](#), C. Da Via [ID 101](#),
W. Dabrowski [ID 85a](#), T. Dado [ID 37](#), S. Dahbi [ID 152](#), T. Dai [ID 106](#), D. Dal Santo [ID 20](#), C. Dallapiccola [ID 103](#),
M. Dam [ID 42](#), G. D'amen [ID 30](#), V. D'Amico [ID 109](#), J.R. Dandoy [ID 35](#), M. D'Andrea [ID 56b,56a](#),
D. Dannheim [ID 37](#), G. D'anniballe [ID 73a,73b](#), M. Danninger [ID 146](#), V. Dao [ID 149](#), G. Darbo [ID 56b](#),
F. Dattola [ID 47](#), S. D'Auria [ID 70a,70b](#), A. D'Avanzo [ID 71a,71b](#), T. Davidek [ID 135](#), J. Davidson [ID 170](#),
I. Dawson [ID 94](#), K. De [ID 8](#), C. De Almeida Rossi [ID 159](#), N. De Biase [ID 47](#), S. De Castro [ID 24b,24a](#),
N. De Groot [ID 115](#), P. de Jong [ID 116](#), H. De la Torre [ID 117](#), A. De Maria [ID 112a](#), S. De Miranda Rimes [ID 81d](#),
A. De Salvo [ID 74a](#), U. De Sanctis [ID 75a,75b](#), F. De Santis [ID 69a,69b](#), A. De Santo [ID 150](#),
J.B. De Vivie De Regie [ID 59](#), K.G. De Vries [ID 116](#), J. Debevc [ID 93](#), D.V. Dedovich³⁸, J. Degens [ID 92](#),
A.M. Deiana [ID 44](#), J. Del Peso [ID 99](#), L. Delagrangé [ID 27](#), F. Deliot [ID 137](#), C.M. Delitzsch [ID 48](#),
M. Della Pietra [ID 71a,71b](#), D. Della Volpe [ID 55](#), A. Dell'Acqua [ID 37](#), L. Dell'Asta [ID 70a,70b](#), M. Delmastro [ID 4](#),
C.C. Delogu [ID 56b,56a](#), P.A. Delsart [ID 59](#), S. Demers [ID 175](#), M. Demichev [ID 38](#), H. Denizli [ID 22a,1](#),
M.G. Depala [ID 92](#), L. D'Eramo [ID 40](#), D. Derendarz [ID 86](#), L. Derin [ID 56b,56a](#), F. Derue [ID 129](#), P. Dervan [ID 92,*](#),
A.M. Desai [ID 1](#), K. Desch [ID 25](#), F.A. Di Bello [ID 73a,73b](#), A. Di Ciaccio [ID 75a,75b](#), L. Di Ciaccio [ID 4](#),
D. Di Croce [ID 37](#), C. Di Donato [ID 71a,71b](#), A. Di Girolamo [ID 37](#), G. Di Gregorio [ID 65](#), A. Di Luca [ID 77a,77b](#),
B. Di Micco [ID 76a,76b](#), R. Di Nardo [ID 76a,76b](#), K.F. Di Petrillo [ID 39](#), M. Diamantopoulou [ID 35](#), F.A. Dias [ID 116](#),
M.A. Diaz [ID 139a,139b](#), A.R. Didenko [ID 38](#), M. Didenko [ID 166](#), S.D. Diefenbacher [ID 18a](#), E.B. Diehl [ID 106](#),
S. Díez Cornell [ID 47](#), C. Díez Pardos [ID 145](#), C. Dimitriadi [ID 148](#), A. Dimitrievska [ID 21](#), A. Dimri [ID 149](#),
Y. Ding⁶¹, J. Dingfelder [ID 25](#), T. Dingley [ID 128](#), I-M. Dinu [ID 28b](#), S.J. Dittmeier [ID 62b](#), F. Dittus [ID 37](#),
M. Divisek [ID 135](#), B. Dixit [ID 92](#), F. Djama [ID 102](#), T. Djobava [ID 153b](#), C. Doglioni [ID 101,98](#), A. Dohnalova [ID 29a](#),
Z. Dolezal [ID 135](#), K. Domijan [ID 85a](#), K.M. Dona [ID 39](#), M. Donadelli [ID 81d](#), B. Dong [ID 107](#), J. Donini [ID 40](#),
A. D'Onofrio [ID 71a,71b](#), M. D'Onofrio [ID 92](#), J. Dopke [ID 136](#), A. Doria [ID 71a](#), N. Dos Santos Fernandes [ID 132a](#),
I.A. Dos Santos Luz [ID 81e](#), P. Dougan [ID 44](#), M.T. Dova [ID 90](#), A.T. Doyle [ID 58](#), M.P. Drescher [ID 54](#),
E. Dreyer [ID 172](#), I. Drivas-koulouris [ID 10](#), M. Drnevich [ID 119](#), D. Du [ID 61](#), T. Du [ID 39](#), T.A. du Pree [ID 116](#),
Z. Duan^{112a}, M. Dubau [ID 4](#), F. Dubinin [ID 38](#), M. Dubovsky [ID 29a](#), E. Duchovni [ID 172](#), G. Duckeck [ID 109](#),
P.K. Duckett⁹⁶, O.A. Ducu [ID 28b](#), D. Duda [ID 51](#), A. Dudarev [ID 37](#), M.M. Dudek [ID 86](#), E.R. Duden [ID 27](#),
M. D'uffizi [ID 101](#), L. Dufflot [ID 65](#), M. Dührssen [ID 37](#), I. Duminica [ID 28g](#), A.E. Dumitriu [ID 28b](#),
M. Dunford [ID 62a](#), T. Duong⁴, A. Duperrin [ID 102](#), A.F. Duque Bran [ID 40](#), H. Duran Yildiz [ID 3a](#),
A. Durglishvili [ID 153b](#), G.I. Dyckes [ID 18a](#), M. Dyndal [ID 85a](#), B.S. Dziedzic [ID 37](#), G.H. Eberwein [ID 128](#),
B. Eckerova [ID 29a](#), J.C. Egan [ID 96](#), S. Eggebrecht [ID 54](#), E. Egidio Purcino De Souza [ID 81e](#), G. Eigen [ID 17](#),
K. Einsweiler [ID 18a](#), T. Ekelof [ID 164](#), P.A. Ekman [ID 98](#), S. El Farkh [ID 36b](#), Y. El Ghazali [ID 61](#),
H. El Jarrari [ID 104](#), A. El Moussaouy [ID 36a](#), I. Elbaz [ID 155](#), D. Elitez [ID 37](#), M. Ellert [ID 164](#),
F. Ellinghaus [ID 174](#), T.A. Elliot [ID 95](#), J. Elmsheuser [ID 30](#), M. Elsayy [ID 118a](#), M. Elsing [ID 37](#),
D. Emelianov [ID 136](#), Y. Enari [ID 82](#), S. Epari [ID 108](#), D. Ernani Martins Neto [ID 86](#), F. Ernst³⁷,
M. Escalier [ID 65](#), C. Escobar [ID 166](#), R. Estevam De Paula [ID 81c](#), E. Etzion [ID 155](#), G. Evans [ID 132a,132b](#),
H. Evans [ID 67](#), L.S. Evans [ID 47](#), S. Ezzarqtouni [ID 36a](#), F. Fabbri [ID 24b,24a](#), L. Fabbri [ID 24b,24a](#), G. Facini [ID 96](#),
V. Fadeyev [ID 138](#), D. Fakoudis [ID 100](#), S. Falciano [ID 74a](#), L.F. Falda Ulhoa Coelho [ID 27](#), F. Fallavollita [ID 110](#),

G. Falsetti ^{43b,43a}, J. Faltova ¹³⁵, C. Fan ¹⁶⁵, K.Y. Fan ^{63b}, Y. Fan ¹⁴, Y. Fang ^{14,112c}, M. Fanti ^{70a,70b}, M. Faraj ^{68a,68c}, Z. Farazpay ⁹⁷, A. Farbin ⁸, A. Farilla ^{76a}, K. Farman ¹⁵², J.N. Farr ¹⁷⁵, M.S. Farrington ⁶⁰, S.M. Farrington ^{136,51}, F. Fassi ^{36e}, D. Fassouliotis ⁹, L. Fayard ⁶⁵, P. Federic ¹³⁵, P. Federicova ¹³³, M. Feickert ¹⁷³, L. Feligioni ¹⁰², D.E. Fellers ^{18a}, C. Feng ^{113b}, Y. Feng ¹⁴, Z. Feng ⁶⁵, B. Fernandez Barbadillo ⁹¹, P. Fernandez Martinez ⁶⁶, C. Fernandez Ruiz ³³, J. Ferrando ⁹¹, A. Ferrari ¹⁶⁴, P. Ferrari ^{116,115}, R. Ferrari ^{72a}, D. Ferrere ⁵⁵, C. Ferretti ¹⁰⁶, M.P. Fewell ¹, D. Fiacco ^{74a,74b}, F. Fiedler ¹⁰⁰, P. Fiedler ¹³⁴, S. Filimonov ³⁸, M.S. Filip ^{28b,s}, A. Filipčič ⁹³, E.K. Filmer ^{160a}, F. Filthaut ¹¹⁵, M.C.N. Fiolhais ^{132a,132c,c}, L. Fiorini ¹⁶⁶, W.C. Fisher ¹⁰⁷, T. Fitschen ¹⁰¹, I. Fleck ¹⁴⁵, P. Fleischmann ¹⁰⁶, T. Flick ¹⁷⁴, M. Flores ^{34d,ag}, L.R. Flores Castillo ^{63a}, M. Foll ¹²⁷, F.M. Follega ^{77a,77b}, N. Fomin ³³, J.H. Foo ¹⁵⁹, A. Formica ¹³⁷, M. Fornasiero ¹⁵⁰, A.C. Forti ¹⁰¹, N. Forti ^{24b,24a}, E. Fortin ¹⁰², A.W. Fortman ^{18a}, L. Foster ^{18a}, L. Fountas ⁹, H. Fox ⁹¹, P. Francavilla ^{73a,73b}, S. Francescato ⁶⁰, S. Franchellucci ²⁰, M. Franchini ^{24b,24a}, S. Franchino ^{62a}, D. Francis ³⁷, L. Franco ⁴⁷, L. Franconi ⁴⁷, M. Franklin ⁶⁰, G. Frattari ²⁷, Y.Y. Frid ¹⁵⁵, N. Fritzsche ³⁷, A. Froch ⁵⁵, D. Froidevaux ³⁷, J.A. Frost ¹³⁶, Y. Fu ¹⁰⁷, S. Fuenzalida Garrido ^{139g}, Y.C. Fujikake ¹³⁸, M. Fujimoto ¹⁴⁹, K.Y. Fung ^{63a}, E. Furtado De Simas Filho ^{81e}, M. Furukawa ¹⁵⁷, M. Fuste Costa ⁴⁷, J. Fuster ¹⁶⁶, A. Gaa ⁵⁴, A. Gabrielli ^{24b,24a}, A. Gabrielli ¹⁵⁹, G. Gagliardi ^{56b,56a}, L.G. Gagnon ^{18a}, S. Galantzan ¹⁵⁵, J. Gallagher ¹, E.J. Gallas ¹²⁸, A.L. Gallen ¹⁶⁴, B.J. Gallop ¹³⁶, K.K. Gan ¹²¹, Y. Gao ⁵¹, Z. Gao ^{112a}, A. Garabaglu ¹⁴¹, F.M. Garay Walls ^{139a,139b}, C. García ¹⁶⁶, A. Garcia Alonso ¹¹⁶, A.G. Garcia Caffaro ¹⁷⁵, J.E. García Navarro ¹⁶⁶, M.A. Garcia Ruiz ^{23b}, M. Garcia-Sciveres ^{18a}, G.L. Gardner ¹³⁰, R.W. Gardner ³⁹, N. Garelli ¹⁶², R.B. Garg ¹⁴⁷, J.M. Gargan ³³, C.A. Garner ¹⁵⁹, C.M. Garvey ^{34a}, V.K. Gassmann ¹⁶², G. Gaudio ^{72a}, A.J. Gavin ⁹⁴, J. Gavranovic ⁹³, I.L. Gavrilenko ^{132a}, C. Gay ¹⁶⁷, G. Gaycken ¹²⁵, A. Gekow ¹²¹, C. Gemme ^{56b}, M.H. Genest ⁵⁹, A.D. Gentry ¹¹⁴, S. George ⁹⁵, T. Geralis ⁴⁵, A.A. Gerwin ¹²², P. Gessinger-Befurt ³⁷, M. Ghani ¹⁷⁰, K. Ghorbanian ⁹⁴, A. Ghosal ¹⁴⁵, A. Ghosh ¹⁶³, A. Ghosh ⁷, B. Giacobbe ^{24b}, S. Giagu ^{74a,74b}, A. Giannini ⁶¹, S.M. Gibson ⁹⁵, D.T. Gil ^{85b}, A.K. Gilbert ^{85a}, B.J. Gilbert ⁴¹, D. Gillberg ³⁵, G. Gilles ¹¹⁶, D.M. Gingrich ^{2,aj}, M.P. Giordani ^{68a,68c}, P.F. Giraud ¹³⁷, G. Giugliarelli ^{68a,68c}, D. Giugni ^{70a}, F. Giuli ^{75a,75b,am}, I. Gkialas ^{9,i}, C. Glasman ⁹⁹, M. Glazewska ²⁰, R.M. Gleason ¹⁶³, G. Glemža ⁴⁷, I. Gnesi ^{24b,24a,an}, Y. Go ³⁰, M. Goblirsch-Kolb ³⁷, B. Gocke ⁴⁸, D. Godin ¹⁰⁸, B. Gokturk ^{22a}, S. Goldfarb ¹⁰⁵, T. Golling ⁵⁵, M.G.D. Gololo ^{34c}, A. Golub ¹⁴¹, J.P. Gombas ¹⁰⁷, A. Gomes ^{132a,132b}, G. Gomes Da Silva ¹⁴⁵, A.J. Gomez Delegido ³⁷, R. Gonçalves ^{132a}, A. Gongadze ^{153c}, F. Gonnella ²¹, J.L. Gonski ¹⁴⁷, R.Y. González Andana ⁵¹, S. González de la Hoz ¹⁶⁶, M.V. Gonzalez Rodrigues ⁴⁷, R. Gonzalez Suarez ¹⁶⁴, S. Gonzalez-Sevilla ⁵⁵, L. Goossens ³⁷, B. Gorini ³⁷, E. Gorini ^{69a,69b}, A. Gorišek ⁹³, T.C. Gosart ¹³⁰, A.T. Goshaw ⁵⁰, M.I. Gostkin ³⁸, S. Goswami ¹²³, C.A. Gottardo ³⁷, S.A. Gotz ¹⁰⁹, M. Goughri ^{36b}, A.G. Goussiou ¹⁴¹, N. Govender ^{34c}, R.P. Grabarczyk ¹²⁸, I. Grabowska-Bold ^{85a}, K. Graham ³⁵, E. Gramstad ¹²⁷, S. Grancagnolo ^{69a,69b}, C.M. Grant ¹, P.M. Gravila ^{28f}, F.G. Gravili ^{69a,69b}, H.M. Gray ^{18a}, M. Greco ¹¹⁰, M.J. Green ¹, C. Grefe ²⁵, A.S. Grefsrud ¹⁷, I.M. Gregor ⁴⁷, K.T. Greif ¹⁶³, P. Grenier ¹⁴⁷, S.G. Grewe ¹¹⁰, K. Grimm ³², S. Grinstein ^{13,x}, R. Groeber ^{al}, E. Gross ¹⁷², J. Grosse-Knetter ⁵⁴, L.H. Grossman ^{18b}, L. Guan ¹⁰⁶, G. Guerrieri ³⁷, R. Guevara ¹²⁷, R. Gugel ¹⁰⁰, J.A.M. Guhit ¹⁰⁶, A. Guida ¹⁹, E. Guilloton ¹⁷⁰, S. Guindon ³⁷, F. Guo ^{14,112c}, J. Guo ^{142a}, L. Guo ⁴⁷, L. Guo ^{112b,u}, Y. Guo ¹⁰⁶, Y. Guo ⁴¹, A. Gupta ⁴⁸, R. Gupta ¹³¹, S. Gupta ²⁷, S. Gurbuz ²⁵, S.S. Gurdasani ⁴⁷, G. Gustavino ^{74a,74b}, P. Gutierrez ¹²², L.F. Gutierrez Zagazeta ¹³⁰, M. Gutsche ⁴⁹, C. Gutschow ⁹⁶, W. Guérin ⁸⁹, C. Gwenlan ¹²⁸, C.B. Gwilliam ⁹², E.S. Haaland ¹²⁷, A. Haas ¹¹⁹, M. Habedank ⁵⁸, C. Haber ^{18a},

R.J. Haberle ¹⁷², H.K. Hadavand ⁸, A. Haddad ⁴⁰, A. Hadeef ⁴⁹, A.I. Hagan ⁹¹, J.J. Hahn ¹⁴⁵, M. Haleem ¹⁶⁹, J. Haley ¹²³, G.D. Hallelwell ¹⁰², J.A. Hallford ⁴⁷, K. Hamano ¹⁶⁸, H. Hamdaoui ¹⁶⁴, M. Hamer ²⁵, S.E.D. Hammoud ⁶⁵, E.J. Hampshire ⁹⁵, L. Han ^{112a}, L. Han ⁶¹, S. Han ¹⁴, K. Hanagaki ⁸², M. Hance ¹³⁸, D.A. Hangal ⁴¹, H. Hanif ¹⁴⁶, M.D. Hank ¹³⁰, J.B. Hansen ⁴², P.H. Hansen ⁴², T. Harenberg ¹⁷⁴, S. Harkusha ¹⁷⁶, M.L. Harris ¹⁰³, Y.T. Harris ²⁵, J. Harrison ¹³, P.F. Harrison ¹⁷⁰, M.L.E. Hart ⁹⁶, N.M. Hartman ¹¹⁰, N.M. Hartmann ¹⁰⁹, R.Z. Hasan ^{95,136}, Y. Hasegawa ¹⁴⁴, D. Hashimoto ¹¹¹, F. Haslbeck ³⁷, S. Hassan ¹²⁷, R. Hauser ¹⁰⁷, M. Haviernik ¹³⁵, C.M. Hawkes ²¹, R.J. Hawkings ³⁷, Y. Hayashi ¹⁵⁷, D. Hayden ¹⁰⁷, R.L. Hayes ¹¹⁶, C.P. Hays ¹²⁸, J.M. Hays ⁹⁴, H.S. Hayward ⁹², M. He ^{14,112c}, Y. He ⁴⁷, Y. He ⁹⁶, N.B. Heatley ⁹⁴, V. Hedberg ⁹⁸, J. Heilman ³⁵, S. Heim ⁴⁷, T. Heim ^{18a}, J.J. Heinrich ¹²⁵, L. Heinrich ¹¹⁰, J. Hejbal ¹³³, M. Helbig ⁴⁹, A. Held ¹⁷³, S. Hellesund ¹⁷, C.M. Helling ¹⁶⁷, F.N.E. Henry ⁵⁸, H. Herde ⁹⁸, Y. Hernández Jiménez ¹⁴⁹, G. Herten ⁵³, R. Hertenberger ¹⁰⁹, L. Hervas ³⁷, M.E. Hespings ¹⁰⁰, N.P. Hessey ^{160a}, J. Hessler ¹¹⁰, R. Hicks ¹³⁰, M. Hidaoui ^{36b}, N. Hidic ¹³⁵, E. Hill ¹⁵⁹, T.S. Hillersoy ¹⁷, S.J. Hillier ²¹, J.R. Hinds ¹⁰⁷, F. Hinterkeuser ²⁵, M. Hirose ¹²⁶, S. Hirose ¹⁶¹, D. Hirschbuehl ¹⁷⁴, B. Hiti ⁹³, J. Hobbs ¹⁴⁹, R. Hobincu ^{28e}, N. Hod ¹⁷², A.M. Hodges ¹⁶⁵, M.C. Hodgkinson ¹⁴³, B.H. Hodgkinson ¹²⁸, A. Hoecker ³⁷, D.D. Hofer ¹⁰⁶, J. Hofer ¹⁶⁶, J. Hofner ¹⁰⁰, M. Holzbock ³⁷, L.B.A.H. Hommels ³³, V. Homsak ¹²⁸, J.J. Hong ⁶⁷, T.M. Hong ¹³¹, B.H. Hooberman ¹⁶⁵, W.H. Hopkins ⁶, M.C. Hoppesch ¹⁶⁵, Y. Horii ¹¹¹, M.E. Horstmann ¹¹⁰, M.M. Horzela ⁵⁴, S. Hou ¹⁵², M.R. Housenga ¹⁶⁵, J. Howarth ⁵⁸, J. Hoya ⁶, M. Hrabovsky ¹²⁴, T. Hryn'ova ⁴, P.J. Hsu ⁶⁴, S.-C. Hsu ¹⁴¹, T. Hsu ⁶⁵, M. Hu ^{18a}, P. Hu ^{63b}, Q. Hu ⁶¹, S. Huang ³³, X. Huang ^{14,112c}, Y. Huang ¹³⁵, Y. Huang ^{112b}, Y. Huang ¹⁴, Z. Huang ⁶⁵, Z. Hubacek ¹³⁴, F. Huegging ²⁵, T.B. Huffman ¹²⁸, M. Hufnagel Maranha De Faria ^{81a}, C.A. Hugli ⁴⁷, M. Huhtinen ³⁷, S.K. Huiberts ¹⁷, R. Hulsken ¹⁰⁴, C.E. Hultquist ^{18a}, D.L. Humphreys ¹⁰³, N. Huseynov ¹², J. Huston ¹⁰⁷, B. Huth ³⁷, J. Huth ⁶⁰, L. Huth ⁴⁷, R. Hyneman ⁷, G. Iacobucci ⁵⁵, G. Iakovidis ³⁰, L. Iconomidou-Fayard ⁶⁵, J.P. Iddon ³⁷, P. Iengo ^{71a,71b}, Y. Iiyama ¹⁵⁷, T. Iizawa ¹⁵⁷, Y. Ikegami ⁸², D. Iliadis ¹⁵⁶, N. Ilic ¹⁵⁹, H. Imam ^{36a}, G. Inacio Goncalves ^{81d}, S.A. Infante Cabanas ^{139c}, T. Ingebretsen Carlson ^{46a,46b}, J.M. Inglis ⁹⁴, G. Introzzi ^{72a,72b}, M. Iodice ^{76a}, V. Ippolito ^{74a,74b}, R.K. Irwin ⁹², M. Ishino ¹⁵⁷, W. Islam ¹⁷³, C. Issever ¹⁹, S. Istin ^{22a,as}, K. Itabashi ¹²⁶, H. Ito ¹⁷¹, R. Iuppa ^{77a,77b}, A. Ivina ¹⁷², F. Ivone ³⁷, S. Izumiyama ¹¹¹, V. Izzo ^{71a}, P. Jacka ¹³⁴, P. Jackson ¹, P.R. Jacobson ⁵⁰, P. Jain ⁴⁷, K. Jakobs ⁵³, J. Jamieson ⁵⁸, W. Jang ¹⁵⁷, S. Jankovych ¹¹⁶, B.K. Jashal ¹³⁶, M. Javurkova ¹⁰³, P. Jawahar ¹⁰¹, L. Jeanty ¹²⁵, J. Jejelava ^{153a,ae}, P. Jenni ^{53,f}, L. Jerala ⁹³, C.E. Jessiman ³⁵, H. Jia ¹⁶⁷, J. Jia ¹⁴⁹, X. Jia ^{110,112c}, C. Jiang ⁵¹, Q. Jiang ^{63b}, S. Jiggins ⁴⁷, M. Jimenez Ortega ¹⁶⁶, J. Jimenez Pena ¹³, S. Jin ^{112a}, A. Jinaru ^{28b}, O. Jinnouchi ¹⁴⁰, P. Johansson ¹⁴³, K.A. Johns ⁷, J.W. Johnson ¹³⁸, F.A. Jolly ⁴⁷, D.M. Jones ¹⁵⁰, E. Jones ⁴⁷, K.S. Jones ⁸, P. Jones ³³, R.W.L. Jones ⁹¹, T.J. Jones ⁹², H.L. Joos ³⁷, R. Joshi ¹²¹, J. Jovicevic ¹⁶, X. Ju ^{18a}, J.J. Junggeburth ³⁷, T. Junkermann ^{62a}, A. Juste Rozas ^{13,x}, M.K. Juzek ⁸⁶, S. Kabana ^{139f}, A. Kaczmaraska ⁸⁶, S.A. Kadir ¹⁴⁷, M. Kado ¹¹⁰, H. Kagan ¹²¹, M. Kagan ¹⁴⁷, A. Kahn ¹³⁰, C. Kahra ¹⁰⁰, T. Kaji ¹⁵⁷, E. Kajomovitz ¹⁵⁴, N. Kakati ¹⁷², N. Kakoty ¹³, S. Kandel ⁸, N. Kanellos ¹⁰, D. Kar ^{34,*}, E. Karentzos ²⁵, K. Karki ⁸, O. Karkout ¹¹⁶, S.N. Karpov ³⁸, Z.M. Karpova ³⁸, V. Kartvelishvili ^{91,153b}, E. Kasimi ¹⁵⁶, J. Katzy ⁴⁷, S. Kaur ³⁵, R. Kavak ¹⁶⁵, K. Kawade ¹⁴⁴, M.P. Kawale ¹²², C. Kawamoto ⁸⁷, E.F. Kay ³⁷, S. Kazakos ¹⁰⁷, K. Kazakova ¹⁰², J.M. Keaveney ^{34a}, R. Keeler ¹⁶⁸, G.V. Kehris ⁶⁰, J.S. Keller ³⁵, J.M. Kelly ¹⁶⁸, J.J. Kempster ¹⁵⁰, O. Kepka ¹³³, J. Kerr ^{160b}, B.P. Kerridge ¹³⁶, B.P. Kerševan ⁹³, L. Keszeghova ^{29a}, R.A. Khan ¹³¹, A. Khanov ¹²³, M. Kholodenko ^{132a},

T.J. Khoo ¹⁹, G. Khoriali ¹⁶⁹, Y. Khoulaki ^{36a}, Y.A.R. Khwaira ¹²⁹, D. Kim ⁶, D.W. Kim ^{18b}, Y.K. Kim ³⁹, N. Kimura ⁹⁶, M.K. Kingston ⁵⁴, F. Kirfel ²⁵, J. Kirk ¹³⁶, A.E. Kiryunin ¹¹⁰, S. Kita ¹⁶¹, O. Kivernyk ²⁵, M. Klassen ¹⁶², C. Klein ³⁵, L. Klein ¹⁶⁹, M.H. Klein ⁴⁴, S.B. Klein ⁵⁵, U. Klein ⁹², A. Klimentov ³⁰, P. Kluit ¹¹⁶, S. Kluth ¹¹⁰, E. Kneringer ⁷⁸, T.M. Knight ¹⁵⁹, A. Knue ⁴⁸, M. Kobel ⁴⁹, D. Kobylianskii ¹⁷², S.F. Koch ³⁷, M. Kocian ¹⁴⁷, P. Kodyš ¹³⁵, D.M. Koeck ¹²⁵, T. Koffas ³⁵, K. Kojima ⁸², O. Kolay ⁴⁹, I. Koletsou ⁴, T. Komarek ⁸⁶, S. Kondo ¹⁵⁷, K. Köneke ⁵⁴, A.X.Y. Kong ¹, T. Kono ¹²⁰, N. Konstantinidis ⁹⁶, P. Kontaxakis ⁵⁵, B. Konya ⁹⁸, R. Kopeliansky ⁴¹, S. Koperny ^{35a}, R. Koppenhofer ⁵³, K. Korcyl ⁸⁶, K. Kordas ^{156,d}, A. Korn ⁹⁶, S. Korn ⁵⁴, I. Korolkov ¹³, B. Kortman ¹¹⁶, O. Kortner ¹¹⁰, S. Kortner ¹¹⁰, W.H. Kostecka ¹¹⁷, M. Kostov ^{29a}, V.V. Kostyukhin ¹⁴⁵, A. Kotsokechagia ³⁷, A. Kotwal ⁵⁰, A. Koulouris ³⁷, A. Kourkoumeli-Charalampidi ^{72a,72b}, O. Kovanda ¹²⁵, R. Kowalewski ¹⁶⁸, W. Kozanecki ¹²⁵, G. Kramberger ⁹³, P. Kramer ²⁵, A. Krasznahorkay ¹⁰³, A.C. Kraus ¹¹⁷, J.W. Kraus ¹⁷⁴, J.A. Kremer ⁴⁷, N.B. Kregel ¹⁴⁵, T. Kresse ¹⁵⁹, L. Kretschmann ¹⁷⁴, J. Kretschmar ⁹², P. Krieger ¹⁵⁹, K. Krizka ²¹, K. Kroeninger ⁴⁸, H. Kroha ¹¹⁰, J. Kroll ¹³³, J. Kroll ¹³⁰, K.S. Krowpman ¹⁰⁷, U. Kruchonak ³⁸, H. Krüger ²⁵, N. Krumnack ⁷⁹, J. Krupa ¹⁴⁷, M.C. Kruse ⁵⁰, O. Kuchinskaia ³⁸, S. Kuday ^{3a}, S. Kuehn ³⁷, R. Kuesters ⁵³, T. Kuhl ⁴⁷, V. Kukhtin ³⁸, Y. Kulchitsky ³⁸, S. Kuleshov ^{139d,139b}, J. Kull ¹, E.V. Kumar ¹⁰⁹, M. Kumar ^{34j}, N. Kumari ⁴⁷, P. Kumari ^{160b}, A. Kupco ¹³³, O. Kuprash ⁵³, H. Kurashige ⁸⁴, L.L. Kurchaninov ^{160a}, O. Kurdysh ⁴, M. Kuze ¹⁴⁰, A.K. Kvam ¹⁰³, J. Kvita ¹²⁴, N.G. Kyriacou ¹⁴¹, M. Laassiri ³⁰, C. Lacasta ¹⁶⁶, H. Lacker ¹⁹, D. Lacour ¹²⁹, E. Ladygin ³⁸, A. Lafarge ⁴⁰, B. Laforge ¹²⁹, T. Lagouri ¹⁷⁵, F.Z. Lahbabi ^{36a}, S. Lai ⁵⁴, W.S. Lai ⁹⁶, I.K. Lakomic ⁵⁴, J.E. Lambert ¹⁶⁸, S. Lammers ⁶⁷, W. Lampl ⁷, C. Lampoudis ¹⁵⁶, G. Lamprinoudis ¹⁶⁹, A.N. Lancaster ¹¹⁷, U. Landgraf ⁵³, M.P.J. Landon ⁹⁴, V.S. Lang ⁵³, A.J. Lankford ¹⁶³, F. Lanni ³⁷, C.S. Lantz ¹⁶⁵, K. Lantzsch ²⁵, A. Lanza ^{72a}, M. Lanzac Berrocal ¹⁶⁶, T. Lari ^{70a}, D. Larsen ¹⁷, L. Larson ¹¹, F. Lasagni Manghi ^{24b}, M. Lassnig ³⁷, H.C. Lau ¹⁶⁸, S.D. Lawlor ¹⁴³, R. Lazaridou ¹⁶³, M. Lazzaroni ^{70a,70b}, E.T.T. Le ¹⁶³, H.D.M. Le ¹⁰⁷, E.M. Le Boulicaut ¹⁷⁵, L.T. Le Pottier ^{18a}, B. Leban ^{24b,24a}, F. Ledroit-Guillon ⁵⁹, T.F. Lee ^{160b}, L.L. Leeuw ^{34h}, M. Lefebvre ¹⁶⁸, C. Leggett ^{18a}, L.M. Lehmann ¹¹⁶, G. Lehmann Miotto ³⁷, M. Leigh ⁵⁵, W.A. Leight ¹⁰³, W. Leinonen ¹¹⁵, A. Leisos ^{156,t}, M.A.L. Leite ^{81c}, C.E. Leitgeb ¹⁹, R. Leitner ¹³⁵, K.J.C. Leney ⁴⁴, T. Lenz ²⁵, S. Leone ^{73a}, C. Leonidopoulos ⁵¹, A. Leopold ¹⁴⁸, J. LePage-Bourbonnais ³⁵, R. Les ¹⁰⁷, C.G. Lester ³³, J. Levêque ⁴, L.J. Levinson ¹⁷², G. Levrini ^{24b,24a}, M.P. Lewicki ⁸⁶, C. Lewis ¹⁴¹, D.J. Lewis ⁴, L. Lewitt ¹⁴³, A. Li ³⁰, B. Li ^{113b}, C. Li ¹⁰⁶, C-Q. Li ¹¹⁰, H. Li ^{113b}, H. Li ¹⁰¹, H. Li ¹⁵, H. Li ⁶¹, H. Li ^{113b}, J. Li ^{142a}, L. Li ^{142a}, R. Li ¹⁷⁵, S. Li ^{142b,142a}, T. Li ⁵, Y. Li ¹⁴, Z. Li ^{14,112c}, Z. Li ⁶¹, S. Liang ^{14,112c}, Z. Liang ¹⁴, M. Liberatore ¹³⁷, B. Liberti ^{75a}, G.B. Libotte ^{81d}, K. Lie ^{63c}, J. Lieber Marin ^{81e}, H. Lien ⁶⁷, H. Lin ¹⁰⁶, S.F. Lin ¹⁴⁹, L. Linden ¹⁰⁹, R.E. Lindley ⁷, J.H. Lindon ³⁷, J. Ling ⁶⁰, E. Lipeles ¹³⁰, A. Lipniacka ¹⁷, A. Lister ¹⁶⁷, J.D. Little ⁶⁷, B. Liu ^{113a}, B.X. Liu ^{112b}, D. Liu ¹⁵⁴, D. Liu ¹³⁸, E.H.L. Liu ²¹, H. Liu ^{112b}, J.K.K. Liu ¹¹⁹, K. Liu ^{142b}, K. Liu ^{142b}, M. Liu ⁶¹, M.Y. Liu ⁶¹, P. Liu ^{113b}, Q. Liu ¹⁴⁷, S. Liu ¹⁴⁹, X. Liu ^{113b}, Y. Liu ^{112b,112c}, Y. Liu ¹⁶⁵, Y.L. Liu ^{113b}, Y.W. Liu ⁶¹, Z. Liu ^{65,j}, S.L. Lloyd ⁹⁴, E.M. Lobodzinska ⁴⁷, P. Loch ⁷, E. Lodhi ¹⁵⁹, K. Lohwasser ¹⁴³, E. Loiacono ¹²³, J.D. Lomas ²¹, I. Longarini ¹⁶³, R. Longo ^{24b,24a,an}, A. Lopez Solis ¹³, N.A. Lopez-canelas ⁷, N. Lorenzo Martinez ⁴, A.M. Lory ¹⁰⁹, M. Losada ^{118a}, G. Lösckce Centeno ⁴, X. Lou ^{14,112c}, P.A. Love ⁹¹, M. Lu ⁶⁵, S. Lu ¹³⁰, Y.J. Lu ¹⁵², H.J. Lubatti ¹⁴¹, C. Luci ^{74a,74b}, F.L. Lucio Alves ^{112a}, F. Luehring ⁶⁷, B.S. Lunday ¹³⁰, O. Lundberg ¹⁴⁸, J. Lunde ³⁷, N.A. Luongo ⁶, M.S. Lutz ¹⁵⁹, A.B. Lux ²⁶, D. Lynn ³⁰, R. Lysak ¹³³, V. Lysenko ¹³⁴, E. Lytken ⁹⁸, V. Lyubushkin ³⁸, T. Lyubushkina ³⁸, M.M. Lyukova ¹⁴⁹, H. Ma ³⁰, K. Ma ⁶¹,

L.L. Ma ^{113b}, W. Ma ⁶¹, Y. Ma ^{113b}, J.C. MacDonald ¹⁰⁰, P.C. Machado De Abreu Farias ^{81e}, D. Macina ³⁷, R. Madar ⁴⁰, T. Madula ⁹⁶, J. Maeda ⁸⁴, T. Maeno ³⁰, P.T. Mafa ^{34f}, H. Maguire ¹⁴³, M. Maheshwari ³³, V. Maiboroda ⁶⁵, A. Maio ^{132a,132b,132d}, K. Maj ^{85a}, O. Majersky ⁴⁷, S. Majewski ¹²⁵, A. Makita ¹⁵⁷, N. Makovec ⁶⁵, V. Maksimovic ¹⁶, B. Malaescu ¹²⁹, J. Malamant ¹²⁷, Pa. Malecki ⁸⁶, F. Malek ^{59,n}, M. Mali ⁹³, D. Malito ⁹⁵, A. Maloizel ⁵, A. Malvezzi Lopes ^{81d}, S. Malyukov ³⁸, J. Mamuzic ⁹³, G. Mancini ⁵², M.N. Mancini ²⁷, G. Manco ^{72a,72b}, S.S. Mandarry ¹⁵⁰, I. Mandić ⁹³, L. Manhaes de Andrade Filho ^{81a}, I.M. Maniatis ¹⁷², J. Manjarres Ramos ⁸⁹, D.C. Mankad ¹⁷², A. Mann ¹⁰⁹, T. Manoussos ³⁷, M.N. Mantinan ³⁹, S. Manzoni ³⁷, L. Mao ^{142a}, X. Mapekula ^{34c}, A. Marantis ¹⁵⁶, R.R. Marcelo Gregorio ¹, G. Marchiori ⁵, C. Marcon ^{70a}, E. Maricic ¹⁶, M. Marinescu ⁴⁷, S. Marium ⁴⁷, M. Marjanovic ¹²², A. Markhoos ⁵³, M. Markovitch ⁶⁵, M.K. Maroun ¹⁰³, M.C. Marr ¹⁴⁶, G.T. Marsden ¹⁰¹, Z. Marshall ^{18a}, S. Marti-Garcia ¹⁶⁶, J. Martin ⁹⁶, T.A. Martin ¹³⁶, V.J. Martin ⁵¹, B. Martin dit Latour ¹⁷, L. Martinelli ^{74a,74b}, V.I. Martinez Outschoorn ¹⁰³, P. Martinez Suarez ³⁷, S. Martin-Haugh ¹³⁶, G. Martinovicova ¹³⁵, V.S. Martoiu ^{28b}, A. Martone ⁸⁹, A.C. Martyniuk ⁹⁶, A. Marzin ³⁷, D. Mascione ^{77a,77b}, L. Masetti ¹⁰⁰, J. Masik ¹⁰¹, A.L. Maslennikov ³⁸, S.L. Mason ⁴¹, P. Massarotti ^{71a,71b}, P. Mastrandrea ^{73a,73b}, A. Mastroberardino ^{43b,43a}, T. Masubuchi ¹²⁶, T.T. Mathew ¹²⁵, J. Matousek ¹³⁵, D.M. Mattern ⁴⁸, K. Mauer ⁴⁷, J. Maurer ^{28b}, T. Maurin ⁵⁸, A.J. Maury ⁶⁵, B. Maček ⁹³, C. Mavungu Tsava ¹⁰², A.E. May ¹⁰¹, E. Mayer ⁴⁰, R. Mazini ^{34j}, S.M. Mazza ¹³⁸, E. Mazzeo ³⁷, J.P. Mc Gowan ¹⁶⁸, S.P. Mc Kee ¹⁰⁶, C.C. McCracken ¹⁶⁷, E.F. McDonald ¹⁰⁵, L.F. Mcelhinney ⁹¹, J.A. Mcfayden ¹⁵⁰, R.P. McGovern ¹³⁰, R.P. Mckenzie ^{34j}, D.J. Mclaughlin ⁹⁶, S.J. McMahan ¹³⁶, C.M. Mcpartland ⁹², R.A. McPherson ^{168,ab}, S. Mehlhase ¹⁰⁹, A. Mehta ⁹², D. Melini ¹⁶⁶, B.R. Mellado Garcia ^{14,ah}, A.H. Melo ⁵⁴, F. Meloni ⁴⁷, A.M. Mendes Jacques Da Costa ¹⁰¹, L. Meng ⁹¹, S. Menke ¹¹⁰, M. Mentink ³⁷, E. Meoni ^{43b,43a}, G. Mercado ¹¹⁷, S. Merianos ¹⁵⁶, C. Merlassino ^{68a,68c}, C. Meroni ^{70a,70b}, J. Metcalfe ⁶, A.S. Mete ⁶, E. Meuser ¹⁰⁰, C. Meyer ⁶⁷, J-P. Meyer ¹³⁷, Y. Miao ^{112a}, R.P. Middleton ¹³⁶, M. Mihovilovic ⁶⁵, L. Mijović ⁵¹, G. Mikenberg ¹⁷², M. Mikestikova ¹³³, M. Mikuž ⁹³, H. Mildner ¹⁰⁰, A. Milic ³⁷, D.W. Miller ³⁹, E.H. Miller ¹⁴⁷, A. Milov ¹⁷², D.A. Milstead ^{46a,46b}, T. Min ^{112a}, I.A. Minashvili ^{153b}, A.I. Mincer ¹¹⁹, B. Mindur ^{85a}, M. Mineev ³⁸, Y. Mino ⁸⁷, L.M. Mir ¹³, M. Miralles Lopez ⁵⁸, M. Mironova ^{18a}, M. Missio ⁴⁰, A. Mitra ¹⁷⁰, V.A. Mitsou ¹⁶⁶, Y. Mitsumori ¹¹¹, P.S. Miyagawa ⁹⁴, R. Mizuhiki ⁸⁴, T. Mkrtchyan ³⁷, M. Mlinarevic ⁹⁶, T. Mlinarevic ⁹⁶, M. Mlynarikova ¹³⁵, L. Mlynarska ^{85a}, C. Mo ^{142a}, S. Mobius ²⁰, M.H. Mohamed Farook ¹¹⁴, S. Mohapatra ⁴¹, M.F. Mohd Soberi ⁵¹, S. Mohiuddin ¹²³, G. Mokgatitwane ^{34j}, R. Mole ²¹, L. Moleri ¹⁷², U. Molinatti ¹²⁸, L.G. Mollier ²⁰, B. Mondal ¹³³, S. Mondal ¹³⁵, K. Mönig ⁴⁷, E. Monnier ¹⁰², L. Monsonis Romero ¹⁶⁶, A. Montella ^{46a,46b}, M. Montella ¹²¹, F. Montereali ^{76a,76b}, F. Monticelli ⁹⁰, S. Monzani ^{68a,68c}, M.E.E. Moors ²⁵, A. Morancho Tarda ⁴², N. Morange ⁶⁵, M. Moreno Llácer ¹⁶⁶, C. Moreno Martinez ⁵⁵, J.M. Moreno Perez ^{23b}, P. Morettini ^{56b}, S. Morgenstern ^{62a}, M. Morii ⁶⁰, M. Morinaga ¹⁵⁷, F. Morodei ^{74a,74b}, P. Moschovakos ³⁷, B. Moser ⁵³, M. Mosidze ^{153b}, T. Moskalets ⁴⁴, P. Moskvitina ¹¹⁵, C.J. Mosomane ^{34b}, J. Moss ³², T. Motta Quirino ^{81d}, A. Moussa ^{36d}, Y. Moyal ^{172,k}, H. Moyano Gomez ¹³, E.J.W. Moyse ¹⁰³, T.G. Mroz ⁸⁶, S. Muanza ¹⁰², M. Mucha ²⁵, J. Mueller ¹³¹, D. Muller ¹⁴⁵, G.A. Mullier ¹⁶⁴, A.J. Mullin ³³, J.J. Mullin ⁵⁰, A.C. Mullins ⁴⁴, A.E. Mulski ⁶⁰, D.P. Mungo ¹⁵⁹, D. Munoz Perez ¹²³, F.J. Munoz Sanchez ¹⁰¹, W.J. Murray ^{170,136}, E. Musajan ⁶¹, M. Muškinja ⁹³, C. Mwewa ⁴⁷, A.J. Myers ⁸, G. Myers ¹⁰⁶, M. Myska ¹³⁴, B.P. Nachman ¹⁴⁷, K. Nagai ¹²⁸, K. Nagano ⁸², R. Nagasaka ¹⁵⁷, J.L. Nagle ^{30,ap}, E. Nagy ¹⁰², A.M. Nairz ³⁷, T. Nakagawa ⁸⁷, Y. Nakahama ⁸², K. Nakamura ⁸², K. Nakkalil ⁵, A. Nandi ^{62b}, H. Nanjo ¹²⁶, E.A. Narayanan ⁴⁴,

Y. Narukawa ¹⁵⁷, L. Nasella ^{70a,70b}, S. Nasri ^{118b}, C. Nass ²⁵, G. Navarro ^{23a}, A. Nayaz ¹⁹,
 S. Nechaeva ^{24b,24a}, F. Nechansky ¹³³, L. Nedic ¹²⁸, A. Negri ^{72a,72b}, M. Negrini ^{24b},
 C. Nellist ¹¹⁶, C. Nelson ¹⁰⁴, K. Nelson ¹⁰⁶, S. Nemecek ¹³³, M. Nessi ^{37,g}, M.S. Neubauer ¹⁶⁵,
 J. Newell ⁹², P.R. Newman ²¹, Y.W.Y. Ng ¹⁶⁵, B. Ngair ^{118a}, H.D.N. Nguyen ¹⁰⁸,
 J.D. Nichols ¹²², R. Nicolaidou ¹³⁷, J. Nielsen ¹³⁸, M. Niemeyer ⁵⁴, J. Niermann ³⁷,
 N. Nikiforou ³⁷, I. Nikolic-Audit ¹²⁹, P. Nilsson ³⁰, G. Ninio ¹⁵⁵, A. Nisati ^{74a}, R. Nisius ¹¹⁰,
 N. Nitika ¹⁷², E.K. Nkadimeng ^{34b}, T. Nobe ¹⁵⁷, D. Noll ¹⁴⁷, T. Nommensen ¹⁵¹,
 M.B. Norfolk ¹⁴³, B.J. Norman ³⁵, L.C. Nosler ^{18a}, M. Noury ^{36a}, J. Novak ⁹³, T. Novak ⁹³,
 P. Novotny ¹⁷², R. Novotny ¹³⁴, L. Nozka ¹²⁴, K. Ntekas ³⁷, D. Ntounis ¹⁴⁷,
 N.M.J. Nunes De Moura Junior ^{81b}, J. Ocariz ¹²⁹, I. Ochoa ^{132a}, A. Odella Rodriguez ¹³,
 S. Oerde ⁴⁷, J.T. Offermann ³⁹, A. Ogrodnik ⁸⁶, A. Oh ¹⁰¹, C.C. Ohm ¹⁴⁸, H. Oide ⁸²,
 M.L. Ojeda ³⁷, Y. Okumura ¹⁵⁷, L.F. Oleiro Seabra ^{132a}, I. Oleksiyuk ⁵⁵, G. Oliveira Correa ¹³,
 D. Oliveira Damazio ³⁰, J.L. Oliver ¹, R. Omar ⁶⁷, A.P. O'Neill ²⁰, Y. Onoda ¹⁴⁰,
 A. Onofre ^{132a,132e,e}, P.U.E. Onyisi ¹¹, M.J. Oreglia ³⁹, D. Orestano ^{76a,76b}, R. Orlandini ^{76a,76b},
 R.S. Orr ¹⁵⁹, L.M. Osojnak ⁴¹, Y. Osumi ¹¹¹, G. Otero y Garzón ³¹, H. Otono ⁸⁸,
 M. Ouchrif ^{36d}, F. Ould-Saada ¹²⁷, T. Ovsiannikova ¹⁴¹, M. Owen ⁵⁸, R.E. Owen ¹³⁶,
 S.A. Oyeniran ¹¹⁴, V.E. Ozcan ^{22a}, F. Ozturk ⁸⁶, N. Ozturk ⁸, S. Ozturk ⁸⁰, H.A. Pacey ¹²⁸,
 K. Pachal ^{160a}, A. Pacheco Pages ¹³, C. Padilla Aranda ¹³, G. Padovano ^{74a,74b},
 S. Pagan Griso ^{18a}, L. Pagani ^{75a,75b}, J. Pampel ²⁵, D.K. Panchal ¹¹, C.E. Pandini ⁵⁹,
 J.G. Panduro Vazquez ¹³⁶, H.D. Pandya ¹, H. Pang ¹³⁷, P. Pani ⁴⁷, G. Panizzo ^{68a,68c},
 L. Panwar ^{129,w}, L. Paolozzi ⁵⁵, S. Parajuli ¹⁶⁵, A. Paramonov ⁶, C. Paraskevopoulos ⁵²,
 D. Paredes Hernandez ^{63b}, S.R. Paredes Saenz ⁵¹, A. Pareti ^{72a,72b}, K.R. Park ⁴¹, T.H. Park ¹¹⁰,
 F. Parodi ^{56b,56a}, J.A. Parsons ⁴¹, U. Parzefall ⁵³, B.A. Paschen ^{18a}, B. Pascual Dias ⁴⁰,
 L. Pascual Dominguez ⁹⁹, E. Pasqualucci ^{74a}, S. Passaggio ^{56b}, F. Pastore ⁹⁵, P. Patel ⁸⁶,
 U.M. Patel ⁵⁰, J.R. Pater ¹⁰¹, T. Pauly ³⁷, A. Paunovic ¹⁶, F. Pauwels ¹³⁵, C.I. Pazos ¹⁶²,
 M. Pedersen ¹²⁷, R. Pedro ^{132a}, O. Penc ¹³³, C.C. Penelaud ¹²⁹, S. Peng ¹⁵, G.D. Penn ¹⁷⁵,
 B.S. Peralva ^{81d}, A.P. Pereira Peixoto ¹⁴¹, L. Pereira Sanchez ¹⁴⁷, D.V. Perepelitsa ^{30,ap},
 G. Perera ¹⁰³, E. Perez Codina ³⁷, M. Perganti ¹⁰, H. Pernegger ³⁷, S. Perrella ^{74a,74b},
 K. Peters ⁴⁷, R.F.Y. Peters ¹⁰¹, B.A. Petersen ³⁷, T.C. Petersen ⁴², E. Petit ¹⁰², V. Petousis ¹³⁴,
 A.R. Petri ^{70a,70b}, T. Petru ¹³⁵, M. Pettee ^{18a}, A. Petukhov ⁸⁰, K. Petukhova ³⁷, R. Pezoa ^{139g},
 L. Pezzotti ^{24b,24a}, G. Pezzullo ¹⁷⁵, L. Pfaffenbichler ³⁷, A.J. Pflieger ⁷⁸, T.M. Pham ¹⁷³,
 T. Pham ¹⁰⁵, P.W. Phillips ¹³⁶, G. Piacquadio ¹⁴⁹, E. Pianori ^{18a}, F. Piazza ¹²⁵, R. Piegai ³¹,
 D. Pietreanu ^{28b}, A.D. Pilkington ¹⁰¹, M. Pinamonti ^{68a,68c}, J.L. Pinfeld ², G. Pinheiro Matos ⁴¹,
 B.C. Pinheiro Pereira ^{132a}, J. Pinol Bel ¹³, A.E. Pinto Pinoargote ¹²⁹, L. Pintucci ^{68a,68c},
 K.M. Piper ¹⁵⁰, A. Pirttikoski ⁵⁵, D.A. Pizzi ³⁵, L. Pizzimento ^{63b}, A. Plebani ³³,
 M.-A. Pleier ³⁰, V. Pleskot ¹³⁵, E. Plotnikova ³⁸, G. Poddar ⁹⁴, R. Poettgen ⁹⁸, L. Poggioli ¹²⁹,
 S. Polacek ¹³⁵, G. Polesello ^{72a}, A. Poley ¹⁴⁶, A. Polini ^{24b}, C.S. Pollard ¹⁷⁰, Z.B. Pollock ¹²¹,
 E. Pompa Pacchi ¹²², N.I. Pond ⁹⁶, D. Ponomarenko ⁶⁷, L. Pontecorvo ³⁷, S. Popa ^{28a},
 G.A. Popeneciu ^{28d}, A. Poreba ^{62a}, D.M. Portillo Quintero ^{160a}, S. Pospisil ¹³⁴, M.A. Postill ¹⁴³,
 P. Postolache ^{28c}, K. Potamianos ¹⁷⁰, P.A. Potepa ^{85a}, I.N. Potrap ³⁸, C.J. Potter ³³, H. Potti ¹⁵¹,
 J. Poveda ¹⁶⁶, M.E. Pozo Astigarraga ³⁷, R. Pozzi ³⁷, A. Prades Ibanez ^{75a,75b}, S.R. Pradhan ¹⁴³,
 J. Pretel ¹⁶⁸, D. Price ¹⁰¹, M. Primavera ^{69a}, L. Primomo ^{68a,68c}, M.A. Principe Martin ⁹⁹,
 R. Privara ¹²⁴, T. Procter ^{85b}, M.L. Proffitt ¹⁴¹, N. Proklova ¹³⁰, K. Prokofiev ^{63c}, G. Proto ¹¹⁰,
 J. Proudfoot ⁶, M. Przybycien ^{85a}, W.W. Przygoda ^{85b}, A. Psallidas ⁴⁵, D. Pudzha ⁵², P. Puhl ⁵⁷,
 H.I. Purnell ¹, D. Pyatiizbyantseva ¹¹⁵, J. Qian ¹⁰⁶, R. Qian ¹⁰⁷, D. Qichen ¹²⁸, Y. Qin ¹³,
 T. Qiu ⁵¹, A. Quadt ⁵⁴, M. Queitsch-Maitland ¹⁰¹, G. Quetant ⁵⁵, R.P. Quinn ¹⁶⁷,
 D. Rafanoharana ¹¹⁰, J.L. Rainbolt ³⁹, S. Rajagopalan ³⁰, E. Ramakoti ³⁸, L. Rambelli ^{56b,56a},

I.A. Ramirez-Berend [ID35](#), K. Ran [ID106,112c](#), S.D. Randles [ID92](#), D.S. Rankin [ID130](#), N.P. Rapheeha [ID34j](#),
 H. Rasheed [ID28b](#), A. Rastogi [ID18a](#), S. Rave [ID100](#), S. Ravera [ID56b,56a](#), B. Ravina [ID37](#), I. Ravinovich [ID172](#),
 M. Raymond [ID37](#), A.L. Read [ID127](#), N.P. Readioff [ID143](#), D.M. Rebuzzi [ID72a,72b](#), A.S. Reed [ID58](#),
 K. Reeves [ID27](#), D. Reikher [ID37](#), A. Rej [ID48](#), C. Rembser [ID37](#), H. Ren [ID61](#), M. Renda [ID28b](#), F. Renner [ID47](#),
 A.G. Rennie [ID58](#), M. Repik [ID55](#), A.L. Rescia [ID56b,56a](#), S. Resconi [ID70a](#), M. Ressegotti [ID56b](#),
 S. Rettie [ID116](#), W.F. Rettie [ID35](#), M.M. Revering [ID33](#), O.L. Rezanova [ID38](#), P. Reznicek [ID135](#), H. Riani [ID36d](#),
 N. Ribaric [ID50](#), B. Ricci [ID68a,68c](#), E. Ricci [ID77a,77b](#), R. Richter [ID110](#), E. Richter-Was [ID85b](#), M. Ridel [ID129](#),
 S. Ridouani [ID36d](#), P. Riedler [ID37](#), E.M. Riefel [ID46a,46b](#), J.O. Rieger [ID116](#), M. Rimoldi [ID34c](#),
 L. Rinaldi [ID24b,24a](#), P. Rincke [ID164,54](#), G. Ripellino [ID164](#), I. Riu [ID13](#), J.C. Rivera Vergara [ID168](#),
 F. Rizatdinova [ID123](#), E. Rizvi [ID94](#), B.R. Roberts [ID39](#), S.S. Roberts [ID138](#), D. Robinson [ID33](#), A. Robson [ID58](#),
 A. Rocchi [ID75a,75b](#), C. Roda [ID73a,73b](#), F.A. Rodriguez [ID117](#), S. Rodriguez Bosca [ID37](#),
 Y. Rodriguez Garcia [ID23a](#), A.M. Rodríguez Vera [ID117](#), S. Roe [ID37](#), J.T. Roemer [ID37](#), O. Røhne [ID127](#),
 R.A. Rojas [ID37](#), Z. Rokavec [ID93](#), C.P.A. Roland [ID129](#), A. Romaniouk [ID78](#), E. Romano [ID72a,72b](#),
 M. Romano [ID24b](#), N. Rompotis [ID92](#), L. Roos [ID129](#), S. Rosati [ID74a](#), L. Roscher [ID47](#), B.J. Rosser [ID39](#),
 E. Rossi [ID128](#), E. Rossi [ID71a,71b](#), L.P. Rossi [ID60](#), L. Rossini [ID53](#), R. Rosten [ID121](#), M. Rotaru [ID28b](#),
 R. Roth [ID37](#), D. Rousseau [ID65](#), D. Rousso [ID47](#), S. Roy-Garand [ID159](#), A. Rozanov [ID102](#),
 Z.M.A. Rozario [ID58](#), Y. Rozen [ID154](#), A. Rubio Jimenez [ID166](#), V.H. Ruelas Rivera [ID19](#), T.A. Ruggeri [ID1](#),
 A. Ruggiero [ID128](#), A. Ruiz-Martinez [ID166](#), A. Rummler [ID37](#), G.B. Rupnik Boero [ID37](#),
 N.A. Rusakovich [ID38](#), S. Ruscelli [ID48](#), H.L. Russell [ID168](#), G. Russo [ID138](#), J.P. Rutherford [ID7](#),
 S. Rutherford Colmenares [ID119](#), M. Rybar [ID135](#), P. Rybczynski [ID85a](#), M.J. Ryczkowski [ID1](#), A. Ryzhov [ID44](#),
 F. Safai Tehrani [ID74a](#), S. Saha [ID1](#), B. Sahoo [ID172](#), A. Saibel [ID166](#), B.T. Saifuddin [ID122](#), M. Saimpert [ID137](#),
 I. Sainz Saenz Diez [ID62a](#), G.T. Saito [ID81c](#), M. Saito [ID157](#), T. Saito [ID157](#), A. Sala [ID70a,70b](#), O.T. Salin [ID65](#),
 A. Salnikov [ID147](#), J. Salt [ID166](#), A. Salvador Salas [ID155](#), F. Salvatore [ID150](#), A. Salzburger [ID37](#),
 D. Sammel [ID53](#), E. Sampson [ID91](#), D. Sampsonidis [ID156,d](#), D. Sampsonidou [ID125](#), M.A.A. Samy [ID58](#),
 J. Sánchez [ID166](#), V. Sanchez Sebastian [ID166](#), H. Sandaker [ID127](#), C.O. Sander [ID47](#), J.A. Sandesara [ID173](#),
 M. Sandhoff [ID174](#), C. Sandoval [ID23b](#), L. Sanfilippo [ID62a](#), D.P.C. Sankey [ID136](#), T. Sano [ID87](#),
 A. Sansar [ID22c](#), A. Sansoni [ID52](#), M. Santana Queiroz [ID18b](#), L. Santi [ID37](#), C. Santoni [ID40](#),
 H. Santos [ID132a,132b](#), L. Santos Pereira Trigo [ID47](#), E. Sanzani [ID24b,24a](#), K.A. Saoucha [ID83b](#),
 J.G. Saraiva [ID132a,132d](#), J. Sardain [ID7](#), S. Sarkar [ID50](#), O. Sasaki [ID82](#), K. Sato [ID161](#), C. Sauer [ID37](#),
 E. Sauvan [ID4](#), P. Savard [ID159,aj](#), R. Sawada [ID157](#), C. Sawyer [ID136](#), L. Sawyer [ID97](#), A.M. Sayed [ID27](#),
 C. Sbarra [ID24b](#), A. Sbrizzi [ID24b,24a](#), R. Scaglioni [ID72a,72b](#), T. Scanlon [ID96](#), J. Schaarschmidt [ID141](#),
 U. Schäfer [ID100](#), A.C. Schaffer [ID65,44](#), D. Schaile [ID109](#), R.D. Schamberger [ID149](#), C. Scharf [ID19](#),
 M.M. Schefer [ID20](#), D. Scheirich [ID135](#), M. Schernau [ID139f](#), C. Scheulen [ID55](#), C. Schiavi [ID56b,56a](#),
 M. Schioppa [ID43b,43a](#), S. Schlenker [ID37](#), T. Schlomer [ID54](#), J. Schmeing [ID174](#), C.R. Schmidt [ID49](#),
 E. Schmidt [ID110](#), M.A. Schmidt [ID174](#), K. Schmieden [ID25](#), C. Schmitt [ID100](#), N. Schmitt [ID100](#),
 S. Schmitt [ID47](#), N.A. Schneider [ID109](#), L. Schoeffel [ID137](#), A. Schoening [ID62b](#), P.G. Scholer [ID35](#),
 E. Schopf [ID145](#), M. Schott [ID25](#), S. Schramm [ID55](#), T. Schroer [ID55](#), H-C. Schultz-Coulon [ID62a](#),
 M. Schumacher [ID53](#), B.A. Schumm [ID138](#), Ph. Schune [ID137](#), H.R. Schwartz [ID7](#), A. Schwartzman [ID147](#),
 T.A. Schwarz [ID106](#), Ph. Schwemling [ID137](#), R. Schwienhorst [ID107](#), F.G. Sciacca [ID20](#), A. Sciandra [ID30](#),
 G. Sciolla [ID27](#), S.A. Scoville [ID131](#), F. Scuri [ID73a](#), C.D. Sebastiani [ID37](#), K. Sedlaczek [ID117](#),
 A. Sehrawat [ID139b](#), S.C. Seidel [ID114](#), B.D. Seidlitz [ID41](#), C. Seitz [ID47](#), J.M. Seixas [ID81b](#),
 G. Sekhniadze [ID71a](#), L. Selem [ID129](#), N. Semprini-Cesari [ID24b,24a](#), A. Semushin [ID176](#),
 V. Senthilkumar [ID116](#), L. Serin [ID65](#), M. Sessa [ID71a,71b](#), H. Severini [ID122](#), F. Sforza [ID56b,56a](#), A. Sfyrla [ID55](#),
 Q. Sha [ID14](#), H. Shaddix [ID117](#), A.H. Shah [ID33](#), R. Shaheen [ID148](#), J.D. Shahinian [ID130](#), M. Shamim [ID37](#),
 L.Y. Shan [ID14](#), M. Shapiro [ID18a](#), A. Sharma [ID37](#), A.S. Sharma [ID167](#), P. Sharma [ID30](#), K. Shaw [ID150](#),
 S.M. Shaw [ID101](#), D. Shemyakin [ID172](#), Q. Shen [ID14](#), D.J. Sheppard [ID146](#), P. Sherwood [ID96](#), L. Shi [ID112b](#),
 X. Shi [ID14](#), S. Shimizu [ID82](#), S. Shirabe [ID88](#), M. Shiyakova [ID38,z](#), M.J. Shochet [ID39](#), D.R. Shope [ID127](#),

B. Shrestha ¹²², S. Shrestha ^{121,ar}, I. Shreyber ³⁸, M.J. Shroff ¹⁰⁴, P. Sicho ¹³³, A.M. Sickles ¹⁶⁵,
 E. Sideras Haddad ^{34j}, A.C. Sidley ¹¹⁶, A. Sidoti ^{24b}, F. Siegert ⁴⁹, Dj. Sijacki ¹⁶, F. Sili ⁶¹,
 J.M. Silva ⁵¹, I. Silva Ferreira ^{81b}, M.V. Silva Oliveira ³⁰, S.B. Silverstein ^{46a}, S. Simion ⁶⁵,
 R. Simoniello ³⁷, E.L. Simpson ¹⁰¹, H. Simpson ¹⁵⁰, L.R. Simpson ⁶, S. Simsek ⁸⁰,
 S. Sindhu ⁵⁴, S.N. Singh ²⁷, S. Singh ³⁰, S. Sinha ⁴⁷, S. Sinha ¹⁰¹, M. Sioli ^{24b,24a},
 K. Sioulas ⁹, I. Siral ³⁷, E. Sitnikova ⁴⁷, J. Sjölin ^{46a,46b}, A. Skaf ⁵⁴, E. Skorda ²¹,
 P. Skubic ¹²², M. Slawinska ⁸⁶, I. Slazyk ¹⁷, I. Sliusar ¹²⁷, V. Smakhtin ¹⁷², B.H. Smart ¹³⁶,
 S.Yu. Smirnov ^{139b}, Y. Smirnov ^{34c}, O. Smirnova ⁹⁸, A.C. Smith ⁴¹, J.L. Smith ¹⁰¹,
 M.B. Smith ³⁵, R. Smith ¹⁴⁷, H. Smitmanns ¹⁰⁰, M. Smizanska ⁹¹, K. Smolek ¹³⁴,
 P. Smolyanskiy ¹³⁴, A.A. Snesarev ³⁸, H.L. Snoek ¹¹⁶, R.M. Snyder ⁵⁰, S. Snyder ³⁰,
 R. Sobie ^{168,ab}, A. Soffer ¹⁵⁵, C.A. Solans Sanchez ³⁷, E.Yu. Soldatov ³⁸, U. Soldevila ¹⁶⁶,
 A.A. Solodkov ^{34j}, S. Solomon ²⁷, A. Soloshenko ³⁸, O.V. Solovyanov ⁴⁰, P. Sommer ⁴⁹,
 A. Sopczak ¹³⁴, A.L. Soppio ⁵¹, F. Sopkova ^{29b}, J.D. Sorenson ¹¹⁴, I.R. Sotarriva Alvarez ¹⁴⁰,
 V. Sothilingam ^{62a}, O.J. Soto Sandoval ^{139c,139b}, S. Sottocornola ⁶⁷, R. Soualah ^{83a}, D. South ⁴⁷,
 N. Soybelman ¹⁷², S. Spagnolo ^{69a,69b}, A.S. Spellman ¹²⁵, D. Sperlich ⁵³, B. Spisso ^{71a,71b},
 L. Splendori ¹⁰², M. Spousta ¹³⁵, E.J. Staats ³⁵, R. Stamen ^{62a}, E. Stanecka ⁸⁶,
 W. Stanek-Maslouska ⁴⁷, M.V. Stange ⁴⁹, B. Stanislaus ^{18a}, M.M. Stanitzki ⁴⁷, G.H. Stark ¹³⁸,
 J. Stark ⁸⁹, P. Staroba ¹³³, P. Starovoitov ^{83b}, R. Staszewski ⁸⁶, C. Stauch ¹⁰⁹,
 G. Stavropoulos ⁴⁵, A. Stefl ³⁷, A. Stein ¹⁰⁰, P. Steinberg ³⁰, B. Stelzer ^{146,160a}, H.J. Stelzer ¹³¹,
 O. Stelzer ^{160a}, H. Stenzel ⁵⁷, T.J. Stevenson ¹⁵⁰, G.A. Stewart ⁴⁷, G. Stoicea ^{28b},
 M. Stolarski ^{132a}, S. Stonjek ¹¹⁰, A. Straessner ⁴⁹, J. Strandberg ¹⁴⁸, S. Strandberg ^{46a,46b},
 M. Stratmann ¹⁷⁴, M. Strauss ¹²², T. Strebler ¹⁰², P. Strizenec ^{29b}, R. Ströhmer ¹⁶⁹,
 D.M. Strom ¹²⁵, R. Stroynowski ⁴⁴, A. Strubig ^{46a,46b}, S.A. Stucci ³⁰, B. Stugu ¹⁷, J. Stupak ¹²²,
 N.A. Styles ⁴⁷, D. Su ¹⁴⁷, S. Su ⁶¹, X. Su ⁶¹, D. Suchy ^{29a}, A.D. Sudhakar Ponnuru ⁵⁴,
 L. Sudit ¹⁷², Y. Sue ⁸², K. Sugizaki ¹³⁰, D.M.S. Sultan ¹²⁸, L. Sultanaliyeva ²⁵, S. Sultansoy ^{3b},
 S. Sun ¹⁷³, W. Sun ¹⁴, S. Sundar Raman ¹⁶⁷, N. Sur ⁹⁸, J.P. Surdutovich ¹²¹, N. Suri Jr ¹⁷⁵,
 M.R. Sutton ¹⁵⁰, M. Svatos ¹³³, P.N. Swallow ³³, S.N. Swatman ³⁷, M. Swiatlowski ^{160a},
 A. Swoboda ³⁷, I. Sykora ^{29a}, M. Sykora ¹³⁵, T. Sykora ¹³⁵, D. Ta ¹⁰⁰, K. Tackmann ^{47,y},
 A. Taffard ¹⁶³, R. Tafirout ^{160a}, Y. Takubo ⁸², M. Talby ¹⁰², N.M. Tamir ¹⁵⁵, A. Tanaka ¹⁵⁷,
 J. Tanaka ¹⁵⁷, R. Tanaka ⁶⁵, M. Tanasini ¹⁴⁹, Z. Tao ¹⁶⁷, S. Tapia Araya ^{139g}, S. Tapprogge ¹⁰⁰,
 A. Tarek Abouelfadl Mohamed ³⁷, S. Tarem ¹⁵⁴, K. Tariq ¹⁴, G. Tarna ³⁷, G.F. Tartarelli ^{70a},
 M.J. Tartarin ^{142b}, P. Tas ¹³⁵, M. Tasevsky ¹³³, E. Tassi ^{43b,43a}, A.C. Tate ¹⁶⁵, Y. Tayalati ^{36e,aa},
 G.N. Taylor ¹⁰⁵, W. Taylor ^{160b}, R.J. Taylor Vara ¹⁶⁶, A.S. Tegetmeier ⁸⁹, P. Teixeira-Dias ⁹⁵,
 J.J. Teoh ¹⁵⁹, K. Terashi ¹⁵⁷, J. Terron ⁹⁹, S. Terzo ¹³, M. Testa ⁵², R.J. Teuscher ^{159,ab},
 A. Thaler ⁷⁸, T. Theveneaux-Pelzer ¹⁰², J.P. Thomas ²¹, E.A. Thompson ^{18a}, P.D. Thompson ²¹,
 E. Thomson ¹³⁰, R.E. Thornberry ³⁰, T.M. Thory-Rao ²¹, C. Tian ⁶¹, Y. Tian ⁵⁵,
 V. Tikhomirov ⁸⁰, Yu.A. Tikhonov ³⁸, D. Timoshyn ¹³⁵, E.X.L. Ting ¹, P. Tipton ¹⁷⁵,
 A. Tishelman-Charny ³⁰, K. Todome ¹⁴⁰, S. Todorova-Nova ¹³⁵, L. Toffolin ^{68a,68c}, M. Togawa ⁸²,
 J. Tojo ⁸⁸, S. Tokár ^{29a}, O. Toldaiev ⁶⁷, G. Tolkachev ¹⁰², M. Tomoto ⁸², L. Tompkins ¹⁴⁷,
 E. Torrence ¹²⁵, H. Torres ⁸⁹, D.I. Torres Arza ^{139g}, E. Torres Reoyo ¹⁶⁶, E. Torró Pastor ¹⁶⁶,
 M. Toscani ³¹, C. Toscirci ³⁹, M. Tost ¹¹, D.R. Tovey ¹⁴³, T. Trefzger ¹⁶⁹, P.M. Tricarico ¹³,
 A. Tricoli ³⁰, I.M. Trigger ^{160a}, S. Trincaz-Duvoid ¹²⁹, D.A. Trischuk ¹⁶⁸, A. Tropina ³⁸,
 D. Truncali ^{75a,75b}, L. Truong ^{34c}, M. Trzebinski ⁸⁶, A. Trzupek ⁸⁶, F. Tsai ¹⁴⁹, A. Tsiamis ¹⁵⁶,
 P.V. Tsiarehsha ³⁸, S. Tsigaridas ^{160a}, A. Tsirigotis ^{156,t}, V. Tsiskaridze ^{153a}, E.G. Tskhadadze ^{153a},
 H.F. Tsoi ¹³⁰, Y. Tsujikawa ⁸⁷, V. Tsulaia ^{18a}, K. Tsuru ¹²⁰, D. Tsybychev ¹⁴⁹, Y. Tu ^{63b},
 A. Tudorache ^{28b}, V. Tudorache ^{28b}, S.B. Tuncay ¹²⁸, S. Turchikhin ^{56b,56a}, I. Turk Cakir ^{3a},
 R. Turra ^{70a}, T. Turtuvshin ^{38,ac}, P.M. Tuts ⁴¹, Y. Uematsu ⁸², F. Ukegawa ¹⁶¹,

P.A. Ulloa Poblete [ID139c,139b](#), G. Unal [ID37](#), A. Undrus [ID30](#), J. Urban [ID29b](#), P. Urrejola [ID139e](#), G. Usai [ID8](#),
 R. Ushioda [ID158](#), M. Usman [ID108](#), F. Ustuner [ID51](#), Z. Uysal [ID80](#), V. Vacek [ID134](#), B. Vachon [ID104](#),
 T. Vafeiadis [ID37](#), A. Vaitkus [ID96](#), C. Valderanis [ID109](#), E. Valdes Santurio [ID46a,46b](#), M. Valente [ID37](#),
 S. Valentinetti [ID24b,24a](#), A. Valero [ID166](#), E. Valiente Moreno [ID166](#), A. Vallier [ID89](#), J.A. Valls Ferrer [ID166](#),
 D.R. Van Arneman [ID116](#), R. Van Den Broucke [ID129](#), A. Van Der Graaf [ID48](#), H.Z. Van Der Schyf [ID34j](#),
 P. Van Gemmeren [ID6](#), M. Van Rijnbach [ID37](#), S. Van Stroud [ID96](#), I. Van Vulpen [ID116](#), P. Vana [ID135](#),
 M. Vanadia [ID75a,75b](#), U.M. Vande Voorde [ID148](#), W. Vandelli [ID37](#), E.R. Vandewall [ID147](#), D. Vannicola [ID155](#),
 R. Vari [ID74a](#), M. Varma [ID175](#), E.W. Varnes [ID7](#), C. Varni [ID85a](#), D. Varouchas [ID65](#), L. Varriale [ID166](#),
 K.E. Varvell [ID151](#), M.E. Vasile [ID28b](#), A. Vasileiadou⁹, L. Vaslin⁸², M.D. Vassilev [ID147](#), A. Vasyukov [ID38](#),
 L.M. Vaughan [ID123](#), R. Vavricka¹³⁵, T. Vazquez Schroeder [ID13](#), J. Veatch [ID32](#), V. Vecchio [ID101](#),
 M.J. Veen [ID103](#), I. Veliscek [ID30](#), I. Velkovska [ID93](#), L.M. Veloce [ID159](#), F. Veloso [ID132a,132c](#),
 A.G. Veltman [ID51](#), S.H. Venetianer [ID162](#), S. Veneziano [ID74a](#), A. Ventura [ID69a,69b](#), A. Verbitskyi [ID110](#),
 M. Verducci [ID73a,73b](#), C. Vergis [ID94](#), M. Verissimo De Araujo [ID81b](#), W. Verkerke [ID116](#),
 J.C. Vermeulen [ID116](#), C. Vernieri [ID147](#), M. Vessella [ID163](#), M.C. Vetterli [ID146,aj](#), A. Vgenopoulos [ID100](#),
 N. Viaux Maira [ID139g,af](#), L. Vicenik [ID134](#), T. Vickey [ID143](#), O.E. Vickey Boeriu [ID143](#),
 G.H.A. Viehhauser [ID128](#), L. Vigani [ID62b](#), M. Vigi [ID110](#), M. Villa [ID24b,24a](#), M. Villaplana Perez [ID166](#),
 E.M. Villhauer³⁹, E. Vilucchi [ID52](#), M. Vincent [ID166](#), M.G. Vincter [ID35](#), A. Visibile [ID116](#), A. Visive [ID116](#),
 C. Vittori [ID162](#), I. Vivarelli [ID24b,24a](#), M.I. Vivas Albornoz [ID47](#), E. Voevodina [ID110](#), F. Vogel [ID109](#),
 J.C. Voigt [ID49](#), P. Vokac [ID134](#), Yu. Volkotrub [ID85b](#), L. Vomberg [ID25](#), E. Von Toerne [ID25](#),
 B. Vormwald [ID37](#), K. Vorobev [ID50](#), M. Vos [ID166](#), K. Voss [ID145](#), M. Vozak [ID37](#), L. Vozdecky [ID122](#),
 N. Vranjes [ID16](#), M. Vranjes Milosavljevic [ID16](#), M. Vreeswijk [ID116](#), N.K. Vu [ID112a](#), R. Vuillermet [ID37](#),
 O. Vujinovic [ID100](#), I. Vukotic [ID39](#), I.K. Vyas [ID35](#), J.F. Wack [ID33](#), A. Wada [ID111](#), S. Wada [ID161](#),
 C. Wagner¹⁴⁷, J.M. Wagner [ID18a](#), W. Wagner [ID174](#), S. Wahdan [ID174](#), H. Wahlberg [ID90](#), C.H. Waits [ID122](#),
 J. Walder [ID136](#), R. Walker [ID109](#), K. Walkingshaw Pass [ID58](#), W. Walkowiak [ID145](#), A. Wall [ID130](#),
 E.J. Wallin [ID98](#), T. Wamorkar [ID147](#), K. Wandall-Christensen [ID166](#), A. Wang [ID61](#), A.Z. Wang [ID138](#),
 C. Wang [ID47](#), C. Wang [ID11](#), H. Wang [ID18a](#), J. Wang [ID63c](#), P. Wang [ID101](#), P. Wang [ID96](#), R. Wang [ID60](#),
 R. Wang [ID106](#), R. Wang [ID6](#), S.M. Wang [ID152](#), S. Wang [ID14](#), T. Wang [ID115](#), T. Wang [ID61](#), W.T. Wang [ID128](#),
 X. Wang [ID165](#), X. Wang [ID142a](#), X. Wang [ID47](#), Y. Wang [ID149](#), Y. Wang [ID114](#), Z. Wang [ID106](#), Z. Wang [ID14](#),
 Z. Wang^{63b}, C. Wanotayaroj [ID82](#), A. Warburton [ID104](#), A.L. Warnerbring [ID145](#), S. Waterhouse [ID96](#),
 A.T. Watson [ID21](#), H. Watson [ID51](#), M.F. Watson [ID21](#), E. Watton [ID37](#), G. Watts [ID141](#), B.M. Waugh [ID96](#),
 J.M. Webb [ID53](#), C. Weber [ID30](#), M.S. Weber [ID20](#), C. Wei [ID61](#), Y. Wei [ID53](#), A.R. Weidberg [ID128](#),
 E.J. Weik [ID119](#), J. Weingarten [ID48](#), C. Weiser [ID53](#), C.J. Wells [ID47](#), T. Wenaus [ID30](#), T. Wengler [ID37](#),
 N.S. Wenke¹¹⁰, N. Wermes [ID25](#), M. Wessels [ID62a](#), A.M. Wharton [ID91](#), A.S. White [ID37](#), A. White [ID8](#),
 M.J. White [ID1](#), D. Whiteson [ID163](#), L. Wickremasinghe [ID126](#), W. Wiedenmann [ID173](#), M. Wielers [ID136](#),
 R. Wierda [ID148](#), C. Wiglesworth [ID42](#), H.G. Wilkens [ID37](#), J.J.H. Wilkinson [ID33](#), S. Williams [ID33](#),
 S. Willocq [ID103](#), D.J. Wilson [ID101](#), P.J. Windischhofer [ID39](#), F.I. Winkel [ID31](#), F. Winklmeier [ID125](#),
 B.T. Winter [ID53](#), M. Wittgen¹⁴⁷, M. Wobisch [ID97](#), T. Wojtkowski⁵⁹, Z. Wolffs [ID116](#), J. Wollrath³⁷,
 M.W. Wolter [ID86](#), H. Wolters [ID132a,132c](#), M.C. Wong¹³⁸, E.L. Woodward [ID41](#), S.D. Worm [ID47](#),
 B.K. Wosiek [ID86](#), K.A. Wozniak [ID55](#), K.W. Woźniak [ID86](#), S. Wozniewski [ID54](#), K. Wraight [ID58](#),
 C. Wu [ID159](#), C. Wu [ID21](#), J. Wu [ID157](#), M. Wu [ID112b](#), M. Wu [ID115](#), S.L. Wu [ID173](#), S. Wu [ID14,ao](#), X. Wu [ID61](#),
 Y.Q. Wu [ID159](#), Y. Wu [ID61](#), Z. Wu [ID102](#), Z. Wu [ID112a](#), J. Wuerzinger [ID110](#), T.R. Wyatt [ID101](#),
 B.M. Wynne [ID51](#), S. Xella [ID42](#), L. Xia [ID112a](#), M. Xie [ID61](#), A. Xiong [ID125](#), I. Xiotidis [ID37](#), D. Xu [ID14](#),
 H. Xu [ID61](#), L. Xu [ID61](#), R. Xu [ID130](#), T. Xu [ID106](#), W. Xu^{112a}, Y. Xu [ID141](#), Z. Xu [ID51](#), R. Xue [ID131](#),
 B. Yabsley [ID151](#), S. Yacoob [ID11](#), Y. Yamaguchi [ID82](#), E. Yamashita [ID157](#), H. Yamauchi [ID161](#),
 T. Yamazaki [ID18a](#), Y. Yamazaki [ID84](#), S. Yan [ID58](#), Z. Yan [ID103](#), C. Yang [ID18a](#), H.J. Yang [ID142a](#),
 H.T. Yang [ID61](#), S. Yang [ID61](#), X. Yang [ID37](#), X. Yang [ID14](#), Y. Yang [ID157](#), Y. Yang⁶¹, W-M. Yao [ID18a](#),
 C.L. Yardley [ID150](#), J. Ye [ID14](#), S. Ye [ID30](#), X. Ye [ID61](#), I. Yeletsikh [ID38](#), B. Yeo [ID18b](#), M.R. Yexley [ID96](#),

T.P. Yildirim ¹²⁸, K. Yorita ¹⁷¹, C.J.S. Young ³⁷, C. Young ¹⁴⁷, I.N.L. Young ⁵⁸, N.D. Young¹²⁵, Y. Yu ⁶¹, J. Yuan ^{14,112c,ao}, M. Yuan ¹⁰⁶, R. Yuan ^{142b}, L. Yue ⁹⁶, M. Zaazoua ⁶¹, B. Zabinski ⁸⁶, I. Zahir ^{36a}, Q.U.A. Zahoor ⁵¹, A. Zaio^{56b,56a}, Z.K. Zak ⁸⁶, T. Zakareishvili ¹⁶⁶, S. Zambito ⁵⁵, J. Zang ¹⁵⁷, R. Zanzottera ^{70a,70b}, O. Zaplatilek ¹³⁴, E. Zaya ¹⁴⁸, C. Zeitnitz ¹⁷⁴, H. Zeng ¹⁴, D.T. Zenger Jr ²⁷, T. Ženiš ^{29a}, S. Zenz ⁹⁴, D. Zerwas ⁶⁵, B. Zhang ¹⁷⁰, D.F. Zhang ¹⁴³, G. Zhang ^{14,ao}, J. Zhang ^{113b}, J. Zhang ⁶, L. Zhang ⁶¹, L. Zhang ^{112a}, P. Zhang ^{14,112c}, R. Zhang ^{112a}, S. Zhang ⁸⁹, Y. Zhang ¹⁴¹, Y. Zhang ⁹⁶, Y. Zhang ⁶¹, Y. Zhang ^{112a}, Z. Zhang ^{18a}, Z. Zhang ^{113b}, Z. Zhang ⁶⁵, H. Zhao ¹⁴¹, T. Zhao ^{113b}, Y. Zhao ³⁵, Z. Zhao ⁶¹, Z. Zhao ⁶¹, A. Zhemchugov ³⁸, J. Zheng ^{112a}, K. Zheng ¹⁶⁵, L. Zheng ^{113b}, X. Zheng ⁶¹, Z. Zheng ¹⁴⁷, D. Zhong ¹⁶⁵, B. Zhou ¹⁰⁶, B. Zhou ^{142b,142a}, N. Zhou ^{142a}, Y. Zhou ¹⁵, Y. Zhou ^{112a}, Y. Zhou⁷, Z. Zhou ⁶¹, J. Zhu ¹⁰⁶, X. Zhu ^{142b}, Y. Zhu ^{142a}, X. Zhuang ¹⁴, K. Zhukov ⁶⁷, P. Ziakas ⁴, N.I. Zimine ³⁸, J. Zinsser ^{62b}, M. Ziolkowski ¹⁴⁵, L. Živković ¹⁶, A. Zoccoli ^{24b,24a}, K. Zoch ³⁷, A. Zografos ³⁷, T.G. Zorbas ¹⁴³, L. Zwalinski ³⁷.

¹Department of Physics, University of Adelaide, Adelaide; Australia.

²Department of Physics, University of Alberta, Edmonton AB; Canada.

^{3(a)}Department of Physics, Ankara University, Ankara; ^(b)Division of Physics, TOBB University of Economics and Technology, Ankara; Türkiye.

⁴LAPP, Université Savoie Mont Blanc, CNRS/IN2P3, Annecy; France.

⁵APC, Université Paris Cité, CNRS/IN2P3, Paris; France.

⁶High Energy Physics Division, Argonne National Laboratory, Argonne IL; United States of America.

⁷Department of Physics, University of Arizona, Tucson AZ; United States of America.

⁸Department of Physics, University of Texas at Arlington, Arlington TX; United States of America.

⁹Physics Department, National and Kapodistrian University of Athens, Athens; Greece.

¹⁰Physics Department, National Technical University of Athens, Zografou; Greece.

¹¹Department of Physics, University of Texas at Austin, Austin TX; United States of America.

¹²Institute of Physics, Azerbaijan Academy of Sciences, Baku; Azerbaijan.

¹³Institut de Física d'Altes Energies (IFAE), Barcelona Institute of Science and Technology, Barcelona; Spain.

¹⁴Institute of High Energy Physics, Chinese Academy of Sciences, Beijing; China.

¹⁵Physics Department, Tsinghua University, Beijing; China.

¹⁶Institute of Physics, University of Belgrade, Belgrade; Serbia.

¹⁷Department for Physics and Technology, University of Bergen, Bergen; Norway.

^{18(a)}Physics Division, Lawrence Berkeley National Laboratory, Berkeley CA; ^(b)University of California, Berkeley CA; United States of America.

¹⁹Institut für Physik, Humboldt Universität zu Berlin, Berlin; Germany.

²⁰Albert Einstein Center for Fundamental Physics and Laboratory for High Energy Physics, University of Bern, Bern; Switzerland.

²¹School of Physics and Astronomy, University of Birmingham, Birmingham; United Kingdom.

^{22(a)}Department of Physics, Bogazici University, Istanbul; ^(b)Department of Physics Engineering, Gaziantep University, Gaziantep; ^(c)Department of Physics, Istanbul University, Istanbul; Türkiye.

^{23(a)}Facultad de Ciencias y Centro de Investigaciones, Universidad Antonio Nariño,

Bogotá; ^(b)Departamento de Física, Universidad Nacional de Colombia, Bogotá; Colombia.

^{24(a)}Dipartimento di Fisica e Astronomia A. Righi, Università di Bologna, Bologna; ^(b)INFN Sezione di Bologna; Italy.

²⁵Physikalisches Institut, Universität Bonn, Bonn; Germany.

²⁶Department of Physics, Boston University, Boston MA; United States of America.

- ²⁷Department of Physics, Brandeis University, Waltham MA; United States of America.
- ²⁸(^a) Transilvania University of Brasov, Brasov; (^b) Horia Hulubei National Institute of Physics and Nuclear Engineering, Bucharest; (^c) Department of Physics, Alexandru Ioan Cuza University of Iasi, Iasi; (^d) National Institute for Research and Development of Isotopic and Molecular Technologies, Physics Department, Cluj-Napoca; (^e) National University of Science and Technology Politehnica, Bucharest; (^f) West University in Timisoara, Timisoara; (^g) Faculty of Physics, University of Bucharest, Bucharest; Romania.
- ²⁹(^a) Faculty of Mathematics, Physics and Informatics, Comenius University, Bratislava; (^b) Department of Subnuclear Physics, Institute of Experimental Physics of the Slovak Academy of Sciences, Kosice; Slovak Republic.
- ³⁰Physics Department, Brookhaven National Laboratory, Upton NY; United States of America.
- ³¹Universidad de Buenos Aires, Facultad de Ciencias Exactas y Naturales, Departamento de Física, y CONICET, Instituto de Física de Buenos Aires (IFIBA), Buenos Aires; Argentina.
- ³²California State University, CA; United States of America.
- ³³Cavendish Laboratory, University of Cambridge, Cambridge; United Kingdom.
- ³⁴(^a) Department of Physics, University of Cape Town, Cape Town; (^b) iThemba Labs, Western Cape; (^c) Department of Mechanical Engineering Science, University of Johannesburg, Johannesburg; (^d) National Institute of Physics, University of the Philippines Diliman (Philippines); (^e) Department of Physics, Stellenbosch University, Matieland; (^f) University of KwaZulu-Natal, School of Agriculture and Science, Mathematics, Westville; (^g) University of South Africa, Department of Physics, Pretoria; (^h) University of Pretoria, Department of Mechanical and Aeronautical Engineering, Pretoria; (ⁱ) University of Zululand, KwaDlangezwa; (^j) School of Physics, University of the Witwatersrand, Johannesburg; South Africa.
- ³⁵Department of Physics, Carleton University, Ottawa ON; Canada.
- ³⁶(^a) Faculté des Sciences Ain Chock, Université Hassan II de Casablanca; (^b) Faculté des Sciences, Université Ibn-Tofail, Kénitra; (^c) Faculté des Sciences Semailia, Université Cadi Ayyad, LPHEA-Marrakech; (^d) LPMR, Faculté des Sciences, Université Mohamed Premier, Oujda; (^e) Faculté des sciences, Université Mohammed V, Rabat; (^f) Institute of Applied Physics, Mohammed VI Polytechnic University, Ben Guerir; Morocco.
- ³⁷CERN, Geneva; Switzerland.
- ³⁸Affiliated with an international laboratory covered by a cooperation agreement with CERN.
- ³⁹Enrico Fermi Institute, University of Chicago, Chicago IL; United States of America.
- ⁴⁰LPC, Université Clermont Auvergne, CNRS/IN2P3, Clermont-Ferrand; France.
- ⁴¹Nevis Laboratory, Columbia University, Irvington NY; United States of America.
- ⁴²Niels Bohr Institute, University of Copenhagen, Copenhagen; Denmark.
- ⁴³(^a) Dipartimento di Fisica, Università della Calabria, Rende; (^b) INFN Gruppo Collegato di Cosenza, Laboratori Nazionali di Frascati; Italy.
- ⁴⁴Physics Department, Southern Methodist University, Dallas TX; United States of America.
- ⁴⁵National Centre for Scientific Research "Demokritos", Agia Paraskevi; Greece.
- ⁴⁶(^a) Department of Physics, Stockholm University; (^b) Oskar Klein Centre, Stockholm; Sweden.
- ⁴⁷Deutsches Elektronen-Synchrotron DESY, Hamburg and Zeuthen; Germany.
- ⁴⁸Fakultät Physik, Technische Universität Dortmund, Dortmund; Germany.
- ⁴⁹Institut für Kern- und Teilchenphysik, Technische Universität Dresden, Dresden; Germany.
- ⁵⁰Department of Physics, Duke University, Durham NC; United States of America.
- ⁵¹SUPA - School of Physics and Astronomy, University of Edinburgh, Edinburgh; United Kingdom.
- ⁵²INFN e Laboratori Nazionali di Frascati, Frascati; Italy.
- ⁵³Physikalisches Institut, Albert-Ludwigs-Universität Freiburg, Freiburg; Germany.
- ⁵⁴II. Physikalisches Institut, Georg-August-Universität Göttingen, Göttingen; Germany.

- ⁵⁵Département de Physique Nucléaire et Corpusculaire, Université de Genève, Genève; Switzerland.
- ⁵⁶(^a) Dipartimento di Fisica, Università di Genova, Genova; (^b) INFN Sezione di Genova; Italy.
- ⁵⁷II. Physikalisches Institut, Justus-Liebig-Universität Giessen, Giessen; Germany.
- ⁵⁸SUPA - School of Physics and Astronomy, University of Glasgow, Glasgow; United Kingdom.
- ⁵⁹LPSC, Université Grenoble Alpes, CNRS/IN2P3, Grenoble INP, Grenoble; France.
- ⁶⁰Laboratory for Particle Physics and Cosmology, Harvard University, Cambridge MA; United States of America.
- ⁶¹Department of Modern Physics and State Key Laboratory of Particle Detection and Electronics, University of Science and Technology of China, Hefei; China.
- ⁶²(^a) Kirchoff-Institut für Physik, Ruprecht-Karls-Universität Heidelberg, Heidelberg; (^b) Physikalisches Institut, Ruprecht-Karls-Universität Heidelberg, Heidelberg; Germany.
- ⁶³(^a) Department of Physics, Chinese University of Hong Kong, Shatin, N.T., Hong Kong; (^b) Department of Physics, University of Hong Kong, Hong Kong; (^c) Department of Physics and Institute for Advanced Study, Hong Kong University of Science and Technology, Clear Water Bay, Kowloon, Hong Kong; China.
- ⁶⁴Department of Physics, National Tsing Hua University, Hsinchu; Taiwan.
- ⁶⁵IJCLab, Université Paris-Saclay, CNRS/IN2P3, 91405, Orsay; France.
- ⁶⁶Centro Nacional de Microelectrónica (IMB-CNM-CSIC), Barcelona; Spain.
- ⁶⁷Department of Physics, Indiana University, Bloomington IN; United States of America.
- ⁶⁸(^a) INFN Gruppo Collegato di Udine, Sezione di Trieste, Udine; (^b) ICTP, Trieste; (^c) Dipartimento Politecnico di Ingegneria e Architettura, Università di Udine, Udine; Italy.
- ⁶⁹(^a) INFN Sezione di Lecce; (^b) Dipartimento di Matematica e Fisica, Università del Salento, Lecce; Italy.
- ⁷⁰(^a) INFN Sezione di Milano; (^b) Dipartimento di Fisica, Università di Milano, Milano; Italy.
- ⁷¹(^a) INFN Sezione di Napoli; (^b) Dipartimento di Fisica, Università di Napoli, Napoli; Italy.
- ⁷²(^a) INFN Sezione di Pavia; (^b) Dipartimento di Fisica, Università di Pavia, Pavia; Italy.
- ⁷³(^a) INFN Sezione di Pisa; (^b) Dipartimento di Fisica E. Fermi, Università di Pisa, Pisa; Italy.
- ⁷⁴(^a) INFN Sezione di Roma; (^b) Dipartimento di Fisica, Sapienza Università di Roma, Roma; Italy.
- ⁷⁵(^a) INFN Sezione di Roma Tor Vergata; (^b) Dipartimento di Fisica, Università di Roma Tor Vergata, Roma; Italy.
- ⁷⁶(^a) INFN Sezione di Roma Tre; (^b) Dipartimento di Matematica e Fisica, Università Roma Tre, Roma; Italy.
- ⁷⁷(^a) INFN-TIFPA; (^b) Università degli Studi di Trento, Trento; Italy.
- ⁷⁸Universität Innsbruck, Department of Astro and Particle Physics, Innsbruck; Austria.
- ⁷⁹Department of Physics and Astronomy, Iowa State University, Ames IA; United States of America.
- ⁸⁰Istinye University, Sariyer, Istanbul; Türkiye.
- ⁸¹(^a) Departamento de Engenharia Elétrica, Universidade Federal de Juiz de Fora (UFJF), Juiz de Fora; (^b) Universidade Federal do Rio De Janeiro COPPE/EE/IF, Rio de Janeiro; (^c) Instituto de Física, Universidade de São Paulo, São Paulo; (^d) Rio de Janeiro State University, Rio de Janeiro; (^e) Federal University of Bahia, Bahia; Brazil.
- ⁸²KEK, High Energy Accelerator Research Organization, Tsukuba; Japan.
- ⁸³(^a) Khalifa University of Science and Technology, Abu Dhabi; (^b) University of Sharjah, Sharjah; United Arab Emirates.
- ⁸⁴Graduate School of Science, Kobe University, Kobe; Japan.
- ⁸⁵(^a) AGH University of Krakow, Faculty of Physics and Applied Computer Science, Krakow; (^b) Marian Smoluchowski Institute of Physics, Jagiellonian University, Krakow; Poland.
- ⁸⁶Institute of Nuclear Physics Polish Academy of Sciences, Krakow; Poland.
- ⁸⁷Faculty of Science, Kyoto University, Kyoto; Japan.
- ⁸⁸Research Center for Advanced Particle Physics and Department of Physics, Kyushu University, Fukuoka ;

Japan.

⁸⁹L2IT, Université de Toulouse, CNRS/IN2P3, UPS, Toulouse; France.

⁹⁰Instituto de Física La Plata, Universidad Nacional de La Plata and CONICET, La Plata; Argentina.

⁹¹Physics Department, Lancaster University, Lancaster; United Kingdom.

⁹²Oliver Lodge Laboratory, University of Liverpool, Liverpool; United Kingdom.

⁹³Department of Experimental Particle Physics, Jožef Stefan Institute and Department of Physics, University of Ljubljana, Ljubljana; Slovenia.

⁹⁴Department of Physics and Astronomy, Queen Mary University of London, London; United Kingdom.

⁹⁵Department of Physics, Royal Holloway University of London, Egham; United Kingdom.

⁹⁶Department of Physics and Astronomy, University College London, London; United Kingdom.

⁹⁷Louisiana Tech University, Ruston LA; United States of America.

⁹⁸Fysiska institutionen, Lunds universitet, Lund; Sweden.

⁹⁹Departamento de Física Teórica C-15 and CIAFF, Universidad Autónoma de Madrid, Madrid; Spain.

¹⁰⁰Institut für Physik, Universität Mainz, Mainz; Germany.

¹⁰¹School of Physics and Astronomy, University of Manchester, Manchester; United Kingdom.

¹⁰²CPPM, Aix-Marseille Université, CNRS/IN2P3, Marseille; France.

¹⁰³Department of Physics, University of Massachusetts, Amherst MA; United States of America.

¹⁰⁴Department of Physics, McGill University, Montreal QC; Canada.

¹⁰⁵School of Physics, University of Melbourne, Victoria; Australia.

¹⁰⁶Department of Physics, University of Michigan, Ann Arbor MI; United States of America.

¹⁰⁷Department of Physics and Astronomy, Michigan State University, East Lansing MI; United States of America.

¹⁰⁸Group of Particle Physics, University of Montreal, Montreal QC; Canada.

¹⁰⁹Fakultät für Physik, Ludwig-Maximilians-Universität München, München; Germany.

¹¹⁰Max-Planck-Institut für Physik (Werner-Heisenberg-Institut), München; Germany.

¹¹¹Graduate School of Science and Kobayashi-Maskawa Institute, Nagoya University, Nagoya; Japan.

¹¹²(^a) Department of Physics, Nanjing University, Nanjing; (^b) School of Science, Shenzhen Campus of Sun Yat-sen University; (^c) University of Chinese Academy of Science (UCAS), Beijing; China.

¹¹³(^a) School of Physics, Nankai University, Tianjin; (^b) Institute of Frontier and Interdisciplinary Science and Key Laboratory of Particle Physics and Particle Irradiation (MOE), Shandong University, Qingdao; (^c) School of Physics, Zhengzhou University; China.

¹¹⁴Department of Physics and Astronomy, University of New Mexico, Albuquerque NM; United States of America.

¹¹⁵Institute for Mathematics, Astrophysics and Particle Physics, Radboud University/Nikhef, Nijmegen; Netherlands.

¹¹⁶Nikhef National Institute for Subatomic Physics and University of Amsterdam, Amsterdam; Netherlands.

¹¹⁷Department of Physics, Northern Illinois University, DeKalb IL; United States of America.

¹¹⁸(^a) New York University Abu Dhabi, Abu Dhabi; (^b) United Arab Emirates University, Al Ain; United Arab Emirates.

¹¹⁹Department of Physics, New York University, New York NY; United States of America.

¹²⁰Ochanomizu University, Otsuka, Bunkyo-ku, Tokyo; Japan.

¹²¹Ohio State University, Columbus OH; United States of America.

¹²²Homer L. Dodge Department of Physics and Astronomy, University of Oklahoma, Norman OK; United States of America.

¹²³Department of Physics, Oklahoma State University, Stillwater OK; United States of America.

¹²⁴Palacký University, Joint Laboratory of Optics, Olomouc; Czech Republic.

- ¹²⁵Institute for Fundamental Science, University of Oregon, Eugene, OR; United States of America.
- ¹²⁶Graduate School of Science, University of Osaka, Osaka; Japan.
- ¹²⁷Department of Physics, University of Oslo, Oslo; Norway.
- ¹²⁸Department of Physics, Oxford University, Oxford; United Kingdom.
- ¹²⁹LPNHE, Sorbonne Université, Université Paris Cité, CNRS/IN2P3, Paris; France.
- ¹³⁰Department of Physics, University of Pennsylvania, Philadelphia PA; United States of America.
- ¹³¹Department of Physics and Astronomy, University of Pittsburgh, Pittsburgh PA; United States of America.
- ¹³²(^a)Laboratório de Instrumentação e Física Experimental de Partículas - LIP, Lisboa;(^b)Departamento de Física, Faculdade de Ciências, Universidade de Lisboa, Lisboa;(^c)Departamento de Física, Universidade de Coimbra, Coimbra;(^d)Centro de Física Nuclear da Universidade de Lisboa, Lisboa;(^e)Departamento de Física, Escola de Ciências, Universidade do Minho, Braga;(^f)Departamento de Física Teórica y del Cosmos, Universidad de Granada, Granada (Spain);(^g)Departamento de Física, Instituto Superior Técnico, Universidade de Lisboa, Lisboa; Portugal.
- ¹³³Institute of Physics of the Czech Academy of Sciences, Prague; Czech Republic.
- ¹³⁴Czech Technical University in Prague, Prague; Czech Republic.
- ¹³⁵Charles University, Faculty of Mathematics and Physics, Prague; Czech Republic.
- ¹³⁶Particle Physics Department, Rutherford Appleton Laboratory, Didcot; United Kingdom.
- ¹³⁷IRFU, CEA, Université Paris-Saclay, Gif-sur-Yvette; France.
- ¹³⁸Santa Cruz Institute for Particle Physics, University of California Santa Cruz, Santa Cruz CA; United States of America.
- ¹³⁹(^a)Departamento de Física, Pontificia Universidad Católica de Chile, Santiago;(^b)Millennium Institute for Subatomic physics at high energy frontier (SAPHIR), Santiago;(^c)Instituto de Investigación Multidisciplinario en Ciencia y Tecnología, y Departamento de Física, Universidad de La Serena;(^d)Universidad Andres Bello, Department of Physics, Santiago;(^e)Universidad San Sebastian, Recoleta;(^f)Instituto de Alta Investigación, Universidad de Tarapacá, Arica;(^g)Departamento de Física, Universidad Técnica Federico Santa María, Valparaíso; Chile.
- ¹⁴⁰Department of Physics, Institute of Science, Tokyo; Japan.
- ¹⁴¹Department of Physics, University of Washington, Seattle WA; United States of America.
- ¹⁴²(^a)State Key Laboratory of Dark Matter Physics, School of Physics and Astronomy, Shanghai Jiao Tong University, Key Laboratory for Particle Astrophysics and Cosmology (MOE), SKLPPC, Shanghai;(^b)State Key Laboratory of Dark Matter Physics, Tsung-Dao Lee Institute, Shanghai Jiao Tong University, Shanghai; China.
- ¹⁴³Department of Physics and Astronomy, University of Sheffield, Sheffield; United Kingdom.
- ¹⁴⁴Department of Physics, Shinshu University, Nagano; Japan.
- ¹⁴⁵Department Physik, Universität Siegen, Siegen; Germany.
- ¹⁴⁶Department of Physics, Simon Fraser University, Burnaby BC; Canada.
- ¹⁴⁷SLAC National Accelerator Laboratory, Stanford CA; United States of America.
- ¹⁴⁸Department of Physics, Royal Institute of Technology, Stockholm; Sweden.
- ¹⁴⁹Departments of Physics and Astronomy, Stony Brook University, Stony Brook NY; United States of America.
- ¹⁵⁰Department of Physics and Astronomy, University of Sussex, Brighton; United Kingdom.
- ¹⁵¹School of Physics, University of Sydney, Sydney; Australia.
- ¹⁵²Institute of Physics, Academia Sinica, Taipei; Taiwan.
- ¹⁵³(^a)E. Andronikashvili Institute of Physics, Iv. Javakhishvili Tbilisi State University, Tbilisi;(^b)High Energy Physics Institute, Tbilisi State University, Tbilisi;(^c)University of Georgia, Tbilisi; Georgia.
- ¹⁵⁴Department of Physics, Technion, Israel Institute of Technology, Haifa; Israel.

- ¹⁵⁵Raymond and Beverly Sackler School of Physics and Astronomy, Tel Aviv University, Tel Aviv; Israel.
- ¹⁵⁶Department of Physics, Aristotle University of Thessaloniki, Thessaloniki; Greece.
- ¹⁵⁷International Center for Elementary Particle Physics and Department of Physics, University of Tokyo, Tokyo; Japan.
- ¹⁵⁸Graduate School of Science and Technology, Tokyo Metropolitan University, Tokyo; Japan.
- ¹⁵⁹Department of Physics, University of Toronto, Toronto ON; Canada.
- ¹⁶⁰^(a)TRIUMF, Vancouver BC; ^(b)Department of Physics and Astronomy, York University, Toronto ON; Canada.
- ¹⁶¹Division of Physics and Tomonaga Center for the History of the Universe, Faculty of Pure and Applied Sciences, University of Tsukuba, Tsukuba; Japan.
- ¹⁶²Department of Physics and Astronomy, Tufts University, Medford MA; United States of America.
- ¹⁶³Department of Physics and Astronomy, University of California Irvine, Irvine CA; United States of America.
- ¹⁶⁴Department of Physics and Astronomy, University of Uppsala, Uppsala; Sweden.
- ¹⁶⁵Department of Physics, University of Illinois, Urbana IL; United States of America.
- ¹⁶⁶Instituto de Física Corpuscular (IFIC), Centro Mixto Universidad de Valencia - CSIC, Valencia; Spain.
- ¹⁶⁷Department of Physics, University of British Columbia, Vancouver BC; Canada.
- ¹⁶⁸Department of Physics and Astronomy, University of Victoria, Victoria BC; Canada.
- ¹⁶⁹Fakultät für Physik und Astronomie, Julius-Maximilians-Universität Würzburg, Würzburg; Germany.
- ¹⁷⁰Department of Physics, University of Warwick, Coventry; United Kingdom.
- ¹⁷¹Waseda University, Tokyo; Japan.
- ¹⁷²Department of Particle Physics and Astrophysics, Weizmann Institute of Science, Rehovot; Israel.
- ¹⁷³Department of Physics, University of Wisconsin, Madison WI; United States of America.
- ¹⁷⁴Fakultät für Mathematik und Naturwissenschaften, Fachgruppe Physik, Bergische Universität Wuppertal, Wuppertal; Germany.
- ¹⁷⁵Department of Physics, Yale University, New Haven CT; United States of America.
- ¹⁷⁶Yerevan Physics Institute, Yerevan; Armenia.
- ^a Also at Affiliated with an institute formerly covered by a cooperation agreement with CERN.
- ^b Also at An-Najah National University, Nablus; Palestine.
- ^c Also at Borough of Manhattan Community College, City University of New York, New York NY; United States of America.
- ^d Also at Center for Interdisciplinary Research and Innovation (CIRI-AUTH), Thessaloniki; Greece.
- ^e Also at Centre of Physics of the Universities of Minho and Porto (CF-UM-UP); Portugal.
- ^f Also at CERN, Geneva; Switzerland.
- ^g Also at Département de Physique Nucléaire et Corpusculaire, Université de Genève, Genève; Switzerland.
- ^h Also at Departament de Física de la Universitat Autònoma de Barcelona, Barcelona; Spain.
- ⁱ Also at Department of Financial and Management Engineering, University of the Aegean, Chios; Greece.
- ^j Also at Department of Modern Physics and State Key Laboratory of Particle Detection and Electronics, University of Science and Technology of China, Hefei; China.
- ^k Also at Department of Physics, Ben Gurion University of the Negev, Beer Sheva; Israel.
- ^l Also at Department of Physics, Bolu Abant İzzet Baysal University, Bolu; Türkiye.
- ^m Also at Department of Physics, King's College London, London; United Kingdom.
- ⁿ Also at Department of Physics, Stellenbosch University; South Africa.
- ^o Also at Department of Physics, University of Fribourg, Fribourg; Switzerland.
- ^p Also at Department of Physics, University of Thessaly; Greece.
- ^q Also at Department of Physics, Westmont College, Santa Barbara; United States of America.

- ^r Also at Faculty of Physics, Sofia University, 'St. Kliment Ohridski', Sofia; Bulgaria.
- ^s Also at Faculty of Physics, University of Bucharest; Romania.
- ^t Also at Hellenic Open University, Patras; Greece.
- ^u Also at Henan University; China.
- ^v Also at Imam Mohammad Ibn Saud Islamic University; Saudi Arabia.
- ^w Also at Indian Institute of Technology (IIT), Jodhpur; India.
- ^x Also at Institutio Catalana de Recerca i Estudis Avancats, ICREA, Barcelona; Spain.
- ^y Also at Institut für Experimentalphysik, Universität Hamburg, Hamburg; Germany.
- ^z Also at Institute for Nuclear Research and Nuclear Energy (INRNE) of the Bulgarian Academy of Sciences, Sofia; Bulgaria.
- ^{aa} Also at Institute of Applied Physics, Mohammed VI Polytechnic University, Ben Guerir; Morocco.
- ^{ab} Also at Institute of Particle Physics (IPP); Canada.
- ^{ac} Also at Institute of Physics and Technology, Mongolian Academy of Sciences, Ulaanbaatar; Mongolia.
- ^{ad} Also at Institute of Physics, Azerbaijan Academy of Sciences, Baku; Azerbaijan.
- ^{ae} Also at Institute of Theoretical Physics, Iliia State University, Tbilisi; Georgia.
- ^{af} Also at Millennium Institute for Subatomic physics at high energy frontier (SAPHIR), Santiago; Chile.
- ^{ag} Also at National Institute of Physics, University of the Philippines Diliman (Philippines); Philippines.
- ^{ah} Also at School of Physics, University of the Witwatersrand, Johannesburg; South Africa.
- ^{ai} Also at The Collaborative Innovation Center of Quantum Matter (CICQM), Beijing; China.
- ^{aj} Also at TRIUMF, Vancouver BC; Canada.
- ^{ak} Also at Università di Napoli Parthenope, Napoli; Italy.
- ^{al} Associated at Università degli Studi di Padova, Padova; Italy.
- ^{am} Also at Università degli Studi Link; Italy.
- ^{an} Also at University and INFN Torino, Torino; Italy.
- ^{ao} Also at University of Chinese Academy of Sciences (UCAS), Beijing; China.
- ^{ap} Also at University of Colorado Boulder, Department of Physics, Colorado; United States of America.
- ^{aq} Also at University of Siena; Italy.
- ^{ar} Also at Washington College, Chestertown, MD; United States of America.
- ^{as} Also at Yeditepe University, Physics Department, Istanbul; Türkiye.
- * Deceased